UNIVERSITY OF OKLAHOMA

GRADUATE COLLEGE

INTERFACIALLY ACTIVE CARBON NANOTUBE HYBRIDS FOR RESERVOIR DEVELOPMENT APPLICATIONS

A DISSERTATION

SUBMITTED TO THE GRADUATE FACULTY

in partial fulfillment of the requirements for the

Degree of

DOCTOR OF PHILOSOPHY

By

MOHANNAD JUAD KADHUM
Norman, Oklahoma
2013

INTERFACIALLY ACTIVE CARBON NANOTUBE HYBRIDS FOR RESERVOIR DEVELOPMENT APPLICATIONS

A DISSERTATION APPROVED FOR THE
SCHOOL OF CHEMICAL, BIOLOGICAL AND MATERIALS ENGINEERING

BY

_____
Dr. Daniel E. Resasco, Chair

_____
Dr. Jeffrey Harwell

_____
Dr. Ben Shiau

_____
Dr. Dimitrios Papavassiliou

_____
Dr. Steven Crossley

Dedication

To my mother and father with love

Acknowledgments

I am deeply thankful for my advisor Dr. Daniel Resasco for his continuous support and guidance through the last four years. Dr. Resasco is a main inspiration for me during my years of study here at OU. He has been like a family for me here and I am honored to work with him and receive my education under his supervision.

I would like to express my gratitude to my family for their support during this scientific journey, my mother and father who have been an inspiration for me.

I would like to thank all my committee members: Dr. Jeffrey Harwell, Dr. Ben Shiau, Dr. Dimitrios Papavassiliou and Dr. Steven Crossley.

I would like to acknowledge all faculty of the department of Chemical, Biological, and Materials Engineering at the University of Oklahoma who were all of great help during the years I spent here. I would like to thank Dr. Richard Mallinson for the best kinetics class, Dr. Lance Lobban, administrative staff and Mr. Alan Miles.

I would like to thank my current and former colleagues at OU who helped me in many ways. Dr. Jimmy Faria, Dr. Pilar Ruiz, Santiago Drexler, Dachuan Shi, Dr. Shaolong Wan, Anh The, Taiwo Omotoso, Wesley Tennyson, Miguel and Daniel Swatske. I would like to acknowledge two special and wonderful colleagues and friends: Tu Pham and Paula Zapata.

I would like to thank my very close friends Mr. Abdulqader Harith and Dr. Haider Hakiri for their help at some point during the last four years.

I would like to acknowledge Advanced Energy Consortium: Member companies include BP America Inc., BG Group, Petrobras, Schlumberger, Statoil, Shell, and Total for funding. Funding was also provided by the Department of Energy DoE EPSCOR (Grant DE-SC0004600). I would like to thank the Center of Interfacial Reaction Engineering (CIRE) and Applied Surfactant Lab (ASL) for valuable interactions.

I would like to acknowledge the institute of international education (IIE) for administering the Iraq Scholars and Leaders Program (ISLP). I would like to thank the wonderful program managers Laila Agily and Heather Theisen-Gandara.

I would like to thank ExxonMobil for funding my scholarship through the Iraqi Scholars and Leaders Program (ISLP) during my years of study in the US.

Table of Contents

List of Tables

List of Figures

Abstract

This work examines the different aspects of stabilizing and propagating interfacially active carbon nanohybrids for oil field applications. The progress achieved during the last four years was quite impressive towards the objective of utilizing nanoparticles for potential in situ applications.

In this work we examined the interactions between nanohybrids and a reservoir-like environment. This has been done by performing a series of adsorption isotherms, column studies, and Coreflood tests. An optimized system of nanohybrids dispersed using binary dispersing polymers (GA and HEC-10) showed almost negligible adsorption of the nanohybrids to crushed Berea sandstone in the order of ≈0.01 mg/g_{sand} in extreme conditions of salinity up to 20% and temperature up to $80^{o}C$. Propagation column studies were performed using crushed Berea sand to propagate nanohybrids dispersions successfully with C/C_o approaching 1 following 5-6 pore volumes of dispersion injection with a P-MWNT concentration as low as 100 ppm. This is because once available adsorption sites get saturated, the nanohybrids dispersion will propagate completely with no significant losses. Coreflood experiments have been performed both in labs at the University of Oklahoma and the Stim-Lab in Duncun, OK. Coreflood results using Stim-Lab standardized core testing verified the previous findings. Ability to propagate nanohybrids dispersion successfully through a 6” length Berea 400 core with C/C_o as high as 97% and particles overall recovery exceeding 84% was demonstrated. Noteworthy is the increased retention of nanoparticles in the

presence of oil phase inside the core because of the nanohybrids interfacial activity. Following successful propagation of nanohybrids through consolidated porous media, novel potential applications have been investigated including using nanohybrids as surfactant carriers and for logging while drilling NMR and EPR reservoir characterization tools.

Series of experiments to investigate the ability of nanohybrids to generate or stabilize foams were conducted. A boost in foam stability was achieved by incorporating nanoparticles during foam generation. Nanohybrids were found to increase foam stability significantly by using concentrations as low as 100ppm of nanohybrids.

As a proof of concept for utilizing nanohybrids in performing in situ reactions for EOR, a series of reaction column studies using catalytically functionalized carbon nanotubes were performed. Reactions have been conducted to investigate the possibility of increasing oil recovery by partial oxidation of tetralin, a molecule containing two carbon rings with an easily oxidizable alpha carbon to produce tetralone, which in turn has less interfacial tension with water than tetralin. Lowering the interfacial tension results in lowering capillary forces which in turn increases oil recovery. It was found that 6% of the residual oil is recovered by conducting partial oxidation reaction using air flow at 90^{o}C and 300 psi, which in turn suggests the viability of this technique for increasing oil recovery.

Chapter 1

Adsorption and Propagation of Interfacially Active Carbon Nanotube Hybrids and Novel Applications

1.1. Introduction

Interfacially active carbon nanotube hybrids exhibit promising properties for potential applications in reservoir technologies [1-5]. Nanoparticles could be used as modifiers of transport properties, as well as nanoscale vehicles for catalyst and contrast agents [6-15]. In-situ catalysis might be used to modify interfacial tension and wettability[1] of rock wall [16-18]. The main requirements for any of these applications are the ability to form stable dispersion and to effectively propagate through the reservoir porous medium under the temperature and salinity conditions that are typical in commercial operations. Suspensions of purified multi-walled carbon nanotubes (P-MWNT) in deionized water and high salinity brine have been prepared using two commercially available polymers, polyvinyl pyrrolidone (PVP) or Gum Arabic(GA) as a primary dispersant and hydroxyethyl cellulose as a secondary salt tolerant dispersant. Stable dispersions were put in contact with crushed Berea sandstone, quantifying the amount of nanotubes lost from suspension to estimate the

[1] Interfacial or surface tension(γ) is the energy per unit area and can be derived from Gibbs-Duhem at constant temperature and composition as $\gamma = \left(\frac{\partial G}{\partial A}\right)_{T,ni}$ [103], details are in Appendix A-1. Wettability can be defined as the tendency of a fluid to preferentially adhere or adsorb to a solid surface in a multi-fluid system [28]. More details are in Chapter 2

adsorption of these nanotubes from suspension onto the walls of the reservoir rocks. Adsorption isotherms were measured from room temperature up to 90^{o}C from aqueous suspensions with salinities up to 20%. These studies demonstrate that combining these two polymers stabilizes suspensions in high-salinity water and minimizes adsorption on the sand walls. It is proposed that this optimized behavior is due to additive electrostatic and steric repulsions. While the polar PVP helps disaggregation by effectively wrapping individual nanotubes (primary dispersant), the bulky HEC inhibits the re-aggregation in saline solutions (secondary dispersant).

Column experiments were conducted to study the propagation of these suspensions through porous media [1]. It was found that a small amount of nanohybrids adsorbed to the sand will be able to saturate available adsorption sites resulting in subsequent injections of nanohybrids to be propagated completely through the column without adsorption. In that sense, ability to reach 100% of the injected concentration with a low particle concentration of 100 ppm and total particle adsorption to the sand of less than 10% at room temperature was shown. With that in mind, successful propagation through porous media allowing for future utilization of these nanohybrids in reservoir applications has been achieved.

1.2. Dispersion Stability of Carbon Nanohybrids

In order to propagate nanohybrids through the pores of reservoir, a stable dispersion must be obtained. Propagating a dispersion of nanotubes in water was found to be an extremely challenging process. Dispersing the nanotubes was done

usually by sonication followed by centrifugation to remove large non dispersed aggregates and filtration [1]. Due to the strong $\pi - \pi$ columbic interaction between hydrophobic tubes, carbon nanotubes tend to flocculate and settle down after few minutes following sonication [19]. This made utilizing them in industrial applications less effective [20, 21]. Using non-ionic polymers such as Polyvinyl Pyrrolidone (PVP) or Gum Arabic (GA) in dispersing SWNT in DI water was found to be successful in producing stable dispersion that can remain stable for months. This is done by disrupting the hydrophobic interface of the tubes with water and the tube-tube interaction in aggregates [22]. For such process, the net energy gain from losing the hydrophobic surface achieved by shielding the nanotube from the water is larger than the energy penalty for forcing a linear polymer into wrapping around a nanotube [23]. Smalley et.al (2001) described in details the forces that result in de-bundling of tubes aggregate. Figure 1- 1 below show possible wrapping arrangement of PVP around a single walled carbon nanotube as suggested by Smalley et al.(2001) .

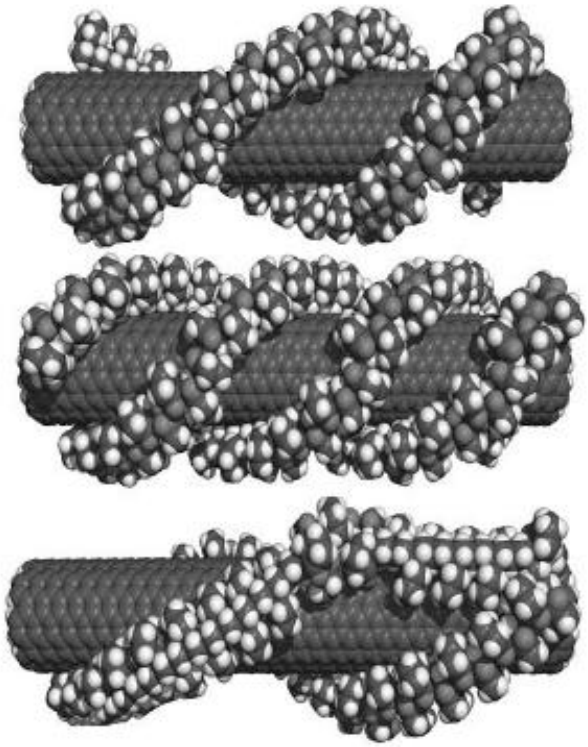

Figure 1- 1: Possible wrapping arrangements of PVP around SWNT as suggested by Smalley et al. (2001).

Figure 1- 2a shows a drawing (not to scale) of one possible conformation of PVP40 wrapped around a nanotube. This was created using Marvin space free software from ChemAxon[2]. In this case, it is hypothesized that PVP40 is wrapping helically around single walled nanotubes. By performing a simple calculation, an estimate can be made of how many rotations a single polymer strand could wrap around P-MWNT of a diameter ranging between 10 and 20nm and an angle ranging between 10 and 60 degrees. An angle of zero was considered as a complete one ring,

[2] ChemAxon is a leader in providing chemical software development platforms and desktop applications for the biotechnology and pharmaceutical industries. www.chemaxon.com

perpendicular to the nanotube. Figure 1- 2b shows the results of this calculation. It is demonstrated that a single strand of PVP40 wraps on average between 1 and 3 times around P-MWNT. This result is in agreement with the assumption stated by Smalley et al. 2001: PVP is physically wrapping around nanotubes in order to stabilize the dispersion; an effect that is possibly initiated by sonication energy following de-bundling of individual tubes. In addition, this result agrees with our research group efforts which concluded that using a PVP molecular weight of 40,000 is an optimum molecular weight for dispersion stability [3]. Calculations resulted in Figure 1- 2b is not taking into account carboxylic groups and/or repulsion on the surface of the tube.

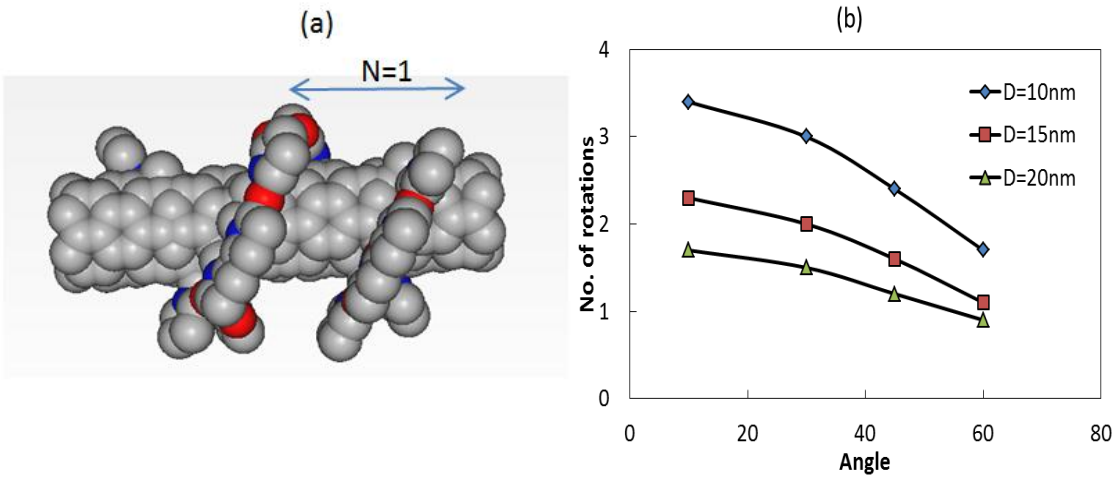

Figure 1- 2: (a) Visualization of PVP40 wrapping around nanotube(gray=carbon, red=oxygen, blue =nitrogen) (b) number of rotations of PVP40 around P-MWNT based on angle and P-MWNT diameter.

In order to have substantial dispersion stability, the electrostatic repulsive forces and Vander Waals attractive forces must be properly balanced. This is also

known as the DLVO theory for colloid stabilization in reference to Derjaguin, Landau, Verwey and Overbeek [24] . As mentioned before, salinity has catastrophic effect on nanoparticles stabilized by PVP or GA alone. This can be explained by the significant shrinkage in the double layer thickness as ionic strength increase as shown below.

$$(1/k) \sim \left(Z_i^2 C_i\right)^{-1/2} \qquad \textbf{Eq. 1- 1}$$

where (1/k) is the double layer thickness (Debye length) , Z_i is the valence of the ion i and C_i is the concentration of ion i [24]. Bohn and McNeal (1983) reported approximate thicknesses of the double layer surrounding colloidal particles. These values are shown in table below. It clearly shows the significant shrinkage in double layer thickness by the inclusion of ions which in turn suppresses the repulsion forces resulting into more collisions and destabilization of dispersion.

Table 1- 1: Approximation of the of double layer surrounding a colloidal particle [25].

Counter ion concentration, mol/L	Double Layer thickness, nm	
	Monovalent	Divalent ions
10^{-5}	100	50
10^{-3}	10	5
10^{-1}	1	0.5

1.3. Propagation Column Studies

Propagating carbon nanotubes through reservoir rock has been studied before. Sending stable dispersions of SWNT/silica dispersed using Polyacrylamide PAA in DI

water through porous media was successful. MWNT/alumina and P-MWNT were dispersed and propagated using PVP as a dispersing agent in DI water. When brine is present, double polymer wrapping of PVP and salt resistant polymers were required in order to disperse and propagate the nanohybrids through porous media [3]. It is hypothesized that carbon nanotubes adsorb to the surface of sand by either single tube adsorption to the surface, or as a large aggregate of poorly dispersed nanotubes. Since the stability of the dispersion is mainly affected by salinity and temperature as has been explained before, the adsorption phenomenon is expected to go high and it is in agreement with experiments as will be demonstrated later. Figure 1- 3 shows a schematic presentation of adsorption hypothesis.

To clarify the mechanism of adsorption, an understanding of the surface charge is necessary. A surface can acquire charges in a number of ways including a) the preferential adsorption of an ion from a solution on an initially uncharged surface such as the adsorption of H^+ and OH^- on insoluble oxides b) dissociation of surface group e.g. ($-COOH \rightarrow COO^- + H^+$) which leaves the surface with a negative charge [24]. Berea sandstone for example has its point of zero charge (PZC) at a pH of 2-5 and therefore anions tend not to adsorb at a pH higher than that [26][3].

[3] Azam et al.(2013) reported a PZC of 8 for Berea with 27% alumina by weight [102]. Some reported PZC for alumina ranging 7-9 and more than 9 for some synthetic aluminas [100]

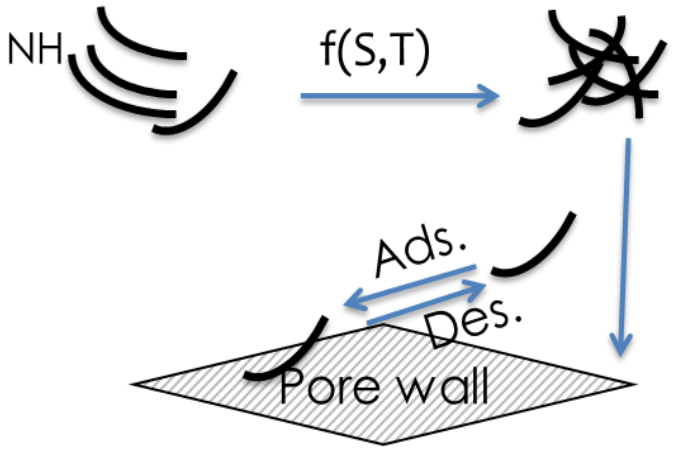

Figure 1- 3: Adsorption phenomena hypothesis.

A proof that nanoparticles are individually wrapped by polymer has been demonstrated in SEM images of a stable P-MWNT dispersion that was sprayed into SEM grid as shown in Figure 1- 4a . The deposited dispersion was diluted 100 times to avoid forming large crystals of salt and high number of nanotubes on top of each other. By focusing the electron beam on the tube we can see that the polymer has completely burned off leaving the tube intact which demonstrates the concept of wrapping polymer around nanotubes [27].

(a) PMWCNT's w/ 200ppm GA, 1600ppm HEC, API

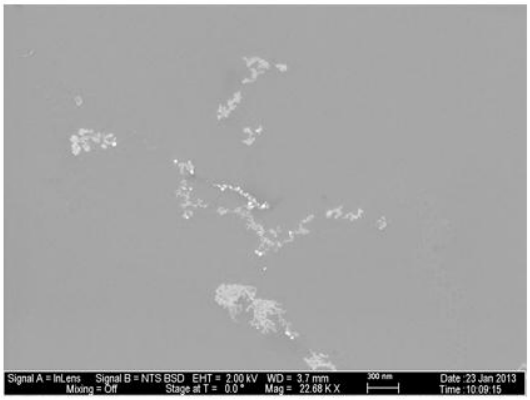

(b) PMWCNT's w/ 200ppm GA, 1600ppm HEC, API

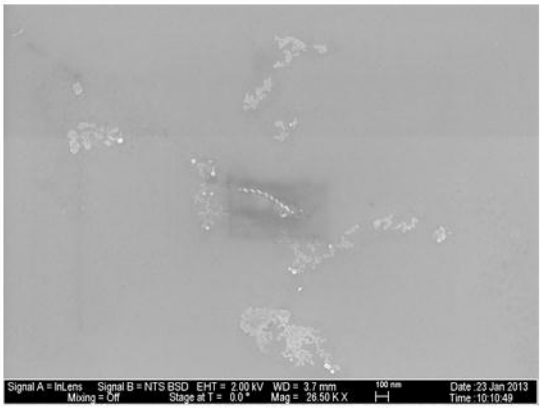

(c)PMWCNT's w/ 200ppm GA, 1600ppm HEC, API Brine

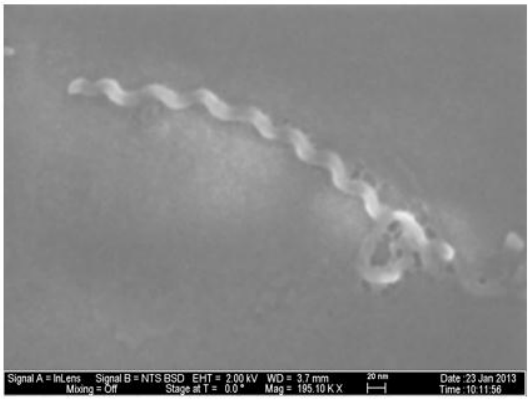

Figure 1- 4: SEM image of P-MWNT (a) initial SEM image,(b) after focusing the beam for few minutes showing the polymer degradation, (c) zoomed in nanotube showing the tube is intact without polymer[27].

1.4. Retention Mechanisms

Throughout the scope of this work, understandings of three retention mechanisms have been developed. The three retention mechanisms are: sedimentation, filtration, and adsorption. Sedimentation takes place because of aggregation of particles into large aggregates that settle down due to the effect of salinity or temperature. This was avoided by the use of system of two polymers as explained earlier. Filtration take place at the pore-throats of sandstone and this is due to the presence of large non-well dispersed aggregates. This is avoided by the pre-filtration of dispersed particles with a micron sized filter to avoid the size exclusion effect of the nanotubes taking place at rock pore throats. Finally adsorption rates can be significantly decreased by the pretreatment or pre-flush of sandstone with polymers which fill up the available adsorption sites reducing or eliminating adsorption of subsequent injections of nanoparticles.

The adsorption of purified multi walled carbon nanotubes on Berea sand has been investigated and quantified. Adsorption isotherms of P-MWNT on crushed Berea sand have been obtained over a wide range of salinity and temperature. Dispersions have been propagated successfully through sand column with minimal adsorption. Understanding the adsorption phenomenon is a very helpful approach to find the optimum way to disperse and propagate nanohybrids through reservoir rock. Table 1-2 summarizes retention mechanisms concept.

Table 1- 2: Retention mechanisms of P-MWNT

	Retention Mechanism		
	Sedimentation	Filtration	Adsorption
Parameters of influence	• Salinity • pH • Temperature	• Aggregation • Nanohybrid size • Pore structure	• Irreversible adsorption • Surface chemistry
Possible Solution	Designed polymers	Pre-filtration	Pre-coating with polymers

1.5. Adsorption Isotherms Experimental

Purified Multi Walled NanoTubes (P-MWNT) were provided by SouthWest Nanotechnologies Inc. (SWeNT), Norman OK. Water was purified and deionized using three ion exchange units from Cole Parmer. Polyvinyl pyrrolidone polymer of molecular weight of 40,000, 55,000, 360,000, and 1,000,000 Daltons were provided by Sigma Aldrich, hydroxyethyl cellulose HEC-10, HEC-25, and another proprietary HEC polymer were provided by DOW Chemicals. Gum Arabic was provided by Acros. The chemical structures of PVP and HEC-10 are shown in Figure 1- 5: (a) PVP and (b) HEC chemical structure.. Berea cores were crushed with a ceramic mortar and sieved through a set of standard sieves (Sieves designations: #60/ 250 µm, #200/ 75 µm) and used only in the range between 75 µm to 250 µm. Such particle size have a surface area of around 1.5m^2/g as reported elsewhere [28-30]. Sodium chloride and calcium chloride were provided by Sigma Aldrich. Standard polymers hydroxyethyl cellulose of molecular weight of 510KD was provided by American Polymer Standards Corporation for gel permeation chromatography (GPC) measurements.

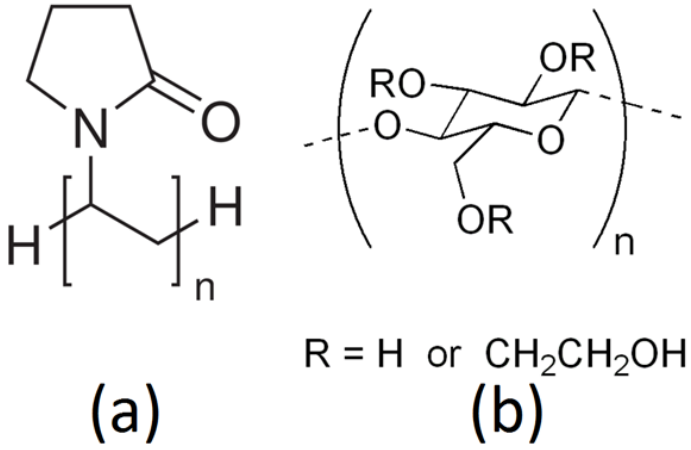

Figure 1- 5: (a) PVP and (b) HEC chemical structure.

Purified multi walled carbon nanotubes were first dispersed in brine or DI water with PVP40 or GA by sonication using 600 W, 20 KHz horn-sonication. HEC-10 stock solution was previously prepared according to guidelines stated elsewhere [31] and added to the dispersed solution of P-MWNT to set the ratio of HEC-10 to PVP40 of 3:1. The solution is sonicated again usually for thirty minutes and centrifuged for one hour at 2000 rpm to settle any large non-dispersed aggregates of P-MWNT. The adsorption experiments were done by adding 10 ml of dispersed P-MWNT solution of known concentration into vials containing 2 g of Berea sandstone of a 75-250 um mesh size. A stirring bar was added and the vials were sealed and placed on a stirrer for 24 hours. The concentration of all solutions was measured using UV-Vis by comparison with calibrations of known sample concentrations [32, 33][4]. The change in

[4] The confidence of UV-Vis measurements has been investigated by measuring the absorbance changes of a stable dispersion of 23ppm P-MWNT stabilized in DI water using PVP40 and HEC-10. 14 different

concentration of P-MWNT reflects the amount adsorbed to the sand for each measurement. The experiments were done covering a range of concentrations and polymer combinations. The salinity used varied up to 20% by weight salt content, keeping a constant ratio of sodium chloride to calcium chloride of 4:1 through all experiments in which brine was used unless otherwise mentioned.

1.5.1. Effect of Polymer Addition Method on Dispersion Stability and Adsorption Rates

In order to produce stable dispersions and successful propagation of carbon nanotubes in brine, a salt resistant polymer was used. A proprietary salt resistant polymer supplied by DOW and another two commercially available polymer (HEC-10 and HEC-25) were tested for dispersion stability and propagation. The technique of mixing polymers was found to be crucial for dispersion stability. It was hypothesized that low molecular weight, highly polarizable PVP polymer is necessary to disperse and disaggregate carbon nanotubes into individual tubes or small aggregates [23]. The salt resistant polymer was then used to prevent re-aggregation and keep the nanotubes well-dispersed in the solution. These concepts have been demonstrated and proven in column propagation studies done by our research team [1]. To explore these concepts further, stable dispersions of P-MWNT were produced in DI water using PVP40 and proprietary DOW by sequential and non-sequential addition of polymers. What is meant by sequential addition is to disperse P-MWNT using PVP40 first by sonication

---

measurements of the same sample have been made over 5 days period resulted in 0.05ppm standard deviation in measurement.

and then add the DOW polymer and repeat sonication. While in non-sequential addition, P-MWNT was dispersed in a solution containing the two polymers. These two cases were compared with a case where PVP40 was used alone. It was found that using sequential addition will result in the least adsorbed amount. The adsorbed amounts were measured using the following equation

$$\boldsymbol{Amount\ adsorbed}\left(\frac{\boldsymbol{mg_{P-MWNT}}}{\boldsymbol{g_{sand}}}\right) = \boldsymbol{Vol.of\ dispersion}\frac{\boldsymbol{(Initial\ conc.-Final\ conc.)}}{\boldsymbol{mass\ of\ sand}} \qquad \text{Eq. 1- 2}$$

Multiple concentrations have been tested in DI water as shown in Figure 1- 6: . In this figure and all adsorption studies reported figures, the x-axis represents the equilibrium concentration of P-MWNT while the y-axis represents the amount adsorbed calculated using Eqn. 1-2. From this figure it is evident that the best polymer system is to disperse the P-MWNT in water and then add the DOW polymer to make the ratio between proprietary DOW and PVP40 to 3:1. Figure 1- 6 shows clearly the beneficial effect of using sequential addition of the two polymers in creating stable dispersion and reducing adsorption.

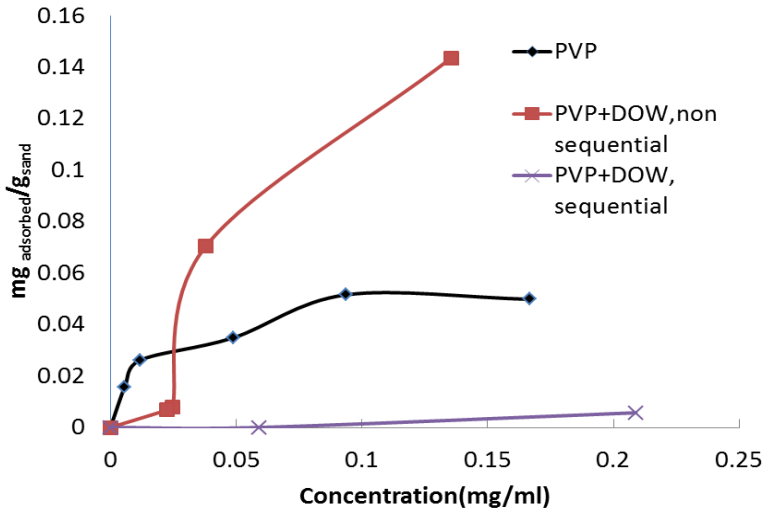

Figure 1- 6: Adsorbed amount using different polymer systems in DI water.

1.5.1.1. Adsorption of P-MWNT Using PVP40 and Proprietary DOW Polymer at Variable Salinity

Adsorption studies of P-MWNT using the combination of PVP40 and proprietary DOW added sequentially were conducted repeatedly for a number of salinities. The salinities tested were 1, 5 and 10% as shown in Figure 1- 7. It was concluded that the amount adsorbed increases with salinity due to the fact that less stable dispersions are present at higher salinity. While the adsorbed amount is in general higher than the case where there was no salt present, the total amount adsorbed for 10% brine is still an order of magnitude lower than what is reported for similar cases of surfactant adsorption on crushed sand as will be demonstrated later.

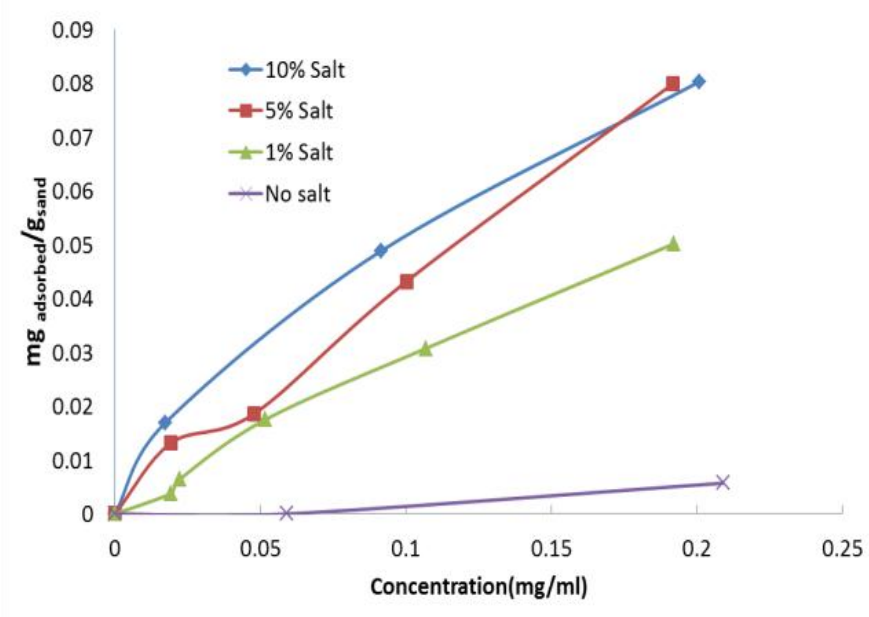

Figure 1- 7: Adsorption rates of P-MWNT dispersed using proprietary DOW and PVP40 combination.

1.5.1.2. Adsorption of P-MWNT Using PVP40 and HEC-10 Polymers at Variable Salinity and Temperature

Salt resistant polymer HEC-10 was also tested, since it is commercially available, for the adsorption and propagation studies. Preliminary results showed the effectiveness of using HEC-10 in both stabilizing dispersion and enhancing propagation. HEC-10 was added to P-MWNT dispersion in the same manner that proprietary DOW was added following the first sonication. The focus was further extended to include the effects of both temperature and salinity on adsorption. Stable dispersions of P-MWNT were produced in DI water using PVP40 and hydroxyethyl cellulose (HEC-10) by sequential and simultaneous addition. In the sequential addition

mode, a suspension containing P-MWNT and PVP40 was sonicated, then added to the hydroxyethyl cellulose (HEC-10), and sonicated for a second time. In the simultaneous addition, P-MWNT was dispersed in a solution containing the two polymers. These two cases were compared with a case where PVP40 was used alone. It was found that the sequential addition resulted in the least adsorbed amount and most stable dispersion even at high salinity.

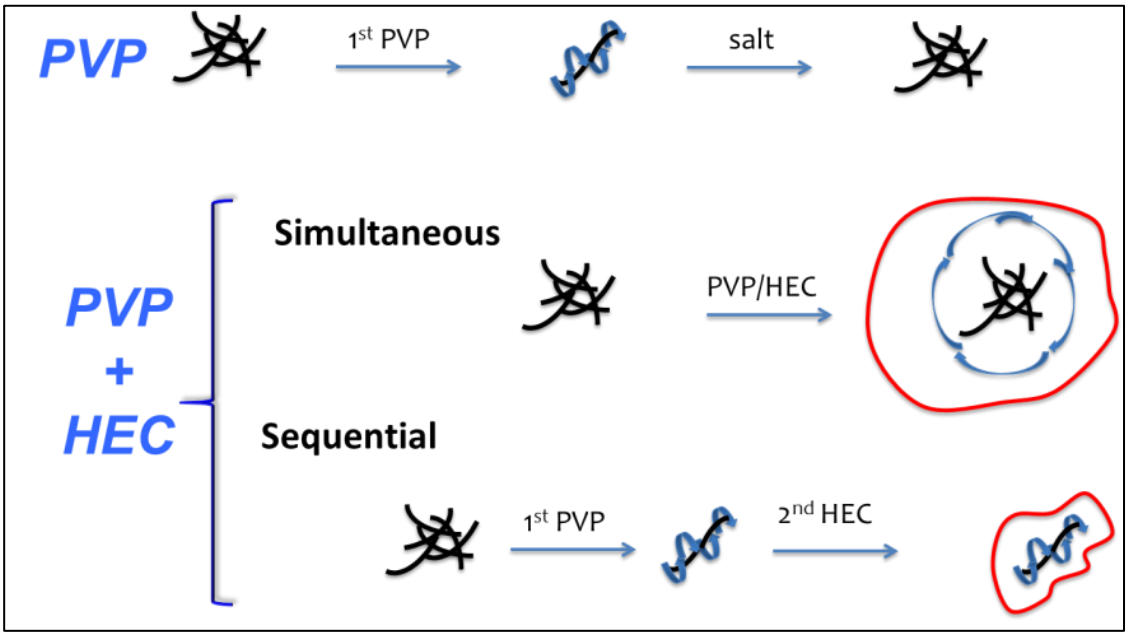

Figure 1- 8: Hypothesized double polymer wrapping for nanotubes [black:nanotubes, blue:PVP, red:HEC].

Figure 1- 8 demonstrates the hypothesis behind simultaneous and sequential polymer addition methods of dispersing P-MWNT. Dispersing P-MWNT in PVP40 solution alone will result in a stable dispersion. Dispersions with PVP40 and P-MWNT alone are salt intolerant and tubes will aggregate once there is strong ionic interaction

present in the solution. However, inclusion of a secondary dispersant, after initially suspending P-MWNT with PVP40 is suggested to keep the tubes well separated by steric repulsion. In this case the dispersion has high salinity tolerance and is very stable at room temperature. The third case, the simultaneous addition of polymer, is expected to encapsulate large aggregates of P-MWNT by both polymers. The P-MWNT aggregates will not be individually separated which will result in a less stable dispersion with larger aggregates that are expected to block pore throats in the rock matrix. Therefore, through all our experiments we have adopted the sequential method of polymer addition to disperse P-MWNT, unless otherwise stated.

Experiments have been done to compare all three methods of dispersion explained earlier in DI water. Figure 1- 9 shows the comparison between the three cases of dispersion explained earlier: sequential addition of polymers, simultaneous addition and dispersing in PVP40 alone. In this figure the x-axis is the equilibrium concentration (final concentration) which is the concentration of P-MWNT in equilibrium with Berea sand after one day of contact. The amount adsorbed to the sand is calculated from the difference in P-MWNT concentration from the initial and final dispersion.

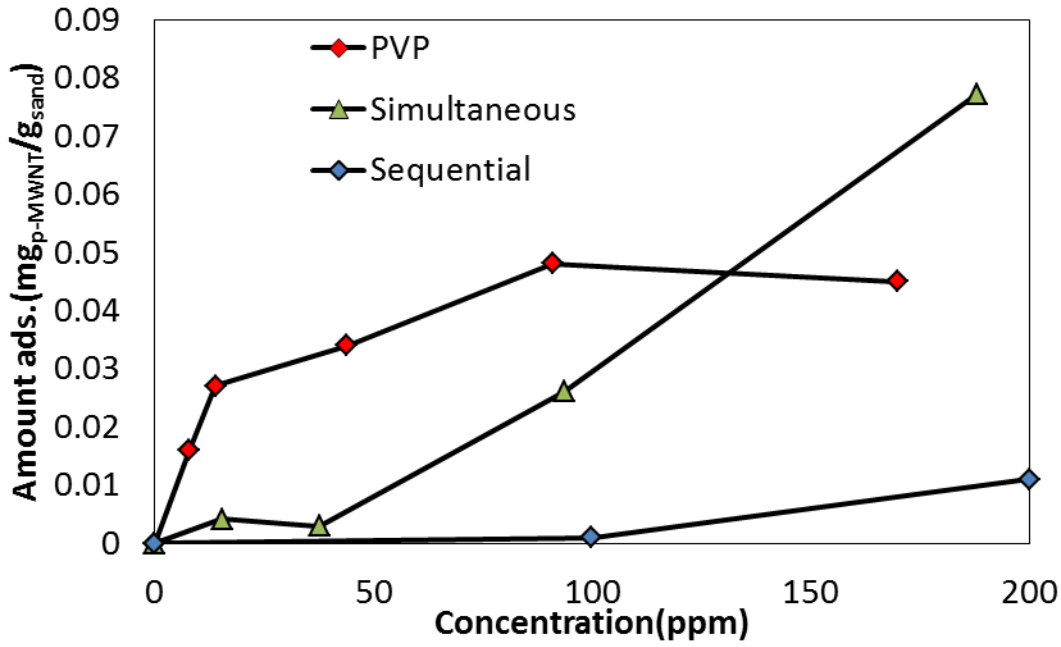

Figure 1- 9: Adsorbed amount using different polymer systems in DI water.

The solutions used in the adsorption isotherm shown in Figure 1- 9 were prepared in three different ways. The adsorption isotherm for the sequential method was prepared by dispersing P-MWNT in solution containing PVP40 by sonication for 2hrs. Then HEC-10 solution was added such that the ratio of HEC-10 to PVP40 was 3:1, and the total polymer concentration was 1000ppm. The solution was further sonicated for 30 minutes after the addition of HEC-10. The second set, the simultaneous method, was prepared by dispersing P-MWNT in a solution containing 1000ppm of both PVP40 and HEC-10 polymer with the same polymer ratio as in the sequential case. This solution was sonicated for two hours and it is expected to have large aggregates of P-MWNT encapsulated by polymer. The third set was dispersed in a solution that has 1000ppm of PVP40 alone. A number of P-MWNT concentrations have been tested ranging between

20 to 200ppm for all experiments. All solutions before mixing them with the sand were centrifuged at 2000rpm for one hour to settle non-dispersed P-MWNT. The adsorption experiments have been done according to the procedure mentioned earlier.

Figure 1- 9 shows clearly the beneficial effect of using sequential addition of the two polymers in creating stable dispersion and reducing adsorption. PVP has been proven as effective dispersant for carbon nanotubes in aqueous solution as it can disrupt the hydrophobic interface with water and the tube-tube interaction in aggregates (Smalley et al. 2001). The secondary dispersant, HEC-10, is hypothesized to create steric repulsion against agglomeration and nanotube-rock interaction. It is expected that by using the two polymers together (simultaneous addition), we were encapsulating large poorly dispersed nanohybrids by the secondary polymer. The resulting dispersion was expected to have relatively large particles, in comparison to the dispersion produced by the sequential method. By dispersing P-MWNT first using the low molecular weight polymer PVP40, the tubes are being individually separated. Therefore, when HEC-10 is added later, the polymer can easily wrap around individual tubes, rather than large agglomerates. By using PVP40 alone a stable dispersion was obtained and moderate adsorption of P-MWNT onto the sand was observed. The amount of adsorption of the PVP40 only system was considerably greater than the amount observed with binary dispersant dispersion prepared by the sequential method. This could be also due to the fact that the pyrene ring of PVP interact with the sand. The resonance structure of PVP is shown in Figure 1- 10. The negative charge of

the carbonyl group in PVP interacts with the silanol group on surface through acid base hydrogen bonding as shown in Figure 1- 11.

.

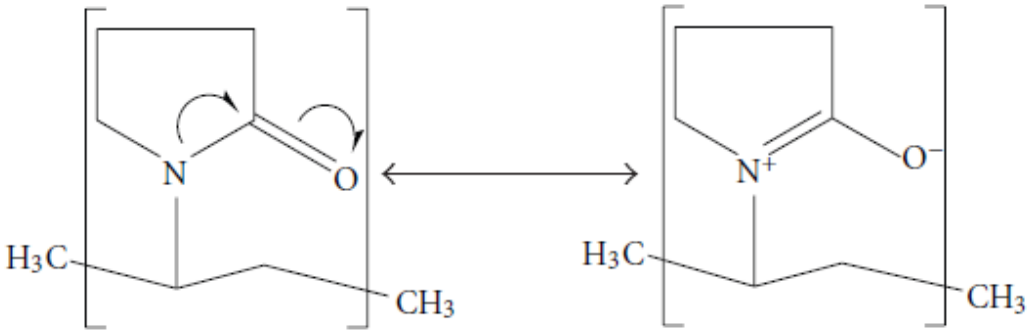

Figure 1- 10: The resonance structure of PVP [34].

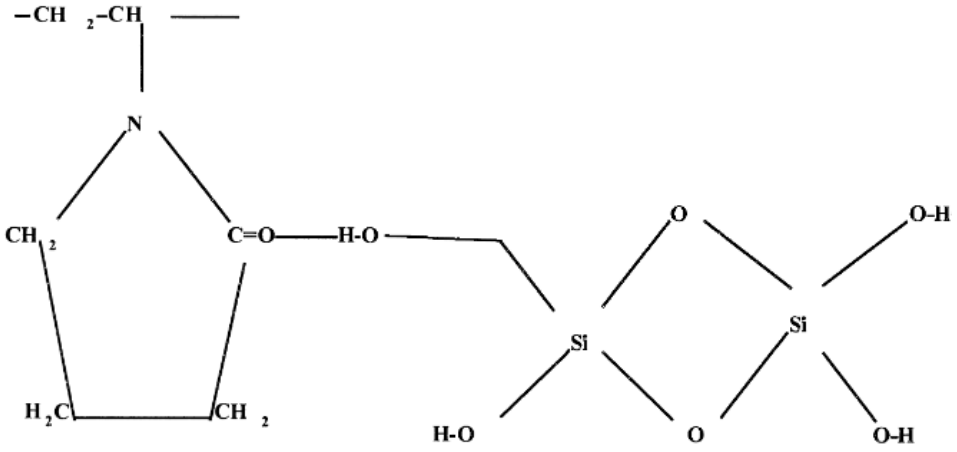

Figure 1- 11: Interaction between silica and PVP [35].

1.5.1.3. Adsorption of P-MWNT Using PVP40 and HEC-10 Polymers at Variable Temperature and Salinity

In order to understand the effect of temperature on adsorption, experiments were done at elevated temperatures. For the following adsorption experiments, the dispersion is prepared using the sequential method as previously described with a fixed total polymer concentration of 1000ppm and a constant ratio between HEC-10 and PVP40 of 3:1. Figure 1- 12 shows the adsorption amount for a number of temperatures. This is done by placing the vials in oil path on top of a heating plate and using a temperature controller to keep the temperature constant throughout the adsorption experiment. Upon examination of Figure 1- 12, it can be observed that the adsorption increased with increasing temperature. This behavior could be explained by the reduction in thermal stability of polymers at high temperatures which affects the dispersion stability at higher temperature or possibly the polymers is reaching the phase separation temperature [36].

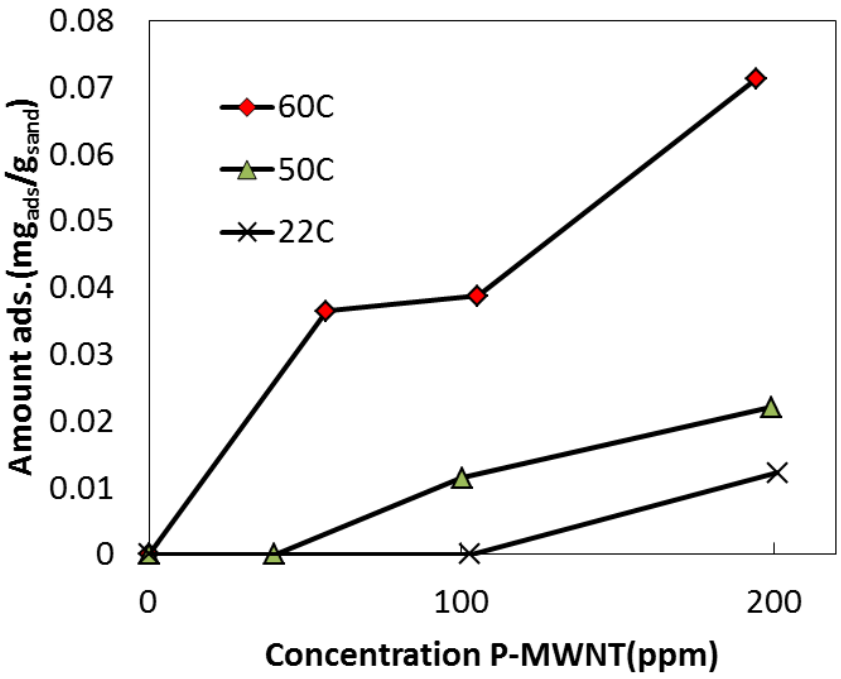

Figure 1- 12: Adsorption isotherms of P-MWNT dispersed using HEC-10 and PVP40 in DI water.

Figure 1- 13a and b demonstrate the effect of temperature on adsorption for 3% and 10% salinity solutions respectively. In this case the saline solution was prepared prior to the experiment by using constant ratio of sodium chloride to calcium chloride of 4:1. Comparing the adsorption at 22^{o}C for the cases of 3% and 10% salinity with the case of DI water we observe the increase in adsorption due to the effect of salinity. The effect of salinity on adsorption can be explained by the fact that the electric double layer decrease significantly as ionic strength increases [24]. Since the Debye length of the P-MWNT decreases with increasing salinity, tubes can approach each other more closely than in DI water. In this case, the Van der Waals attraction

forces between the particles have more influence, resulting in faster particle agglomeration and higher adsorption. In both Figure 1- 13a and Figure 1- 13b we also observe the trend of increased adsorption with temperature which is similar to what we observed in Figure 10 with DI water case.

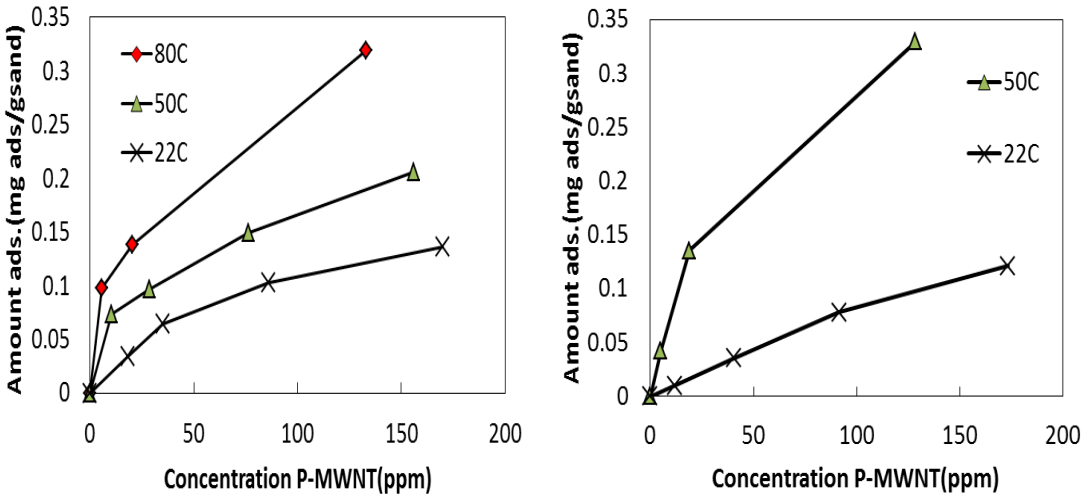

(a) (b)

Figure 1- 13: Adsorption of P-MWNT in (a) 3% brine solution (b) 10% brine solution.

Figure 1- 14 shows a comparison of the adsorption of a typical surfactant (Neodol 25-3S) to crushed Berea sandstone as reported by Peru and Lorenz 1990 and the adsorption of P-MWNT at the equivalent testing conditions. This figure shows the low adsorption values observed for P-MWNT in comparison to Neodol 25-3S. Hirasaki et al.(2013) reported 1.3-1.5 mg/g for a number of surfactants experiments in an effort to use sacrificial agents to reduce anionic surfactant adsorption [37]. The comparison

shown in Figure 1- 14 is to demonstrate the low adsorption of nanohybrids and is by no mean to be generalized for all surfactants.

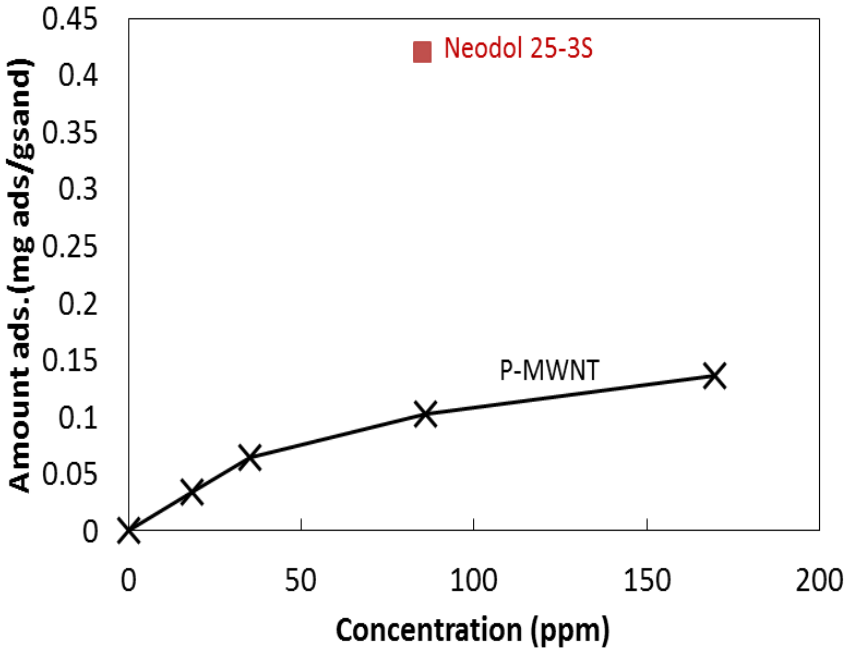

Figure 1- 14: Adsorption comparison of P-MWNT versus Neodol 25-3S at 3% salinity.

1.5.1.4. Effect of Pretreatment with Polymers on Adsorption

It was suggested that adsorption to the crushed Berea can be reduced by occupying the available adsorption sites with polymers. Therefore, a step was added to the experiment to confirm this theory by pre-treating the sand with a polymer solution. Once some of the available adsorption sites in Berea sand have been covered with polymer, the nanohybrids dispersion will adsorb less to the Berea sand. The adsorption experiments in this part were done by adding 5 ml of polymer/ brine solution without nanoparticles present in the solution and stirring for one hour at

room temperature. Then 5 ml of P-MWNT dispersion was added to pre-treat the sand, and the mixture was stirred for 24hrs. Finally, the absorbed amount was quantified using UV-Vis. The brine concentration was kept constant in all batches, including the pretreatment polymer solution at 10% by weight. It was found that the adsorption amount was much lower when the sand was pretreated with polymer solution first. The particle adsorption decreased by more than 50% using pretreatment. This indicates that available adsorption sites were partially saturated by polymer adsorption to the sand. Figure 1- 15 shows adsorption at 22 ^{o}C for the different systems of polymers studied to identify which polymer system prevents particle adsorption the best. Three pre-treatment polymers were studied: 1000ppm of PVP40, 1000ppm of HEC-10 and 1000ppm combined polymer concentration with HEC-10 and PVP40 (at a ratio of 3:1, respectively). All pretreatment experiments resulted in reduced adsorption to the sand, however it was observed that the mixture of both polymers prevents particle adsorption the most. The particle adsorption at higher temperature was also tested, and it was confirmed that pretreatment still reduces adsorption at higher temperature. In light of known interactions of pyrene ring in PVP with silanol groups on the surface and adsorption of HEC on silica [35, 38], it is understood that both polymers will adsorb to the surface however the hydrodynamic differences in propagation experiments might give slightly different results.

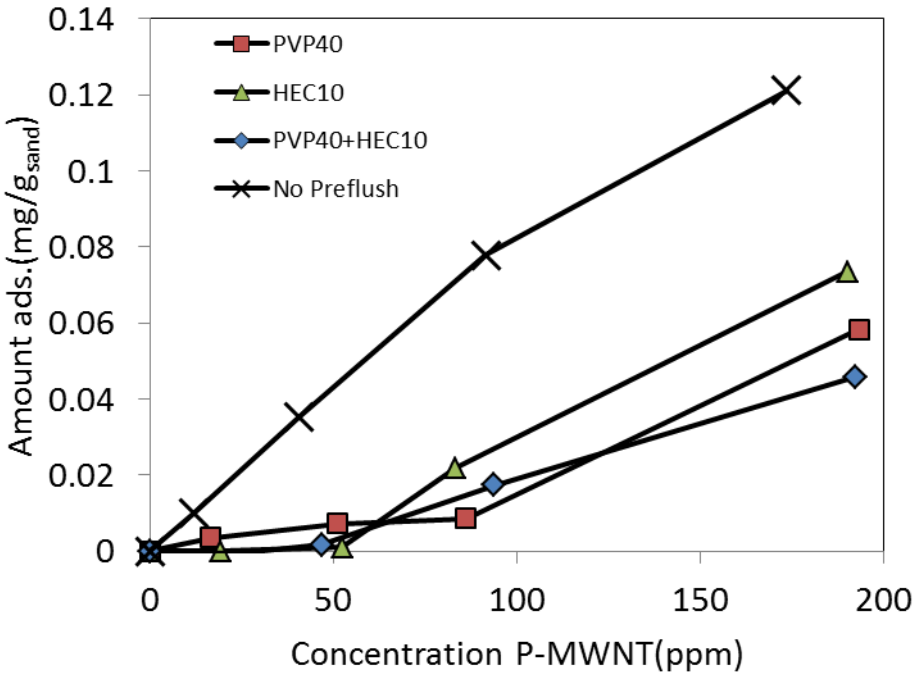

Figure 1- 15: Effect of pretreatment with polymers on adsorption.

Figure 1-16 show clearly this effect for 22 ^{o}C and 50 ^{o}C. At the point, comparing the value of surfactant adsorption reported into that of P-MWNT adsorption. Neodol 25-3S adsorption was about 0.42mg/g and with pretreatment of sand we were able to reduce adsorption of P-MWNT down to about 0.02mg/g at similar conditions. That is about 20 times lower adsorption for the case of P-MWNT which suggests that we have a very efficient dispersion for propagation through porous media as will be demonstrated in the column studies part of this work.

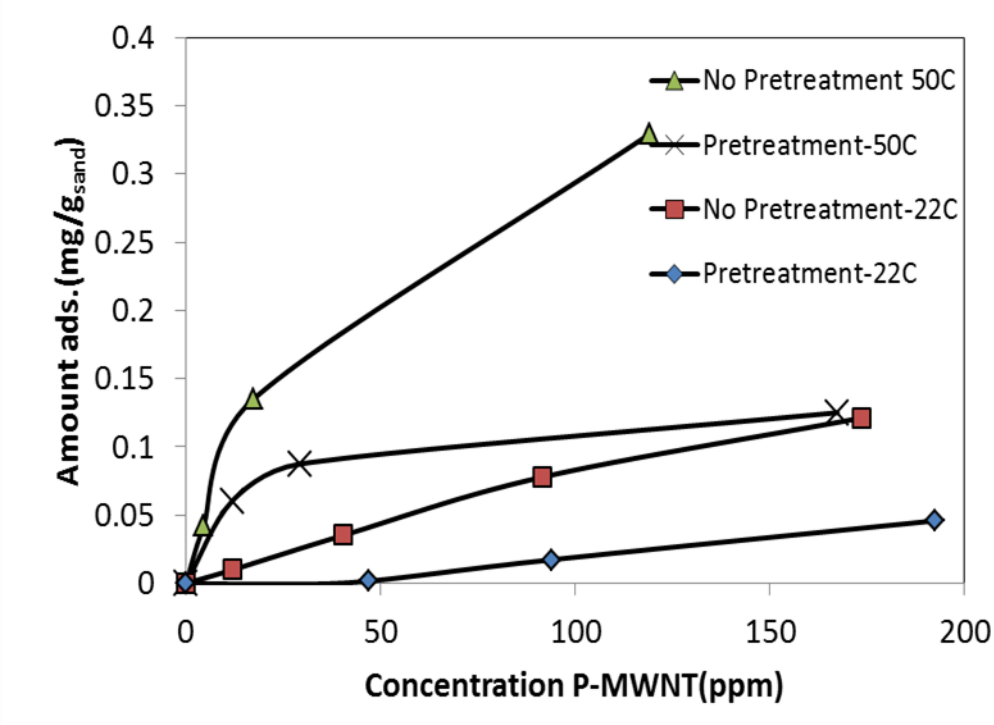

Figure 1- 16: Effect of pretreatment with polymers on adsorption at 22 and 50°C.

1.5.2 Comparison Between Adsorption Isotherms and Column Studies

Column studies were done using glass column purchased from Kimble/Kontes Co. The column was connected to peristaltic pump as shown in Figure 1- 17. The porosity and permeability of the crushed Berea were 35% and 4.1D respectively. Experiments were run using a number of dispersions and pretreatment (pre-flush) procedures to compare adsorption isotherms with column propagation studies. A no pretreatment experiment should reflect the highest adsorption in both batch adsorption test and propagation column studies. Table 1- 3 shows the adsorption values and cumulative recoveries for four different cases: no pretreatment (pre-flush), pretreatment with PVP40, HEC-10, and PVP40 and HEC-10 together.

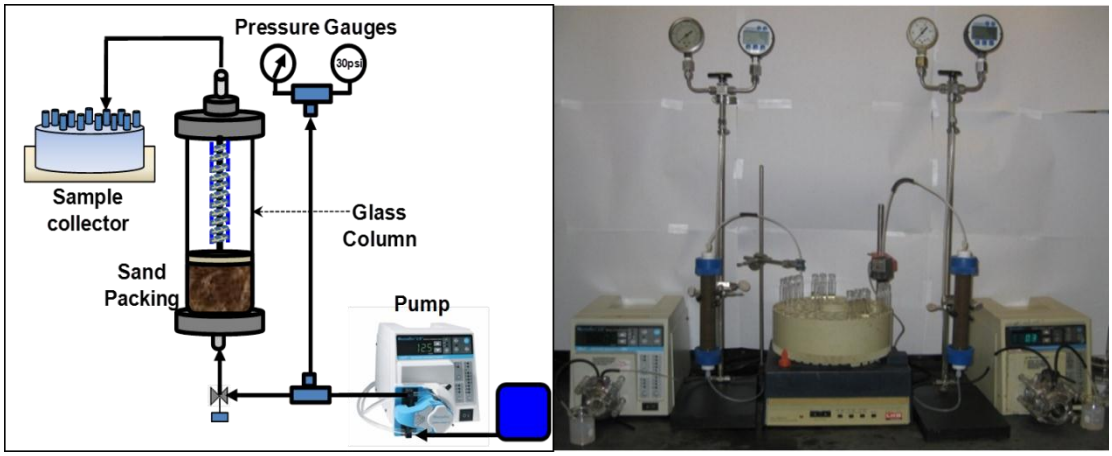

Figure 1- 17: Packed column setup for analysis of propagation through porous media.

Table 1- 3: Quantitative comparison between adsorption isotherms and column studies.

Pretreatment	Adsorption, mg/g_{sand}	Column Recovery, %
No pretreatment	0.08	61
PVP40	0.01	84
HEC10	0.02	95
PVP40+HEC10	0.015	96

Good agreement between adsorption isotherms and column propagation studies is demonstrated in Table 1- 3. The reduction in adsorption observed by pretreating sand with polymers corresponds to increased recovery in polymer pre-flushed columns.

1.5.3. Main Conclusions for PVP40/HEC-10 System

Adsorption of carbon nanotubes on crushed Berea sandstone is affected mainly by salinity, temperature, method of polymer addition and size of nanohybrids (or nanohybrids aggregates). Higher temperatures resulted in greater adsorption because most polymers suffer from thermal degradation at high temperature and/or the solubility of nonionic polymers decreases in water at higher temperatures, approaching a phase separation point. The pretreatment of sand with polymers greatly reduced adsorption because this pretreatment reduces the number of sites readily available for adsorption. Systems that resulted in the least adsorption were in agreement with column studies performed by our group: systems demonstrating reduced adsorption corresponded to systems showing better propagation in sand pack studies.

The binary polymer system used in order to generate the proper characteristics of the P-MWNT dispersions for transport in porous media under high ionic conditions, i.e. maximum reduction of particle losses due to adsorption or straining (filtration). This binary system consists of PVP40 (to generate stable dispersions of P-MWNT) and HEC-10 (to reduce the adsorption onto sandstone of these polymer coated nanoparticles).

Pre-flushing the column with a polymer solution seems to have a desirable effect on the final transport of the particles through the porous media, which is hypothesized to occur by occupying sites available for nanotubes adsorption, improving overall transport of these particles in porous media.

Although thorough sonication and centrifugation is used in the preparation of the nanohybrids dispersion, there are still particle agglomerates at the end of this process that are large enough to be filtrated out during transport through the sand pack, making it important to additionally filtering the dispersion before it is being injected into the porous media.

1.6. Adsorption of P-MWNT Using Gum Arabic as a Primary Dispersant

Gum Arabic(GA) which is a water soluble polysaccharide produced by Acacia Senegal trees [39, 40] has been used as a primary dispersing polymer instead of PVP40. 80% of GA consists mainly of highly branched polysaccharide and 20% of polysaccharide-protein complex. Figure 1- 18 shows GA structure which consists of arbinogalactan polysaccharide (AG) and arabinogalactan-protein complex(AGP) [41]. The selection was based on the work reported elsewhere on GA ability to disperse SWNT [20] and MWNT [42]. It is also for the expected PVP phase separation due to the interaction between PVP and metal cations present in the reservoir fluids [43, 44].

In an earlier part of this work we have demonstrated how using two non-ionic polymers, one with low molecular weight and highly polarizable (primary dispersant) is able to de-bundle P-MWNT aggregates into individual tubes while the second polymer with large molecular weight and salt tolerance (secondary dispersant) is able keep the tubes separated even in the presence of high ionic strength. In this part of the work a different primary dispersant was studied. Adsorption experiments have been done

using GA instead of PVP40 as a primary dispersant while retaining HEC-10 as a secondary dispersant.

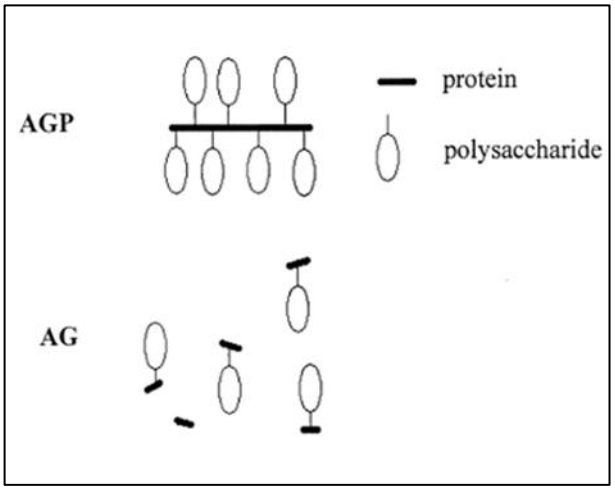

Figure 1- 18: Gum Arabic Structure [41].

P-MWNT samples of a number of concentrations were dispersed in GA by sonication for two hours and then secondary dispersant polymer HEC-10 was added and the suspensions were sonicated again for another 30 minutes. The final dispersions ranged between 20 and 200ppm of P-MWNT, 200ppm of GA and 1600ppm of HEC-10. The dispersion was then centrifuged for one hour at 2000rpm. All dispersions, unless otherwise stated, were prepared in 10% brine with a sodium chloride to calcium chloride ratio of 4:1. Adsorption experiments have been done by mixing 10ml of dispersion with 2g of crushed Berea sand and stirring for 24hrs. A number of concentrations have been tested, and the adsorption of P-MWNT to sand has been quantified using UV-Vis spectrophotometry. Figure 1- 19 shows a comparison

between the adsorption of P-MWNT using GA or PVP40 as primary dispersants. HEC-10 was used as a secondary dispersant at two temperatures 22 and 50^{o}C. PVP40 was used as a primary dispersant in an earlier work done by our research group. Appreciable adsorption has been observed using PVP40 as primary dispersant. We can see clearly that a dispersion made using GA adsorbs less to the crushed Berea sand. This can be explained by the high tendency of PVP40 to adsorb to crushed Berea sand due to the electrostatic attraction that results from a difference in charge on the PVP40 pyrene ring and silanol groups on the sand particles [44].

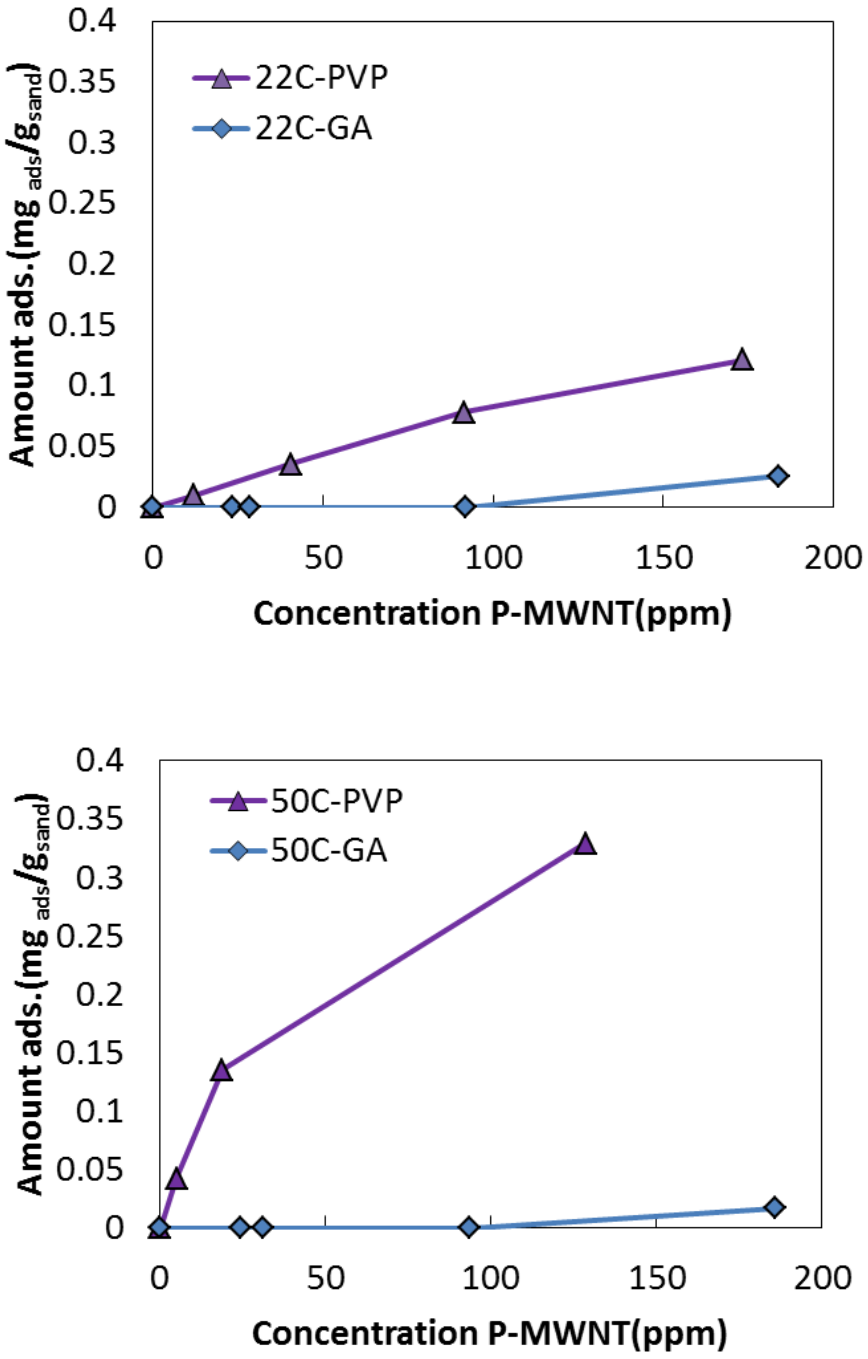

Figure 1- 19: Adsorption of P-MWNT using two different primary dispersants at 22°C [top] and 50°C [bottom].

Adsorption experiments have been performed using the same system mentioned earlier: GA and HEC-10. The only change was that experiments were repeated at 80°C and the results are shown Figure 1- 20. From this figure, we observe the low to negligible adsorption at low concentration ranging between 25-100 ppm. It was suggested that this relatively high adsorption at 80°C is due to the low concentration of GA. Therefore the use of a constant ratio of GA to P-MWNT of 2:1 was suggested. Experiments were repeated using this constant ratio of GA to P-MWNT and total HEC-10 polymer concentration of 1600 ppm. As shown in Figure 1- 20, the use of constant ratio between GA and P-MWNT reduced adsorption considerably as shown in the black line with black squares. These sets of data are very important due to the fact that we observed significant adsorption of P-MWNT using PVP as primary dispersion at this high temperature as shown in earlier parts of this work.

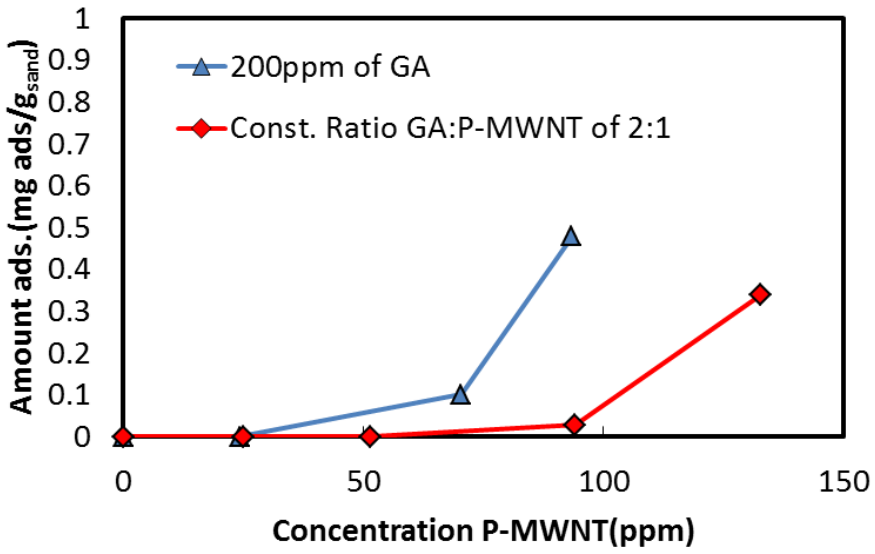

Figure 1- 20: Adsorption isotherms of P-MWNT at 80°C.

Although adsorption experiments performed using GA at 80°C were successful in reducing adsorption, the adsorption was not entirely eliminated at this temperature. A filtration step was suggested to be done on the centrifuged samples of the supernatant prior to the adsorption experiments. The dispersions were filtered using 1um filter and then added to the crushed sand. Figure 1- 21 shows the adsorption measurements at 80 and 90°C using pre-filtered P-MWNT dispersions. The data series represented with triangles indicate almost zero adsorption at 80°C, and the data series represented with squares showed very low adsorption at 90°C which corresponds to around 30% of total P-MWNT concentration.

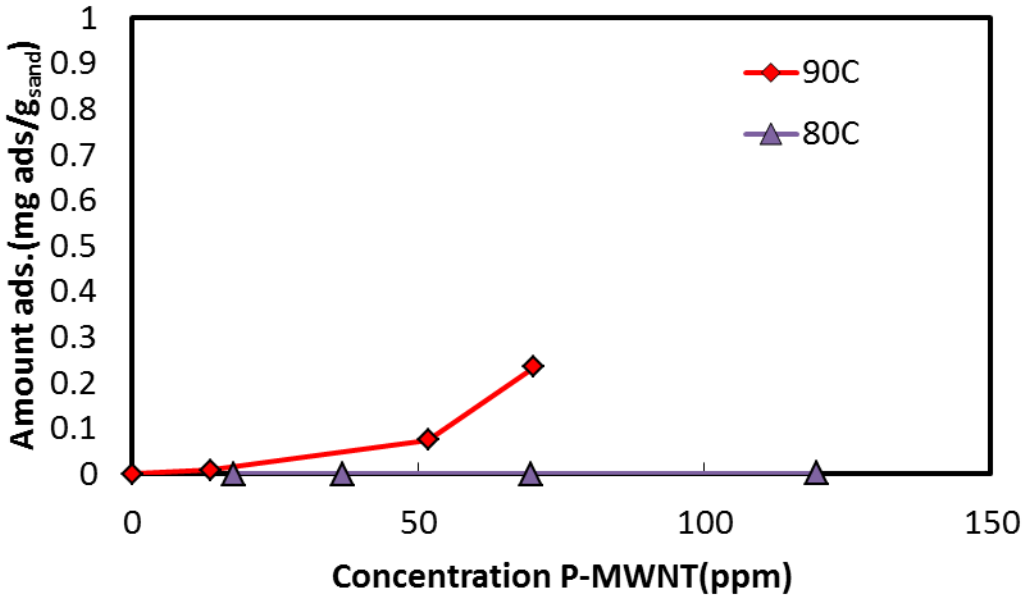

Figure 1- 21: Adsorption of P-MWNT using pre-filtered dispersions at high temperature.

Using the most stable dispersion, adsorption experiments have been repeated at 20% salinity to check for the effect of swamping the dispersion with higher ionic strength. It was found that this system of dispersing polymer is able to remain stable at this salinity and 80^{o}C as shown in Figure 1- 22. Considering the fact that 20% of the total salt used in our experiment is calcium chloride, a divalent cation Ca^{+2} is more effective is destabilizing nanoparticle dispersion than monovalent cation Na^{+}. The critical salt concentration(CSC) for Na^{+} is about 100 times more than for Ca^{+2} which shows the robustness of this dispersing polymer system in tolerating salinity [45].

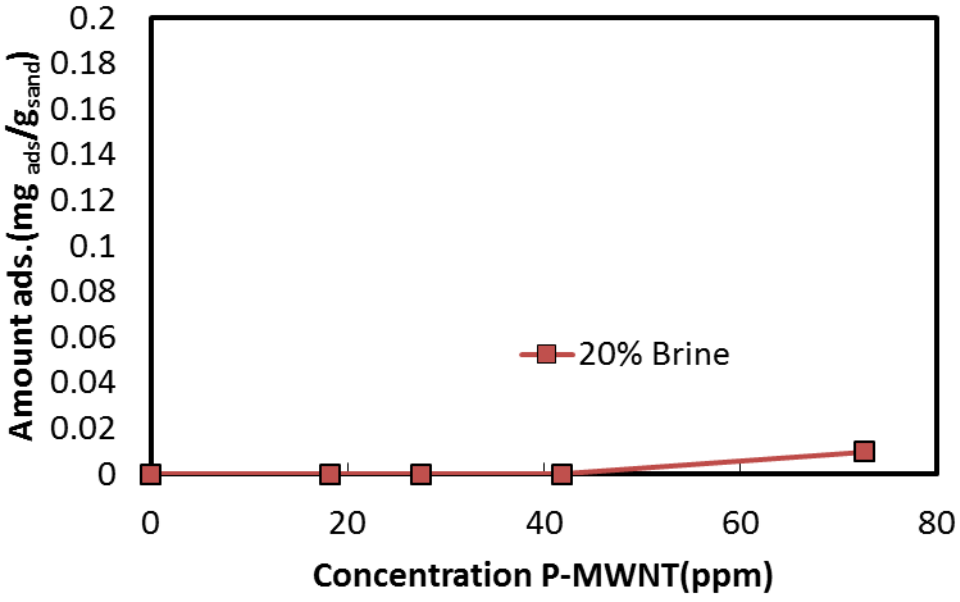

Figure 1- 22: Adsorption isotherms in 20% salinity brine and at 80^{o}C.

1.6.1. Polymer Concentration Enhancement Study

Adsorption experiments have been performed to investigate the effect of HEC-10 concentration on dispersion stability and adsorption isotherm. From previous experiments we found that the best recipe for dispersing P-MWNT is using twice as much of primary dispersant (GA) and 1600ppm of secondary dispersant (HEC-10) at 80^{o}C. Experiments have been done to optimize HEC-10 concentration needed for the measurement. Adsorption isotherms were repeated using 800ppm of HEC-10. Figure 1- 23 shows that using less of HEC-10 resulted in significant adsorption correspond to about 20% of the nanotube adsorbed to the sand.

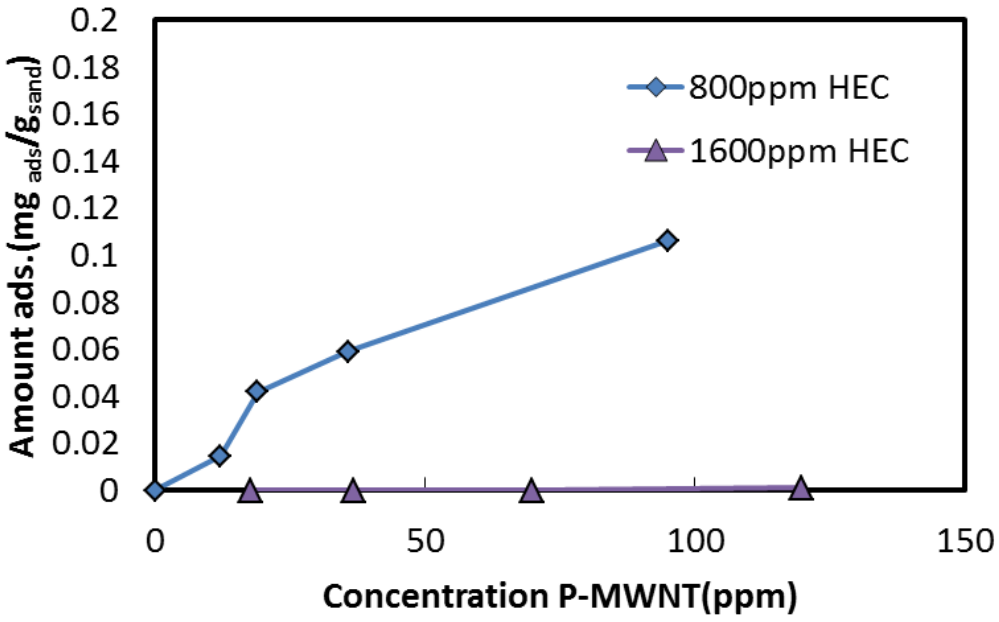

Figure 1- 23: Effect of HEC-10 concentration on P-MWNT adsorption at 80^{o}C.

1.6.2. Comparison between HEC-10 and HEC-25

Hydroxylethyl cellulose (HEC-25) Dow Chemicals has been investigated for the ability to stabilize P-MWNT dispersions. HEC-25 was added in the same manner as HEC-10. A study to scan the changes in concentration of P-MWNT through filtration and adsorption steps has been measured. Four samples of each dispersion using two concentration of secondary dispersant, HEC-10 and HEC-25 of 800 and 1600ppm were analyzed. Table in Appendix B-1 list all the changes in concentration investigated for HEC-25 samples after filtration and adsorption. The main observation is the huge loss of P-MWNT particles through the filtration step corresponds to about 70% of the initial concentration for the case were 800 ppm of HEC-25 and 50% for the case of 1600ppm of HEC-25. This in comparison to the HEC-10 data for the same two concentrations of 800 and 1600 ppm was much higher. The loss in filtration step was around 45% at 800 ppm and 35% for 1600 ppm of HEC-10. So the first conclusion drawn conforms to the understanding that HEC-10 works the best in stabilizing dispersions. On other hand, the adsorption isotherms of HEC-25 show interesting observation. The data are plotted in Figure 1- 24. In this Figure, dispersions filtered previously show slightly observable adsorption by using 1600 ppm of HEC-25 as secondary dispersant. Although the dispersion prepared using HEC-25 has low adsorption, it is of no match for the superior effect observed for HEC-10 at the same concentration. While adsorption using 800ppm HEC-25 is slightly lower than the case were 800 ppm of HEC-10 used, the starting concentrations are much lower and the particles loss by filtration is much more. This can also explained if we consider that loosely stabilized particles are filtered out

leaving a small fraction of the more stable dispersion which shows very low adsorption to the sand.

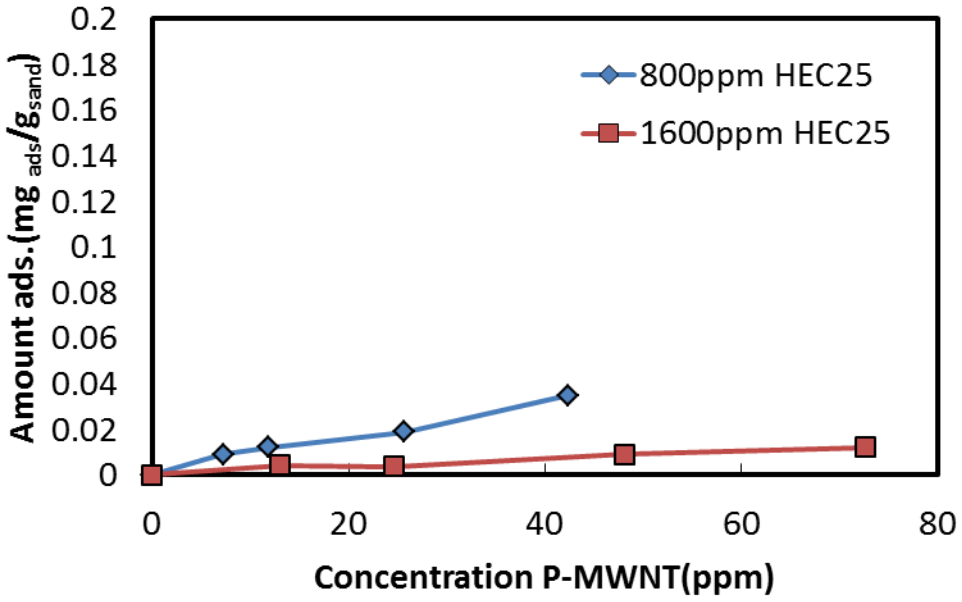

Figure 1- 24: Adsorption isotherms using HEC-25 as dispersant at 80°C.

Efforts have been done to understand the difference in functionalization between HEC-10 and HEC-25 using elemental analysis. Four samples have been analyzed using this technique and showed no significant difference in percentage of carbon, hydrogen as shown in appendix C-1.

1.6.3. High Concentration Dispersion

High concentration dispersions of P-MWNT in the range between 500-1000ppm were desired to be investigated for stability measurements and adsorption and propagation studies. One limitation to scaling up the concentrations of all constituents was the high viscosity encountered resulting from HEC-10 concentrated dispersion and pressure drop increase across reservoir rock. It was suggested to keep the ratio between GA and P-MWNT of 2:1 and increasing the amount of HEC-10 in the dispersion by a factor of 2. Dispersion prepared using 500ppm of P-MWNT, 1000ppm of GA and 3200ppm of HEC-10 was studied for filtration procedure adjustments. This was done by using system of filters: Whatman Grade 1, 5 and Grade B were the pore sizes were 11, 2.5 and 1um respectively. A dispersion of 160mL was divided into four solutions of 40 mL each and they were filtered differently from each other to understand the effect of filtration on particles loss. The four steps are numbered from 1 to 4. Number 1 is by using Grade 1, 5 and B consecutively. Number 2 is by using Grade 1 and B consecutively. Number 3 is by using Grade 5 and B consecutively. Number 4 is just the normal way using Grade B. It was hypothesized that doing filtration by this way could help reduce particle loss through filtration encountered as a result of large aggregates fish down smaller ones as they fill the pores of the filter. Figure 1- 25 summarizes he results from the four different filtrations as shown below. The values below the x-axis correspond to the percentage loss from the original dispersion.

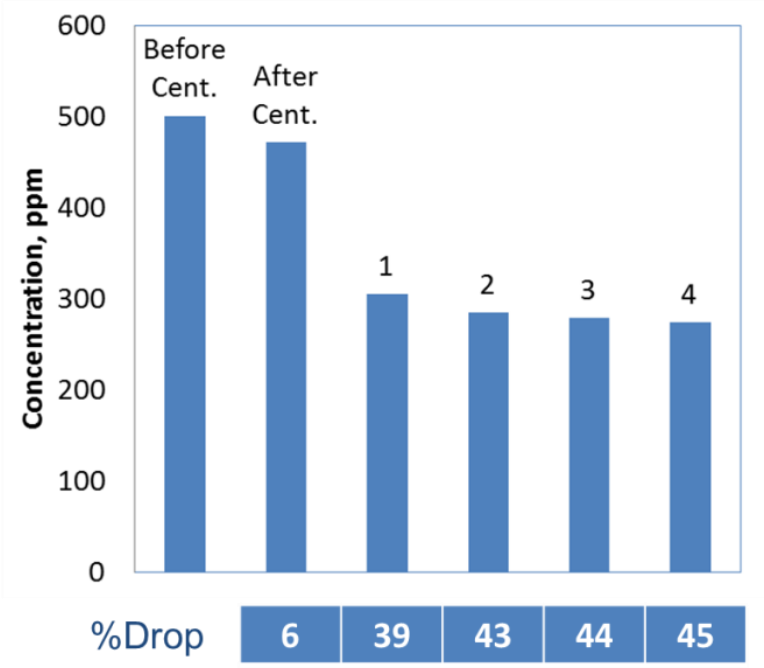

Figure 1- 25: Filtration loss using a number of filtration techniques.

It was found that using three filtration steps (filtration number 1) reduces particle loss. However, the difference in concentration is not significant between all filtration sequences. Using three filters showed little enhancement overall; however, the particles loss using different filter combinations correspond to 40% of the nanoparticles being trapped by the filter.

1.6.4. Comparison with Column Studies

Adsorption isotherms demonstrated unprecedented results using GA as a primary dispersant. Adsorption was less than 0.01 mg/g of sand in general up to a temperature of 80^{o}C and 20% salinity. Column studies were done using 100 ppm of P-

MWNT dispersed in 200ppm of GA and 1600ppm of HEC-10 polymer. Results are shown in Figure below.

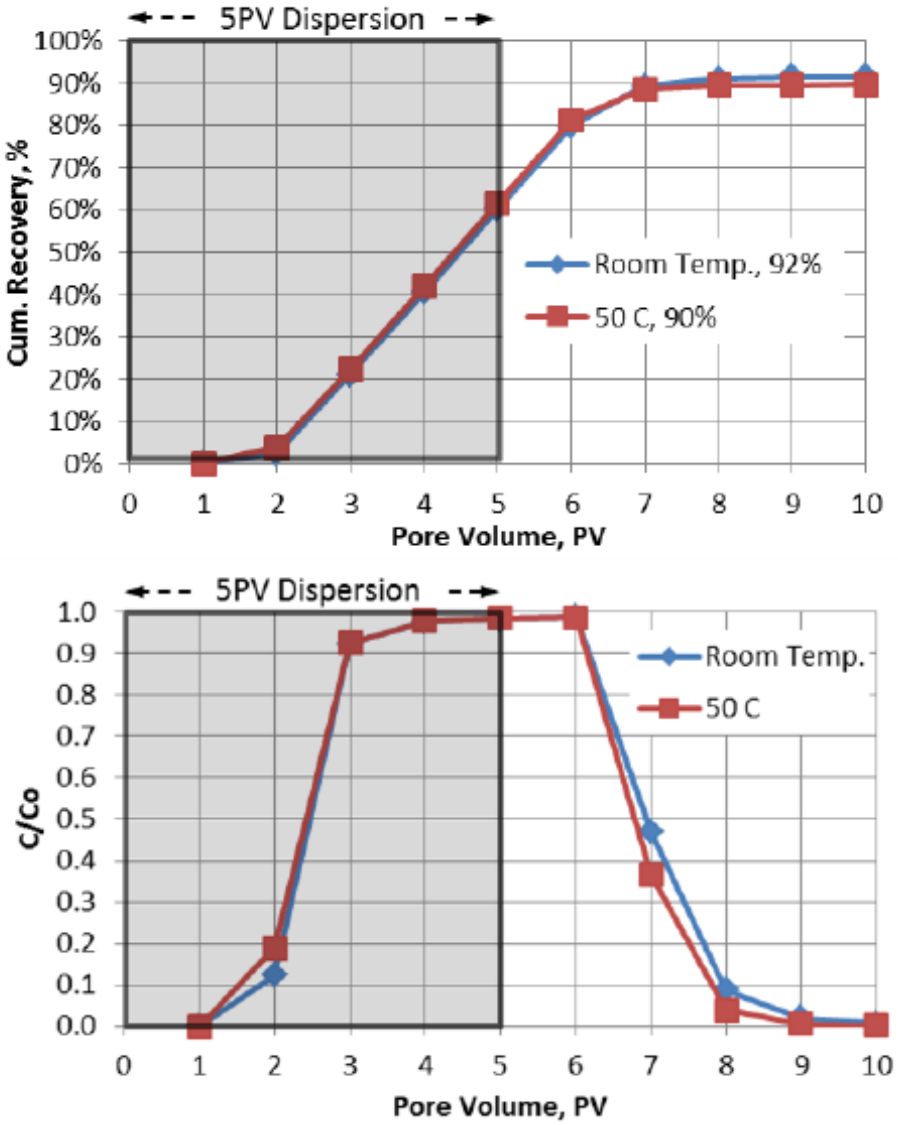

Figure 1- 26 Propagation of MWNT in the HEC-10/GA binary dispersant system at room temperature and 50°C. (Above: cumulative recovery. Below: normalized concentration) [27].

Figure 1- 26 shows a particle recovery of 92% and a normalized particle concentration approaching 100%. Although a slightly lower overall particle recovery has been observed using GA instead of PVP40 at room temperature, a better stability and propagation has been observed at 50^{o}C and higher.

1.6.5. Main Conclusions for GA/HEC-10 System

Stable carbon nanohybrids dispersions using two dispersing polymers GA and HEC-10 have shown outstanding tolerance at harsh reservoir conditions up to 20% salinity and a temperature up to 80^{o}C. The adsorption of P-MWNT to the crushed Berea sand was in the order of 0.01 mg/g of sand at 80^{o}C. Thermal stability studies of polymers at 90^{o}C shown the degradation of HEC-10 at that temperature as expected while GA visual observation suggests that this polymer degrade aerobically at high temperature which explains the adsorption observed at that temperature.

Column studies in accordance with adsorption isotherm have shown the beneficial effect of using GA instead of PVP40 as a primary dispersant in reducing retention of P-MWNT especially at 50^{o}C. The higher C/C_o and the faster breakthrough of P-MWNT suggest more interaction between PVP and Berea sand which explain the higher particle retention observed by using PVP as primary dispersant.

1.7. Polymer Stability and Characterization

1.7.1. Thermal Stability of Gum Arabic and HEC-10

From previous adsorption experiments we observed almost negligible adsorption at 80^{o}C and some adsorption at 90^{o}C therefore we performed some thermal stability measurements of fresh polymer samples to understand the impact of high temperature on polymer stability. Stock solutions of 2000 ppm of HEC-10 and 5000 ppm of GA both in 10% brine were treated for a time ranging from one day up to one week and compared with fresh untreated polymer samples both aerobically and anaerobically. Anaerobic experiments were done by allowing a stream of high purity nitrogen to flow through a glove bag which contains a stirrer and brine vials to allow for any oxygen to be flushed out of the system. Previously weighed polymer samples were added slowly to the vials while stirring to avoid fisheyes formation and gelation of HEC-10 polymer. The vials were sealed inside the glove bag and transported to an oven kept at 90^{o}C. Figure 1- 27a and b shows viscosity measurements for HEC-10 in aerobic and anaerobic degradation respectively. In these two figures we observe the trend of decreasing viscosity with increased treatment time which indicates significant polymer degradation; however, there are no significant differences between the aerobic and anaerobic cases. This behavior of degradation was also expected to take place as reported elsewhere [36, 46].

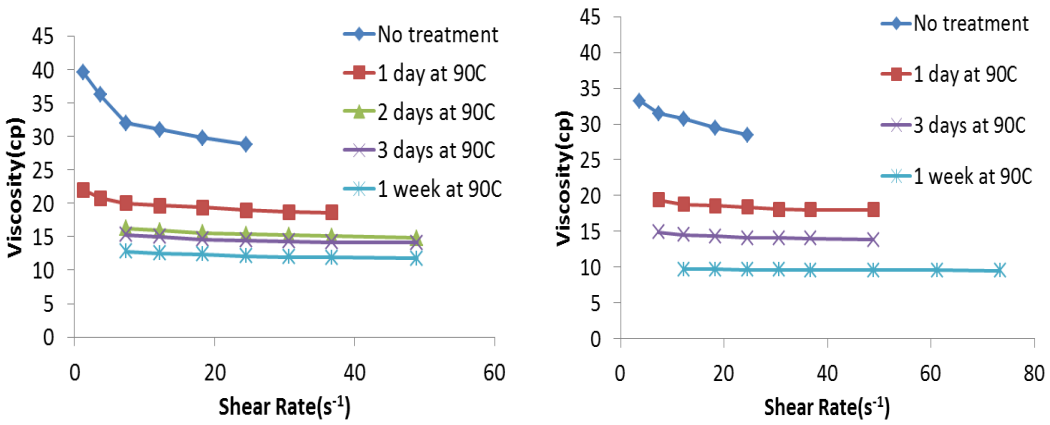

Figure 1- 27: HEC-10 viscosity measurements with different treatment times at 90°C at (a) aerobic conditions (b) anaerobic conditions.

Similar experiments were repeated for 5000 ppm GA polymer solutions. Figure 1- 28a and Figure 1- 28b show visual observations since no reliable viscosity measurements were obtained due to the low viscosity of the initial stock solution of GA. From visual observations, we conclude that the aerobic degradation of GA at this 90°C which explain the loss of some particles at this temperature in comparison to adsorption measurements at 80°C.

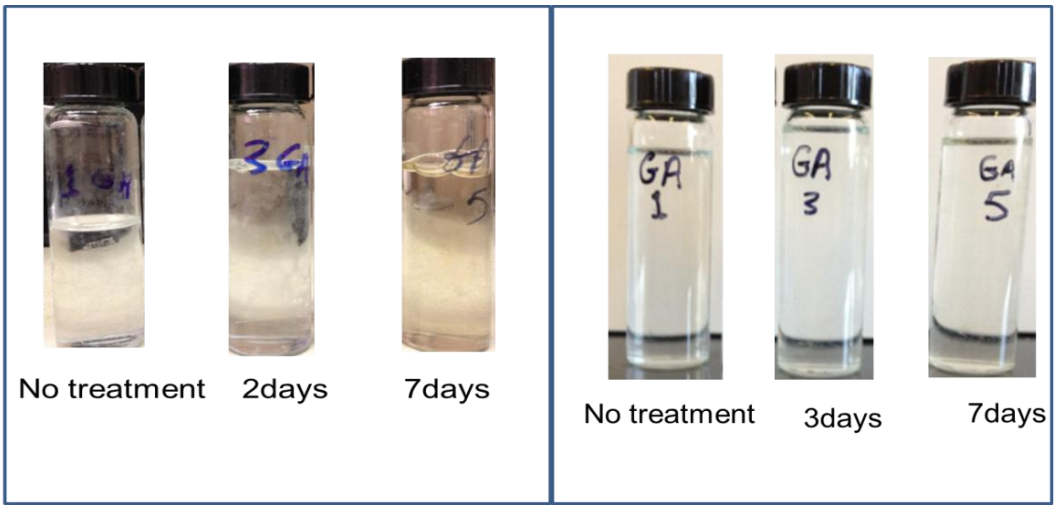

(a) (b)

Figure 1- 28: Visual observation of GA treated at 90°C at (a) aerobic conditions (b) anaerobic conditions.

1.7.2. Gel Permeation Chromatography (GPC)

As a continuous effort to understand the dual effect of polymer on stability we have performed gel permeation chromatography (GPC) also known as size exclusion chromatography (SEC) of HEC-10. GPC studies were done to identify HEC molecular weight and the significance of this molecular weight on dispersion stabilization and any possible molecular weight changes that can take place due to the effect of sonication [47]. GPC column can separate polymers depending on size using a column as shown in Figure 1- 29. Figure 1- 30 shows the setup used for analysis consisting of an HPLC pump pumping the HPLC grade water connected to an inline auto sampler. The whole stream is flowing through Waters columns (Ultrahydrogel WAT011535) with a

molecular weight resolution between 2K and 4M. Polymer will elute from the column depending on the size and will be analyzed using the differential refractometer.

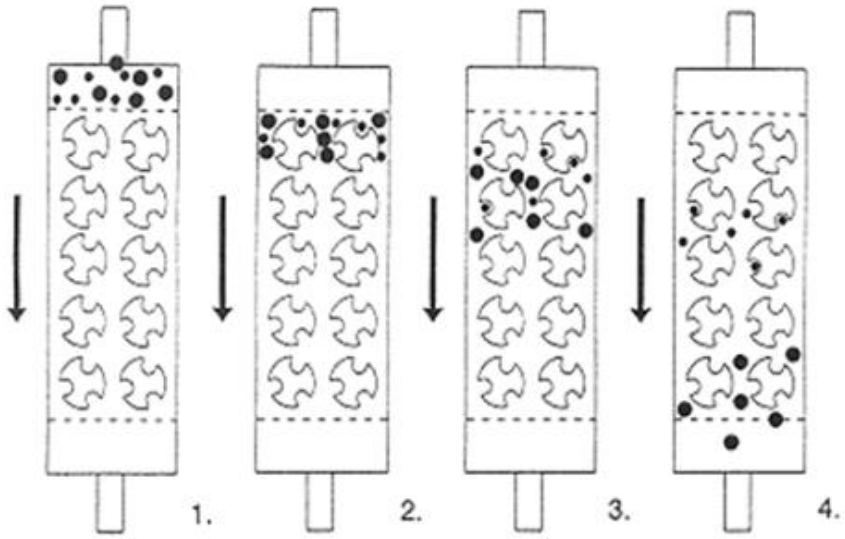

Figure 1- 29: GPC of two macromolecular sizes: (1) sample mixture before entering; (2) upon the head of the column; (3) size separation begins; (4) complete resolution [48].

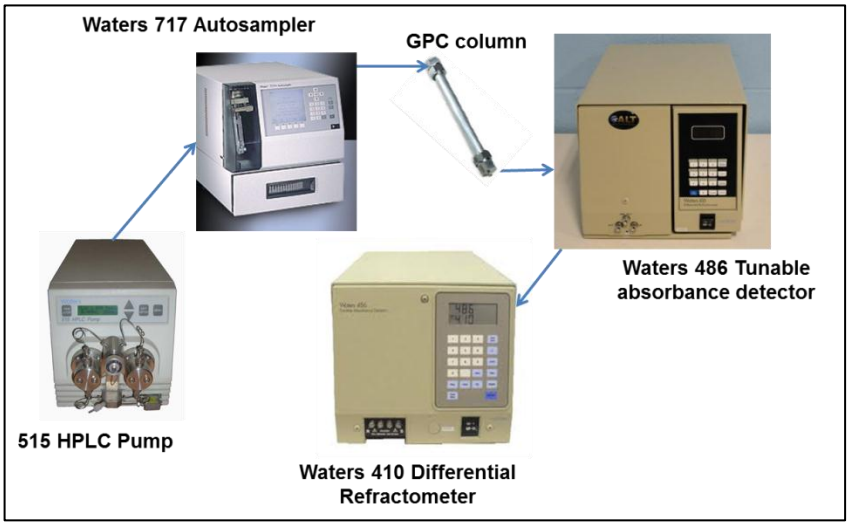

Figure 1- 30: GPC experimental setup.

Figure 1- 31 shows the differential refractometer measurements done on two samples of polymer, HEC-10 were compared with a standard HEC polymer of a molecular weight of 510KD obtained from American Polymer Standards Corporation[5]. Standard polymer solution was dissolved in HPLC grade water. 0.1M of sodium nitrate was used to avoid interaction between polymer and column packing [48]. We observe that both polymers have the same retention time around 13 minutes which indicates that both polymers have similar molecular weights. The small peaks around 26 and 30 minutes correspond to possible gas bubbles or small segments of polymer escaping the GPC column at a later time [49, 48].

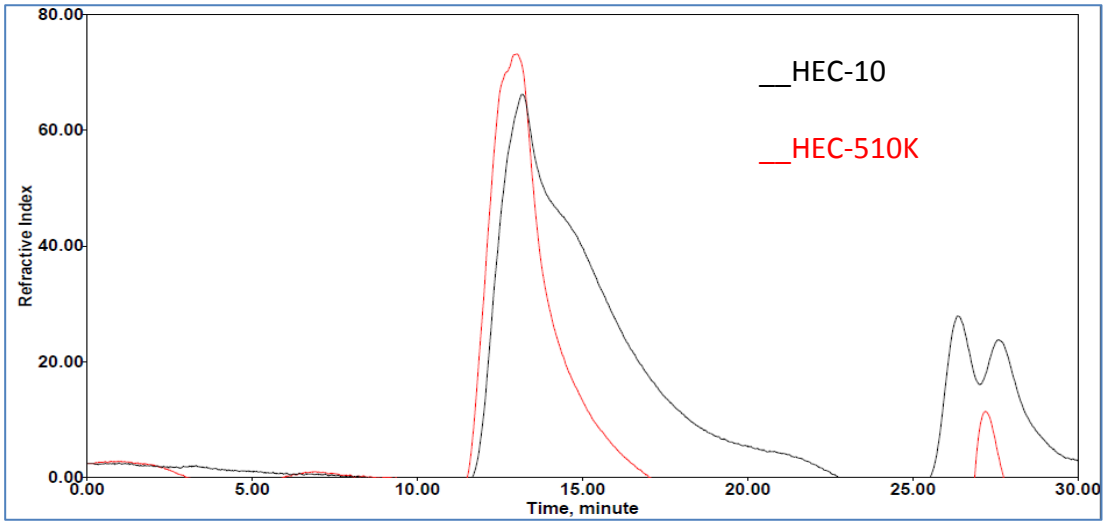

Figure 1- 31: Differential refractometer measurements of HEC-10 and HEC-510K.

[5]American Polymer Standards Corporation is a provider for molecular weight determination services and polymer standards and GPC columns. http://www.ampolymer.com/

The effect of sonication on HEC-10 was investigated by sonicating a 100ml solution containing 2000ppm of HEC-10 for different times ranging from 30 minutes up to 2 hrs. It was found that possible degradation could take place; however, this degradation does not appear to be severe as shown in Figure 1- 32. From this Figure we can expect the degradation after two hours to reduce the polymer weight after two hours down to around 400-450KD based on comparison made with Hydroxylethyl cellulose sample of 250KD molecular weight(HEC-250K). This is not likely to significantly change the dispersion stability.

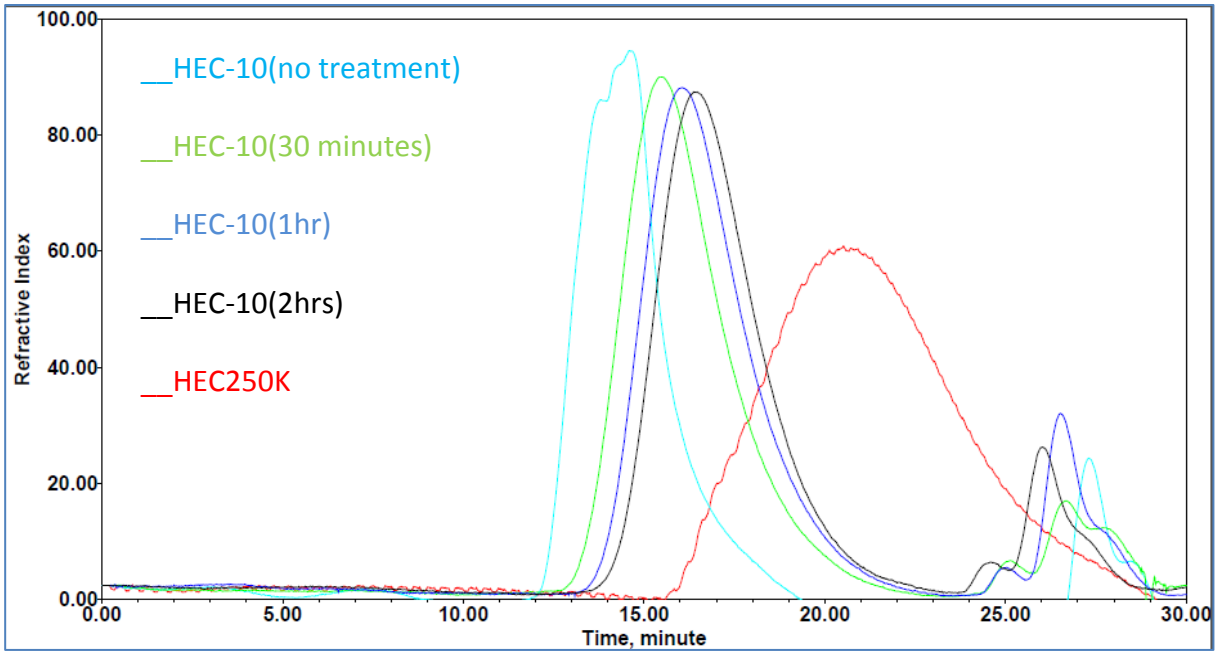

Figure 1- 32: Effect of Sonication on HEC-10 molecular weight.

1.8. Coreflooding Experiments

Three retention mechanisms (sedimentation, filtration, and Adsorption) have been explained earlier and methods to eliminate or reduce the impact of these mechanisms have been suggested. In connection to the previous concepts, it is of importance to highlight some of the similarities involved in the flow of a chemical solution through porous media as in Eq. 1-3 or the flow of nanoparticles as in Eq 1-4. Equation describing such phenomena is called mass balance, diffusion equation, or filtration equation depending on the academic community and usage [50-52]

$$\boldsymbol{D\frac{\partial^2 C}{\partial x^2}-\frac{q}{A\emptyset}\frac{\partial C}{\partial x}=\frac{\partial C}{\partial t}+\left(\frac{1-\emptyset}{\emptyset}\right)\rho_r\frac{\partial C_r}{\partial t}} \qquad \textbf{Eq. 1- 3}$$

where D is dispersion coefficient, C is the concentration, x is the distance in linear coordinate, q is the flow rate, A is the cross section area, t is the time, $\emptyset$ is the porosity, ρ_r is the rock density, and C_r concentration on the solid surface. Equation 1-4 describes particle adsorption as

$$\boldsymbol{D\frac{\partial^2 C}{\partial x^2}-v_p\frac{\partial C}{\partial x}=\frac{\partial C}{\partial t}+\frac{\rho_B}{\theta}\frac{\partial S}{\partial t}} \qquad \textbf{Eq. 1- 4}$$

where v_p is the particle flow velocity, ρ_B is the porous media density, S is a surface concentration related to adsorption and desorption [51]. The reason to highlight equations here is because adsorption phenomenon is time dependent and while core flood data are obtained at much shorter times than reservoir residence time, it can lead to underestimation of adsorption [50]. In both equations 1-3 and 1-4 we notice the three terms from left corresponding to molecular diffusion, convective and

accumulation terms. In this case of nanoparticles adsorption inside solid rock is not only affected by electrostatic/steric factor but also by hydrodynamic factors such as the flow velocity, nanoparticle size and for grain geometry in unconsolidated porous media [53].

1.8.1. Coreflood Testing

Coreflooding experiments of stable dispersions have been tested in a core flood test setup located in our labs at the university of Oklahoma. The core flood experiments depicted in Figure 1- 33 consists of a syringe pump filled with silicone oil connected to four pushing pistons which will be filled with injected fluids. A core holder can be used with core samples lengths up to 6" is situated inside a heating oven controlled by a temperature controller. Pressure transducers are connected to a computer to record pressure changes through all experiment. The effluent stream of the core holder is connected to a sample collector. Sample unit are collected and analyzed using UV-Vis as explained earlier.

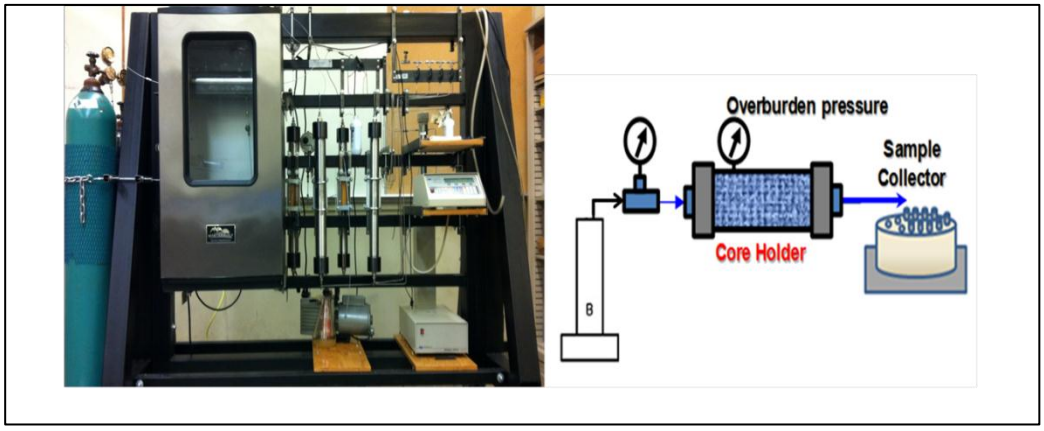

Figure 1- 33: Coreflooding test unit.

P-MWNT was dispersed in GA stock solution by sonication for two hours and then HEC-10 solution was added to prepare the dispersion used in experiments. The final dispersion is 100 ppm of P-MWNT, 200 ppm of GA and 1600 ppm of HEC-10. The solution was centrifuged for 1 hour at 2000 rpm and filtered using 1mm glass filter (grade B). Two cores of Berea sandstone were tested with permeabilities of 460 and 250mD. The injection temperature was 50^{o}C and the overburden pressure was 1000psi. The back pressure was set to 500psi. Early experiments have been done using two cores of Berea with measured permeabilities of 460 and 253mD. The breakthrough of a 100ppm dispersion of nanotubes is shown below. The core tested were both 1" in diameter. Five pore volumes of dispersion were injected at 50^{o}C and 5 pore volumes of brine post flush. The recovery of particles is shown in Figure 1- 34. In this figure we observed that the concentration is approaching C/C_o of 1 after 5 pore volumes of injection with the 460 mD core. The core with the lower permeability did not reach a plateau of C/C_o after 5 pore volumes. This means that we could see a higher concentration if we keep injecting dispersion.

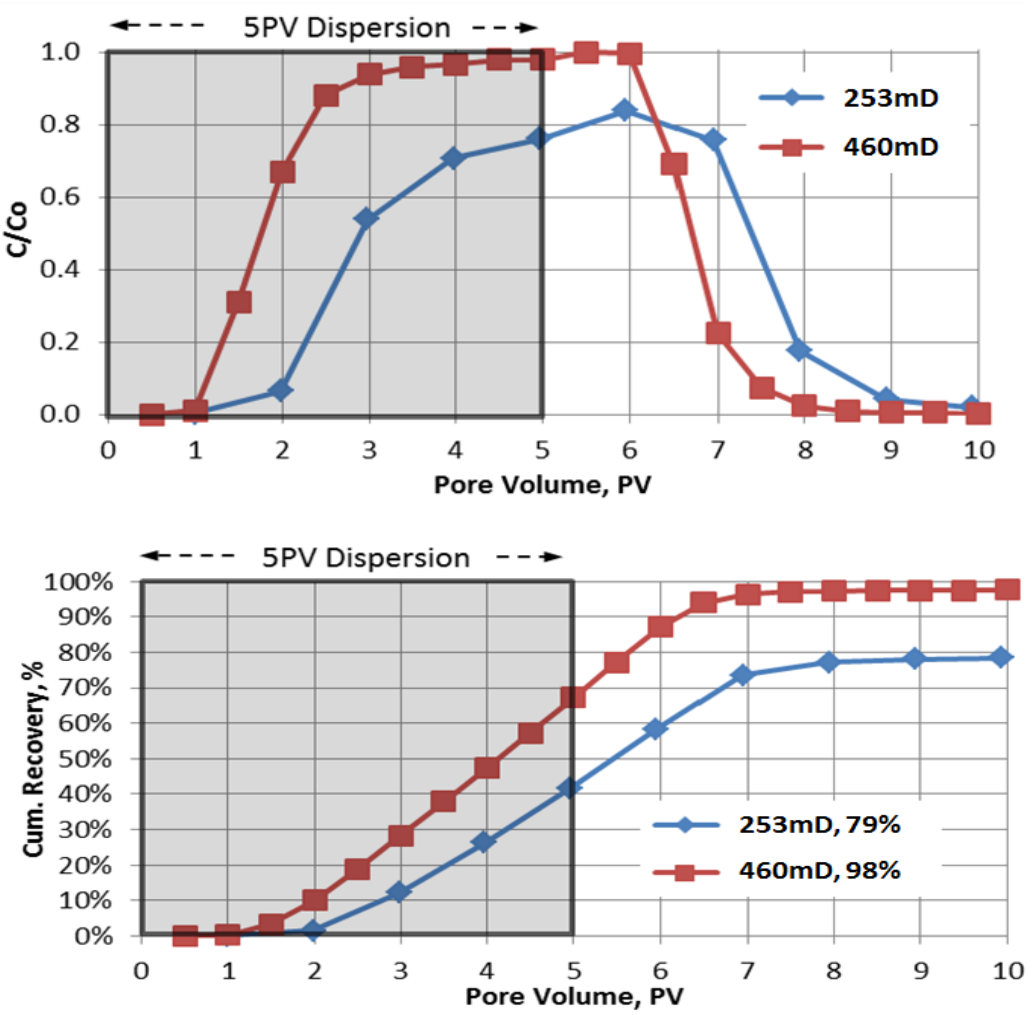

Figure 1- 34: Core flood experiments at OU lab [Top] normalized concentration of nanohybrids [bottom] cumulative recovery.

The total cumulative recovery was 98% for the 460 mD core and 79% for the 253mD core. The transport of particles showed little to no retention at the sand face and we were able to propagate the dispersion successfully. These results was encouraging to test the propagation through a standard core testing in Collaboration with Stim Lab as will be demonstrated later. Figure 1- 35 shows a photo of the 253mD

core plug after dispersion propagation. The 253mD core has been pre-flush with 1600ppm of HEC-10 polymer. Despite the fact that we got 79% recovery for this core, it is anticipated that some of the particles were trapped at the sand face due to size exclusion by the polymer pre-flush. The test with the 460mD core was run with sonicated polymer pre-flush and that eliminated greatly particle retention at the sand face. It is noteworthy to mention that all later runs including the Stim-Lab ones were done without polymer pre-flush and demonstrated outstanding propagation. The entrapments of particles at the sand face were very low as will be demonstrated later.

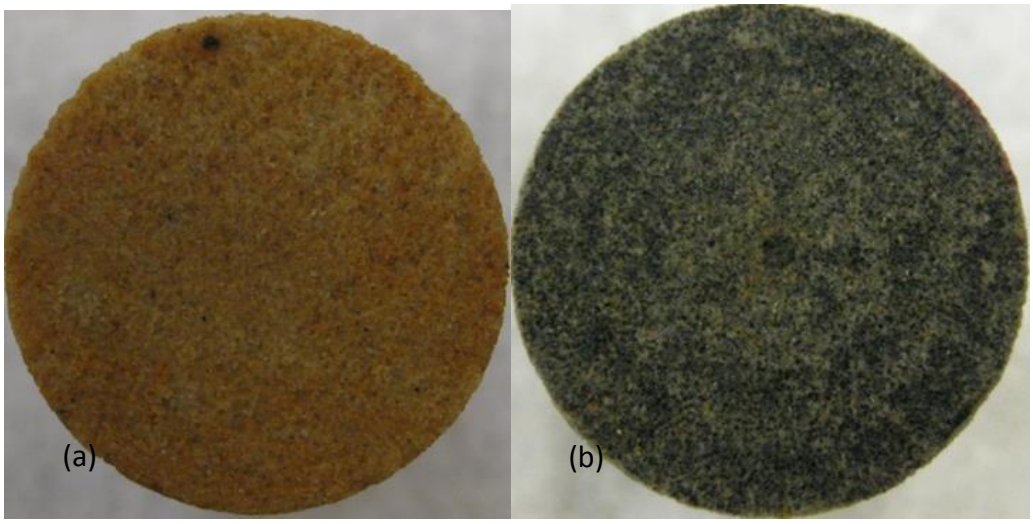

Figure 1- 35: Photo of core plug face after propagation of MWNT through a) 460mD b)253mD.

1.8.2. Verification of Coreflooding (Standardized Testing)

Core flooding experiments of dispersed P-MWNT through core samples have been repeated in collaboration with Stim Lab; an affiliate of Core Laboratories. A dispersion was prepared as following: Purified multi-walled nanotubes (P-MWNT) was dispersed in a solution containing GA by sonication for 2 hrs. HEC-10 stock solution was added to the dispersion and sonicated again for another thirty minutes and then centrifuged for 1 hour at 2000rpm and filtered using 1 micron filter paper. All solutions were in 10% brine with sodium chloride to calcium chloride ratio of 4:1. The details of dispersion preparation were explained in detail before. Table 1- 4 lists all details for both runs at Stim Lab and the physical properties of the cores used.

Table 1- 4: Standardized testing parameters.

Permeability klinkenberg, mD	200
Temperature, ^{o}C	65.5
Salinity, %	10
Core length, inch	6
Core diameter, inch	1.5
Flow rate, ml/min	2
Berea 400 core porosity, %	20

The two cores were pre-flushed with 10% brine prior to the test. The first core was run with no oil present. The brine flow rate was ramped up to 40 mL/min to remove loose clay particles from the core pores. The flow rate was then slowed down to 2ml/min and kept for a while until pressure stabilizes. 8 pore volumes of dispersion

were injected followed by 4 pore volume of brine post-flush. The second run was slightly different. It was done by injecting ¼ pore volume of Isopar L oil and then ramping the flow rate of brine up to 40ml/min collecting any oil coming out of the column and then settling the flow rate of brine down to 2ml/min and letting the pressure stabilize before starting to inject the dispersion. The oil saturation (S_{or}) prior to dispersion injection was found to be 0.21. Figure 1- 36 shows concentration and cumulative recovery of both experiments. In this figure, propagation data show faster breakthrough for the case where oil is present due to the smaller pore volume. This is because of the fraction of the pore volume taken up by the oil. Table 1- 5: lists the maximum concentrations attainable in both cases, overall cumulative recovery and amount adsorbed per gram of dry core.

Table 1- 5: Core-Lab run propagation data.

Core	Without Oil	With Oil
Max. C/C_o	97	95
Cum. Recovery, %	85	80
Adsorption, mg/g_{core}	0.03	0.04

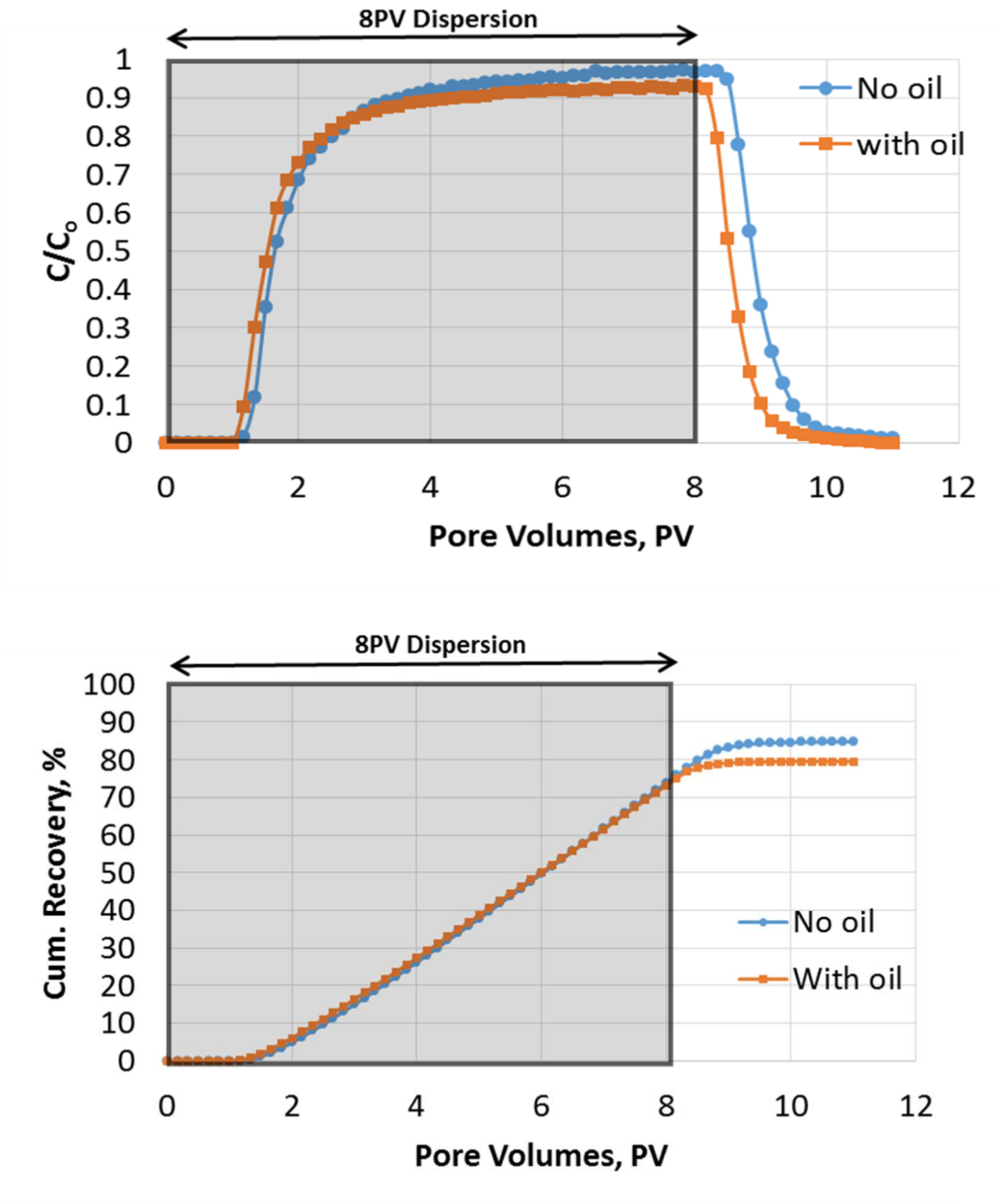

Figure 1- 36 Normalized concentration of particles(C/C_o)[Top] and nanohybrids cumulative recovery[bottom].

By inspecting adsorption values reported in Table 1- 5 we can conclude there is significant retention of particles in the second core where oil is present. The nanoparticles have higher adsorption in that case indicating that particles got retained at the oil/water interface due to their interfacial activity. It is important to mention from inspecting C/C_o that the concentration never reached a plateau in all cases which signifies the possibility of saturating adsorption sites allowing for further injections to propagate completely without retention. Figure 1- 37 shows the sand face for both cores with small sparse patches of particles deposited at the entrance.

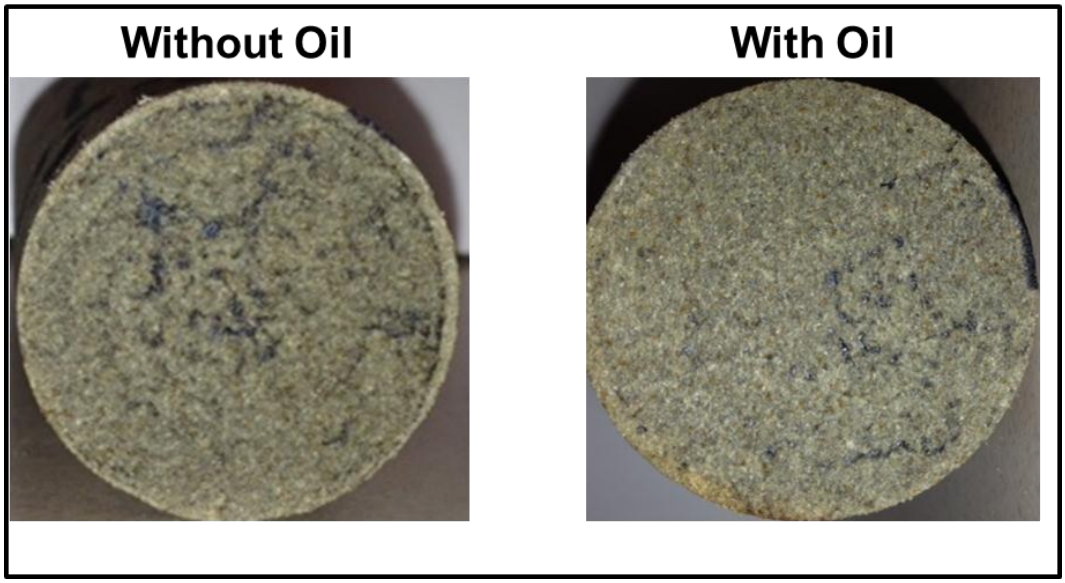

Figure 1- 37: Core entrance photos for both core runs with and without oil.

Since the core which has oil retained 5% more of the particles or 33% more than the oil-free core, it is expected that the difference is due to the adsorption of

nanoparticles at the oil/water interface. This means that the nanoparticles can be used for the detection of oil phase presence so it can act as a tracer. Understanding of both interactions of nanoparticles with rock and oil phase is necessary for that objective. Another core flood experiment with higher concentration was run at our labs here at OU and it came in agreement with our previous result as will be demonstrated in the next section.

The pressure drop for the two Stim–Lab tests was recorded as well and is shown in Figure 1- 38. In this Figure we observed that the pressure drop is not significant (≈2psi) for the oil-free core. However, the pressure increases (5-7psi) as dispersion injection continues. This is mainly because of viscosity change since HEC-10 contributes towards viscosity. Water viscosity at 40^{o}C is around 0.6cp while our normal filtered dispersion has a viscosity ranging between 1-1.5cp at same temperature. This explains the two to three fold increase in pressure and agrees with a Darcy's law interpretation.

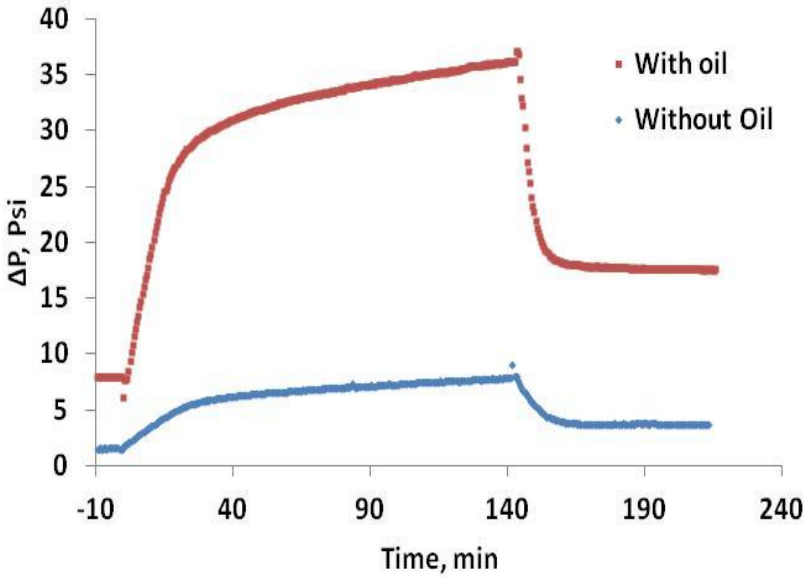

Figure 1- 38: Pressure drop for Stim-Lab runs.

This increase in pressure drop in the presence of oil can be explained in terms of relative permeability in two phase flow. Relative permeability can be defined as the ratio of the effective permeability of the phase to the absolute permeability at a specific saturation [54]. Relative permeabilities of oil and water in a two phase flow system can be defined accordingly as following

$$k_{ro} = \frac{k_o}{k} \qquad \textbf{Eq. 1- 5}$$

$$k_{rw} = \frac{k_w}{k} \qquad \textbf{Eq. 1- 6}$$

where k_{ro} and k_{rw} are the relative permeabilities of oil and water respectively, k_o and k_w are the effective permeabilities of oil and water respectively and k is the absolute permeability of the porous media [55]. Nikjoo and Hashemi(2012) reported relative

permeability curves for a 172mD core and 22% porosity core which has very close permeability and porosity to the Berea core run by Stim Lab. At 0.75 water saturation the relative permeability of water is around 15% of its original value [56].

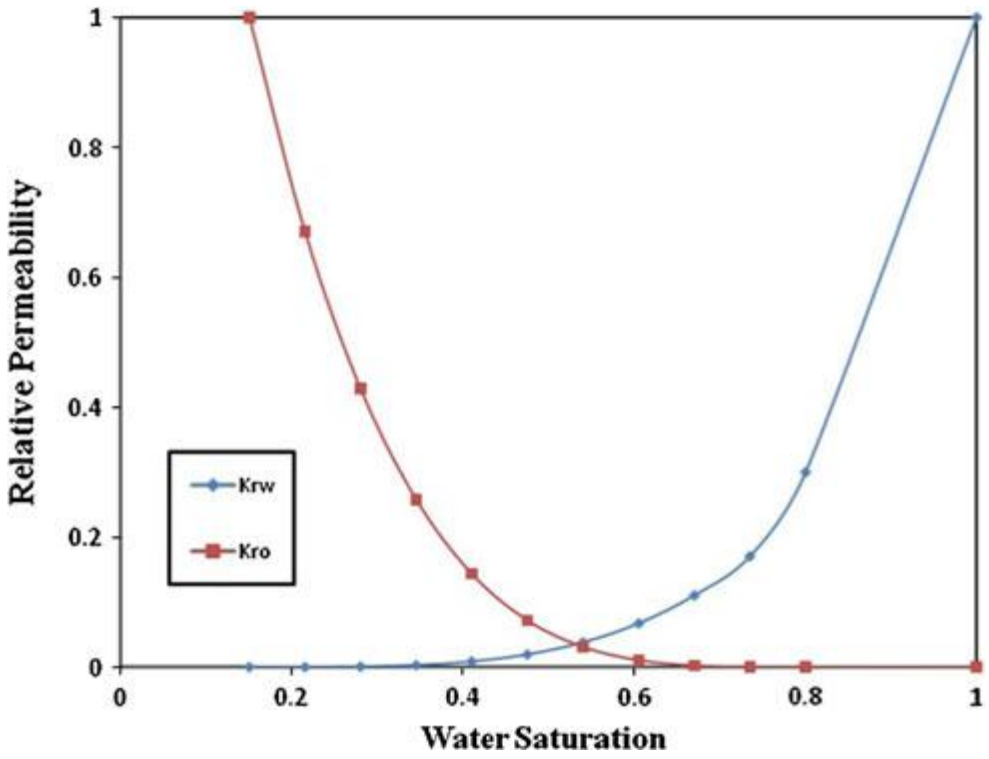

Figure 1- 39 relative permeability curves of 172mD core reported by Nikjoo and Hashemi (2012).

1.8.3. High Concentration Coreflooding Experiment

Experiments were conducted using the same setup described in previous section. The nanoparticle concentration and polymers were twice as much as the earlier experiments and the dispersion was prepared the same way mentioned earlier.

In this case the dispersion was filtered twice using the 1micron filter paper. The core tested was 200mD with 1” in diameter, 2” length. The dispersion flow rate was 1ml/min. A flow rate ramped up to 20 mL/min with brine prior to the dispersion injection in the same way as the Stim Lab runs. Once the pressure stabilized, 8 pore volumes of dispersion were injected followed by 4 pore volumes of brine post flush. The temperature was kept at 65.5^{o}C. The concentration and cumulative recovery for this run is shown in Figure 1- 40.

Figure 1- 40 shows the slightly higher recovery overall of the 2” high concentration core in comparison with the 6” core ran by Stim Lab, these is mainly is expected because of the double filtration of the dispersion, The total cumulative recovery for this 2” run was 88.5% in comparison to 85% for the 6” core. The adsorption was 0.02 mg/g_{core} for the 2” core in comparison to 0.03 mg/g_{core} for the 6” case.

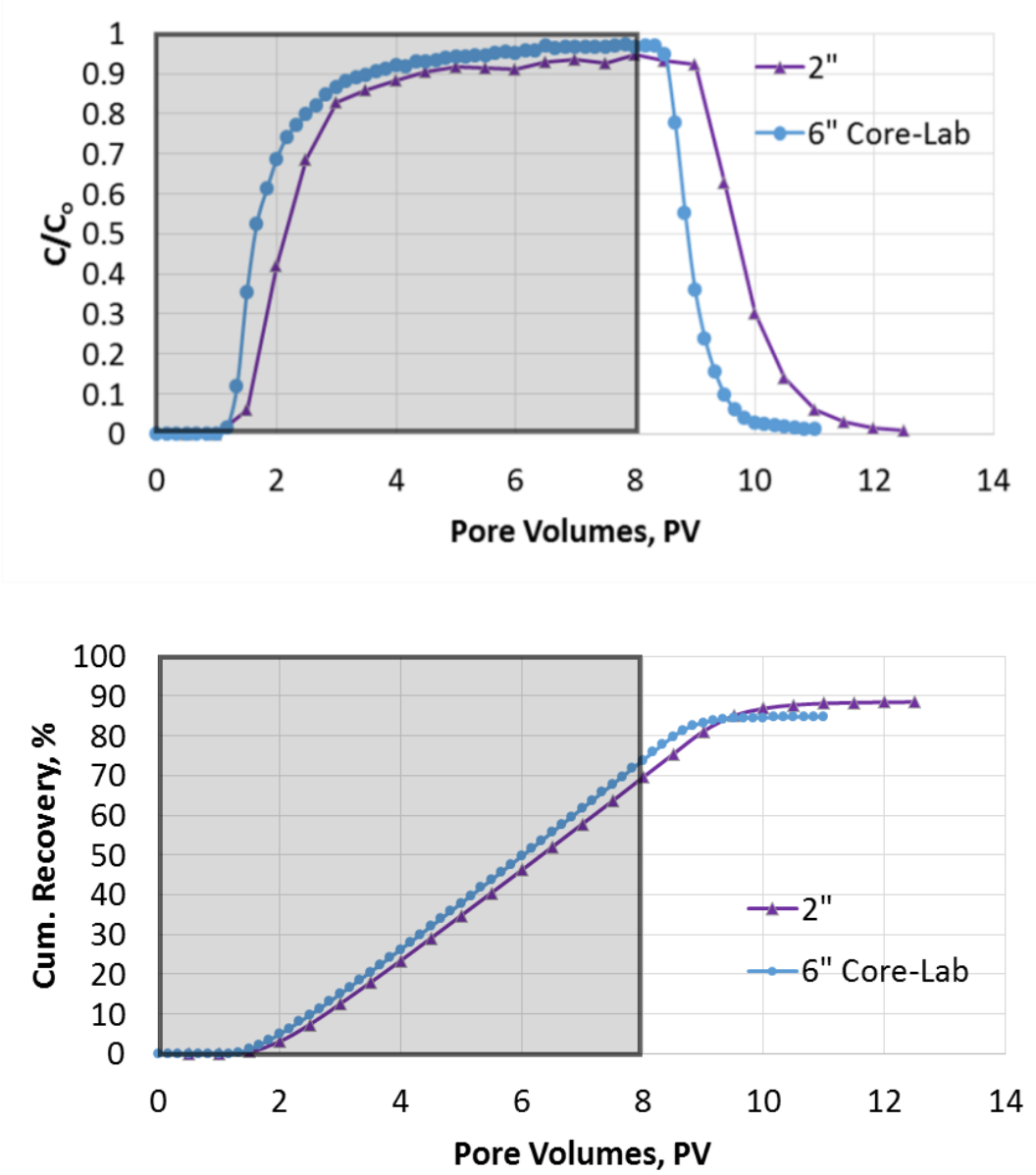

Figure 1- 40: Coreflood using 200ppm P-MWNT dispersion [Top] and nanohybrids cumulative recovery [bottom].

Coreflood runs conducted in our labs at the University of Oklahoma were in good agreement with the standardized runs at Stim-Lab, Duncan, OK. Successful

propagation of nanohybrids through cores of 200mD permeability and 6” length was achieved. The particle recoveries through all core runs were usually greater than 80%. Adsorption values were less than 0.03mg/g_{core}. This value in comparison to surfactant at mild conditions highlighted earlier in this work is more than an order of lower magnitude. The successful propagation of nanohybrids through consolidated porous media is a first step into utilizing nanohybrids in novel reservoir applications.

1.9. Oil Saturated Column Test

Column tests in the presence of a standard oil phase were conducted using Isopar L. Isopar L is an isoparaffinic oil mostly of C_{11}-C_{13} with 2% aromatics [57]. Two sets of tests one using high pressure high temperature stainless steel column connected to a syringe pump (reaction setup) or a glass column connected to a peristaltic pump as described earlier. These set of tests were done to investigate the interactions of nanoparticles with the water oil interface.

1.9.1. Stainless Steel Column Tests

Stainless steel column of 1” in diameter and 5” in length was packed with crushed Berea sandstone of size 75-250um. The whole setup for the experiment in stainless steel column is described in the reaction part of this work (Chapter 2).The column was pre-saturated with isopar-L oil. The column was then water flooded with water to remove excess oil. The residual oil saturation was quantified in each case. Two runs have been done one using P-MWNT and the second using sulfonated

multiwall nanotubes (SO_3-MWNT). The sulfonation of multiwalled nanotubes as shown in Figure 1- 41 started by treating 1g of P-MWNT with 50mL of 16M nitric acid at 80^{o}C under stirring for 3hrs. This will create carboxylic acid group on the surface resulting in oxidized multiwall nanotubes (oxidized-MWNT). Oxidized-MWNT is washed with distilled water and dried. Oxidized-MWNT was also tested in subsequent work in foams and other applications. For the preparation of SO_3-MWNT, oxidized-MWNT was treated with 20mL of sulfuric acid and 200mL of acetic anhydride for 2hrs under continuous stirring at 70^{o}C. The sulfonated nanohybrids was washed repeatedly and dried in vacuum oven [58-60].

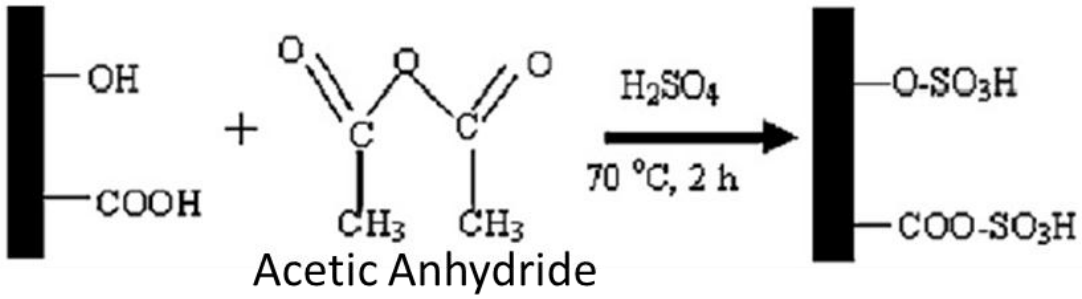

Figure 1- 41: Sulfonation of P-MWNT [58].

100ppm dispersions of both P-MWNT and SO_3-MWNT were prepared the same way in 500ppm GA and DI water. The flow rate was set to 1mL/min and temperature of 65^{o}C. The column was 5" in length and 1" in diameter and was pre-saturated with isopar L. Prior to dispersion injection, S_{or} was evaluated as shown in Table 1- 6:. Figure

1- 42 shows the effluent of column for the case of SO_3-MWNT dispersion injection. The red color is due to the oil soluble dye Sudan III.

Table 1- 6: Sulfonated and purified nanohybrids injection in stainless steel column.

Dispersion	P-MWNT	SO_3-MWNT
Max. C/C_o	1	0.97
Cum. Rec., %	98	87
S_{or}	0.27	0.24
% reduction S_{or}	0	3

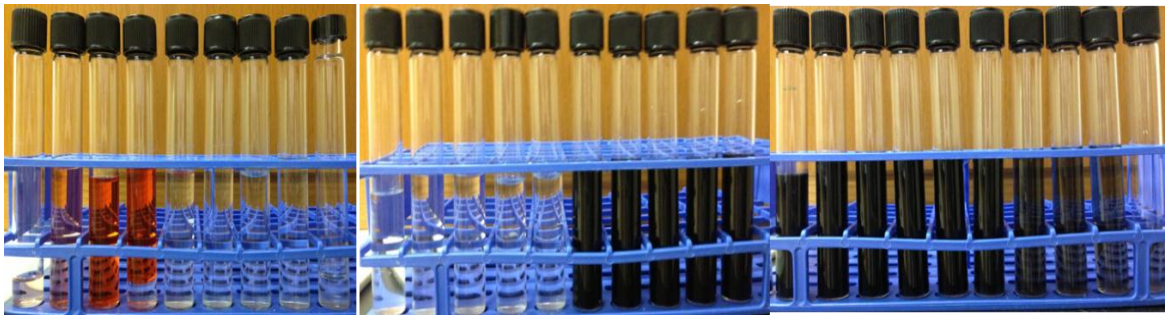

Figure 1- 42: SO_3-MWNT dispersion injection in the presence of oil phase.

The effluent normalized concentration and cumulative recovery is shown in Figure 1- 43. A recovery of 98% of P-MWNT is in agreement with previous column tests and indicate little to no interaction with either the sand or the oil phase while the

functionalized SO_3-MWNT show more retention. The increased retention of SO_3-MWNT could be due to different functional group or more interaction with oil phase.

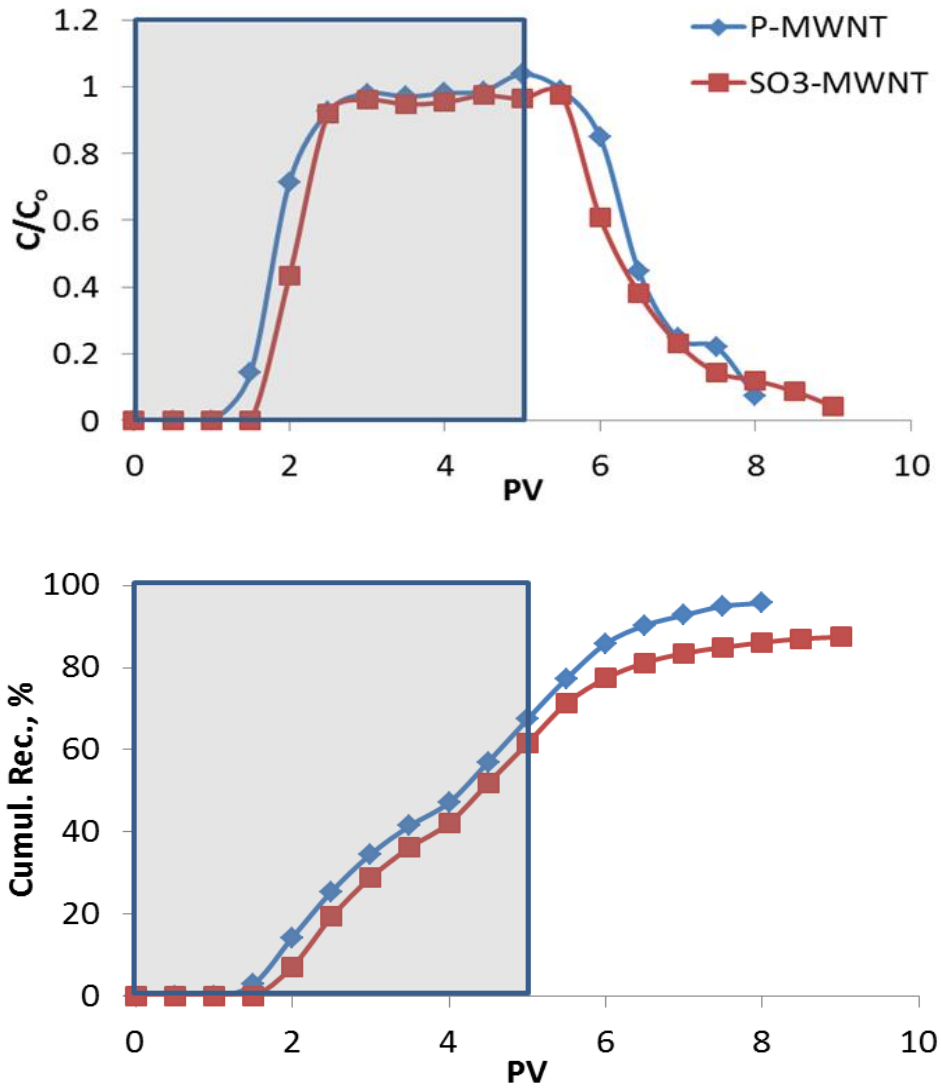

Figure 1- 43: Effluent normalized concentration [Top] and cumulative recovery [Bottom] of P-MWNT and SO_3-MWNT in oil saturated sand packed column.

1.9.2. Glass Column Tests

Interaction of nanoparticles with the oil phase has been tested before in core flood experiments. Higher retention/adsorption of particles has been observed in the presence of oil. However, fast flow rate were expected to result in underestimation of adsorption effect. Therefore, column tests with and without oil presence has been tested by stopping the flow for 24 hours inside the column and allowing dispersion to interact with the oil phase. Table below summarizes the experiment parameters.

Table 1- 7 Investigating flow stoppage in the presence of oil.

Test 1(with oil)	Test 2(W/O oil)
Brine pre flush	2PV brine
1 PV of Isopar L	
2PV brine	
5PV of 500ppm Alfoterra 123-8S	5PV of dispersion(500ppm Alfoterra
Stop flow for 24hrs	Stop flow for 24hrs
2PV brine post flush	2PV brine post flush

Higher retention in the presence of oil was observed. Taking into account the small PV available for nanohybrids adsorption because a fraction of the pore volume occupied by the oil phase. S_{or} was found to be 0.26. The particles recovery in the presence of oil is 79% and 83% for the oil free column. This means there is 24% increase in retention of particles in oil treated column for 25% less PV due to the presence of oil.

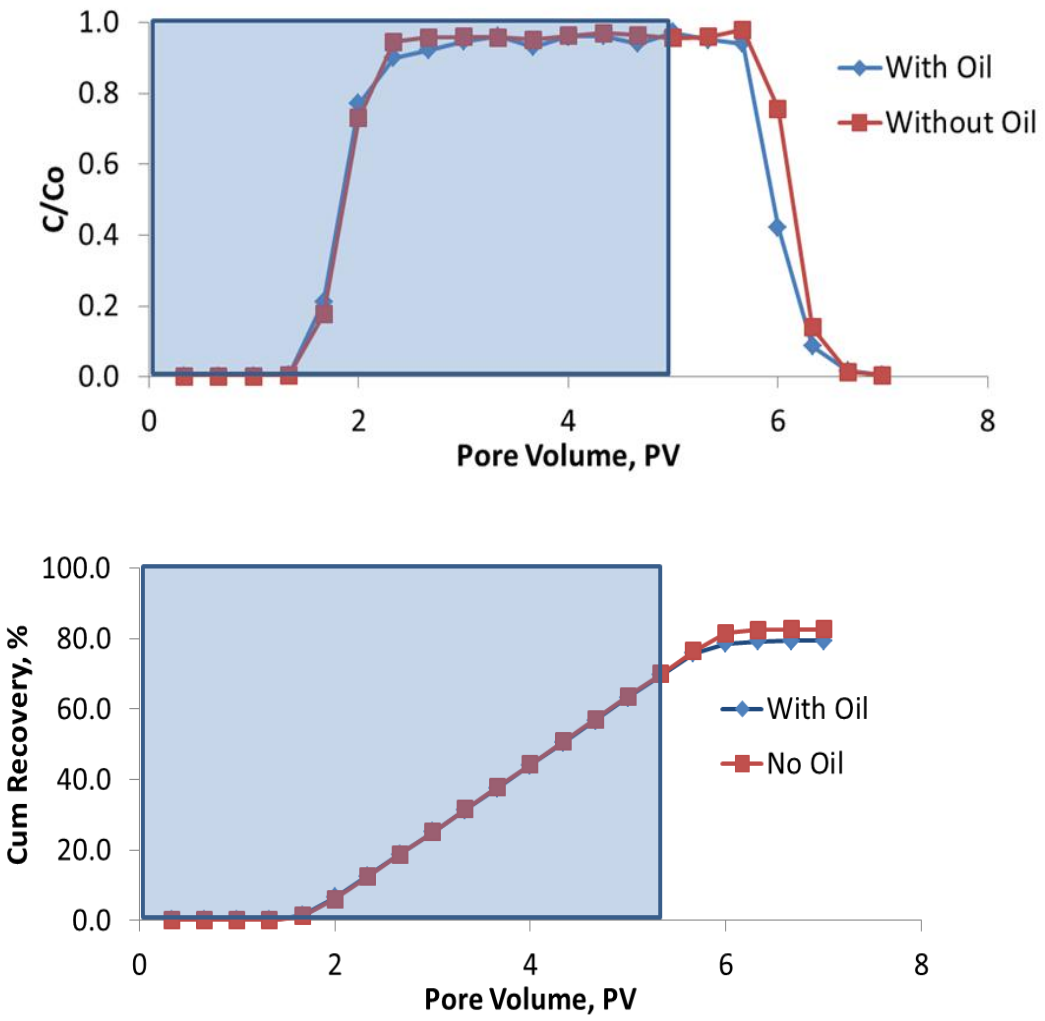

Figure 1- 44: Effect of flow stoppage on particle retention in oil pretreated column.

1.10. Nanohybrids as Surfactants Carriers

Surfactant flooding is one of the techniques widely adopted for chemical EOR. The main objective is to drop interfacial tension of the oil water interface [50, 61-63]. One of the main drawbacks to adopting this technique in many cases is the huge losses of surfactant by adsorption to the reservoir rock making the economics for such

operations unfavorable [64-67]. To avoid such losses, it was suggested to use a carrier to deliver surfactants to the oil water interface. These carriers should be less than 100nm in size and are completely dispersible in brine [68]. They should be designed to release their contents at the oil/water interface to result in oil solubilization. Lowering interfacial tension will increase capillary number (N_c)[6] and ease oil mobilization. This idea has many challenges and limitations and is still under investigation. Therefore, we suggested using nanohybrids as surfactant carriers. Surfactants tend to adsorb strongly on nanotubes and they have the ability to act as dispersing agents for nanohybrids [2, 69-71]. Earlier work suggested using SDBS to disperse SWNT [2, 72-74]. The dispersion of nanotubes can be achieved successfully by adsorption of surfactant systems such as SDS, Triton X-100, and SDBS as shown in Figure 2-33. This is mostly by surfactant alkyl chain adsorption along the nanotube [75].

[6] Capillary Number (N_c) can be defined as the ratio between viscous forces to interfacial tension forces. $N_c = \frac{v\mu}{\sigma}$ where v is the Darcy velocity μ is the mobilizing fluid's viscosity, σ is the oil-water interfacial tension [99]. Capillary Number at the end of a water flood process has a value of $\sim 10^{-7}$. In order to reduce the residual oil saturation to 50% of its original value, Capillary Number must be increased by three orders of magnitude [62, 101].

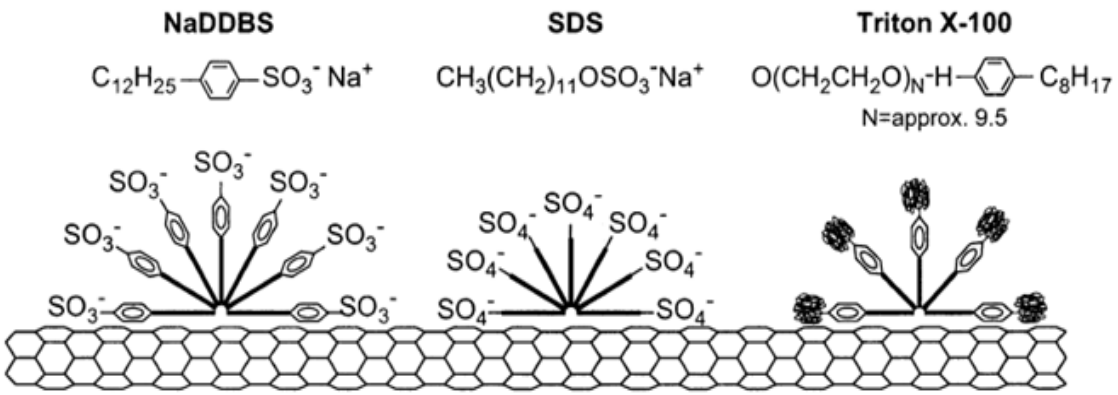

Figure 1- 45: Schematic representation of how surfactant adsorb onto the nanotube surface [75].

Suggested surfactant delivery system is employed by minimizing the adsorption of surfactant onto the reservoir rock by presenting an alternative surface for the surfactant to adsorb onto. Surfactant stabilized nanohybrids dispersions are expected to travel through the reservoir with minimal retention. As the nanohybrids reach the oil/water interface, surfactants desorb from the nanohybrids surface and adsorb at the water oil interface. Figure 1- 46 demonstrates the concept of surfactant delivery using nanohybrids.

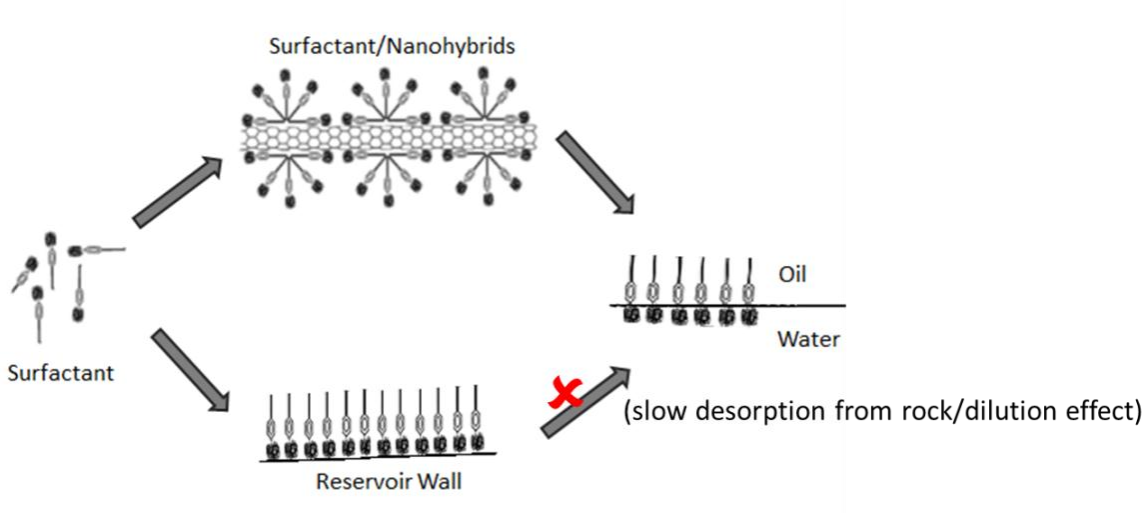

Figure 1- 46: Suggested surfactants delivery system.

1.10.1. Preliminary Column Studies Using Surfactants

1.10.1.1 Alfoterra 123-8S

Column studies using anionic sulfate surfactant Alfoterra 123-8S was conducted initially to evaluate the possibility of surfactant delivery using nanohybrids. Alfoterra 123-8S is a branched hydrophobe with 8 propoxylate group. Figure 1- 47 shows the chemical structure of Alfoterra surfactant [76].

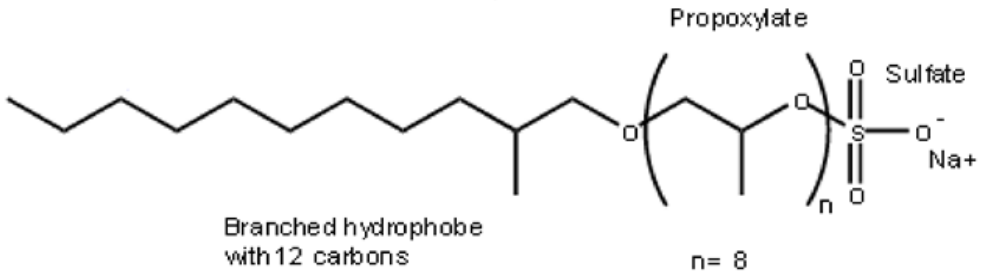

Figure 1- 47: Alfoterra 123-8S Sasol Surfactants [76].

Two sand packed column tests have been conducted using glass column of 3" length and 1" in diameter. The flow rate was set to 0.5mL/min. both experiments were done in 10% API brine and room temperature. Table below list the injection sequence for both tests. Figure 1- 48 shows the effluent for Test 2.

Table 1- 8: Injection sequence for glass column tests.

Test 1	Test 2
Brine pre flush	Brine pre flush
1 PV of Isopar L	1 PV of Isopar L
2PV brine	2PV brine
5PV of 500ppm Alfoterra 123-8S	5PV of dispersion(500ppm Alfoterra 123-8S and 100ppm of SO_3-MWNT)
2PV brine post flush	2PV brine post flush
S_{or}=0.26	S_{or}=0.29 (traces of oil observed after

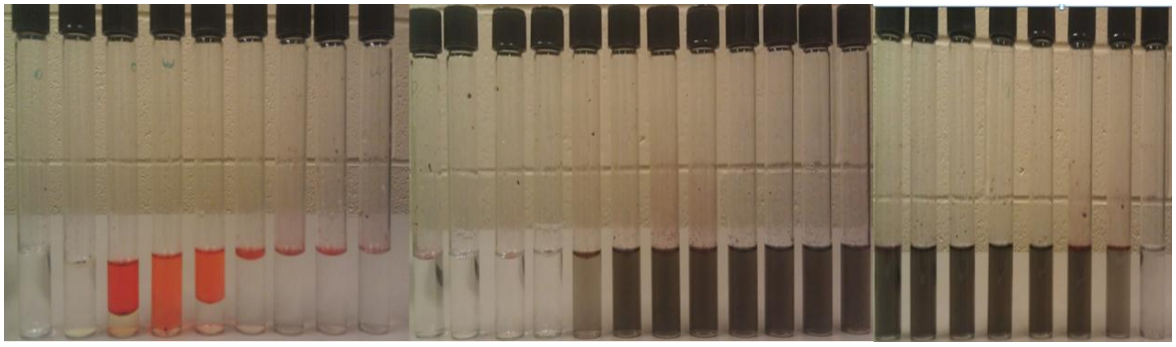

Figure 1- 48: Effluent of test 2 using Alfoterra 123-8S and SO_3-MWNT.

Traces of oil observed leaving the column was encouraging to perform full study of surfactant stabilized by nanohybrids starting with identification of possible surfactant candidates, phase behavior studies, dispersion stabilization by surfactant and adsorption isotherms.

1.10.1.2. Dispersion Stability and Adsorption Isotherms Using Alfoterra AF-23

Ability of AF-23 to stabilize nanohybrids dispersion has been investigated under a number of conditions. Studies were done with DI and brine and will be dealt with in further details below. Figure 1- 49 shows the chemical structure of AF-23.

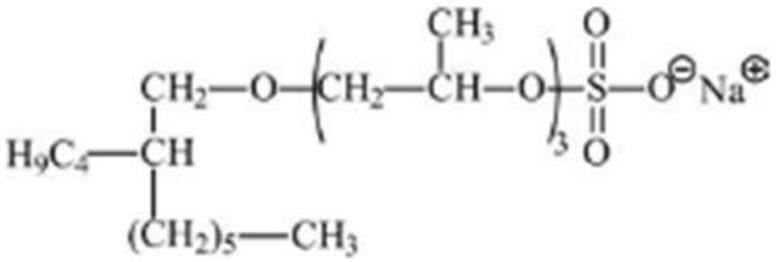

Figure 1- 49: Alfoterra AF-23 [77].

Nanohybrids dispersion was prepared in DI water using 500 and 1000ppm of AF-23. The dispersion is sonicated for 2hrs, centrifuged for 1hr at 2000rpm and filtered using 1um filter paper. 10 mL of the stable dispersion was added to 2g of sand and stirred for 12 hrs and the concentrations were as shown in Table 1- 9.

Table 1- 9: P-MWNT dispersion stabilized by AF-23 in DI water.

Surf. Conc., ppm	P-MWNT Concentration, ppm				Ads. $mg_{P\text{-}MWNT}/g_{sand}$
	Sonicated	Centrifuged	Filtered	12 hrs adsorption	
500	100	97	82	77	0.025
1000	100	96	91	88	0.015

It is quite obvious that higher concentration of surfactant results in higher stability and lower adsorption. This could possibly due to extra free surfactant in 1000ppm case available that adsorb readily to the replace the desorbed surfactant. Column studies using this surfactant was done using surfactant only and nanohybrid stabilized by surfactant dispersion.

A column injection of 100ppm P-MWNT stabilized by 500ppm of AF-23 were injected in similar manner to Table 1- 8. The S_{or} was found to be 0.4 and we observed a delay of particles breakthrough in spite of the high S_{or} value which should facilitate particle breakthrough as shown in Figure 1- 50. This indicated that surfactant adsorption is higher due to the presence of oil in column and that surfactant is not adsorbed to the rock is shown in adsorption isotherms reported in Table 1- 9. Efforts were also made to stabilize nanohybrids dispersions using Alfoterra AF-23 alone or combination with any of the polymers (GA and HEC-10) in the presence of brine were not successful. Table **1- 10** lists trials made in that effort.

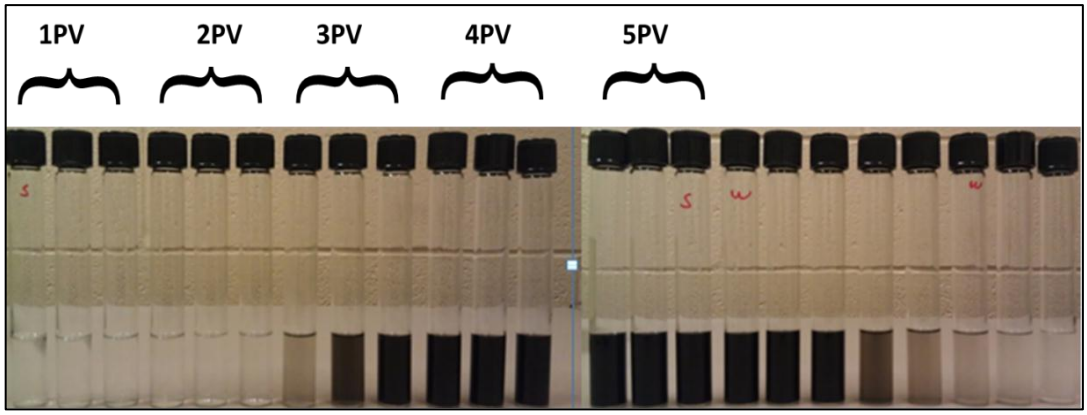

Figure 1- 50 Particle breakthrough for P-MWNT stabilized by AF-23.

Table 1- 10: Stabilization trials using number of combinations in API brine.

Trial #	Primary Dispersant, Salinity	Secondary Dispersant	Result
1	AF-23, Brine	N/A	✗
2	AF-23, DI	HEC-10, Brine	✗
3	AF-23+GA, Brine	HEC-10, Brine	✗
4	AF-23+GA, DI	HEC-10, Brine	✗
5	GA+AF-23, DI	HEC-10, DI	Add brine after 2nd sonication, ✗

After all these trials, a shift in strategy was necessary to incorporate binary/ternary surfactant systems to be used with the standard oil (Isopar L). The following section will shed spot light on this work.

1.10.2. Binary and Ternary Surfactant System Identification and Testing

The identification of a matching surfactant depends on the nature of the oil phase. This is done by identifying the equivalent alkane carbon number (EACN). All oils have corresponding EACN that can be easily identified for pure oils or measured using standard surfactants. Benzene has an EACN of 0, toluene has EACN of 1, while hexane decane, and hexadecane have EACN values of 6, 10, and 16 respectively [78]. Once EACN is identified, a matching surfactant system can be tested for compatibility and then dispersion stability, adsorption isotherms and column studies consecutively can be conducted for successful nanohybrids and surfactant propagation to the O/W interface.

1.10.2.1 EACN Identification

The EACN of isopar L was identified based on phase behavior studies using 5g of 2.5% AF 8-41S and 5 mL of isopar L. Salinity scan for Winsor III microemulsion with different salinities were investigated. As salinity increases, the solubility of surfactant in water phase decreases. At high salt concentration, the surfactant preferentially dissolves into the oil phase and very little partitioning takes place [79]. Optimum salinity can be identified highest surfactant concentration at the interface resulting in lowest IFT [80] as shown in Figure 1- 51.

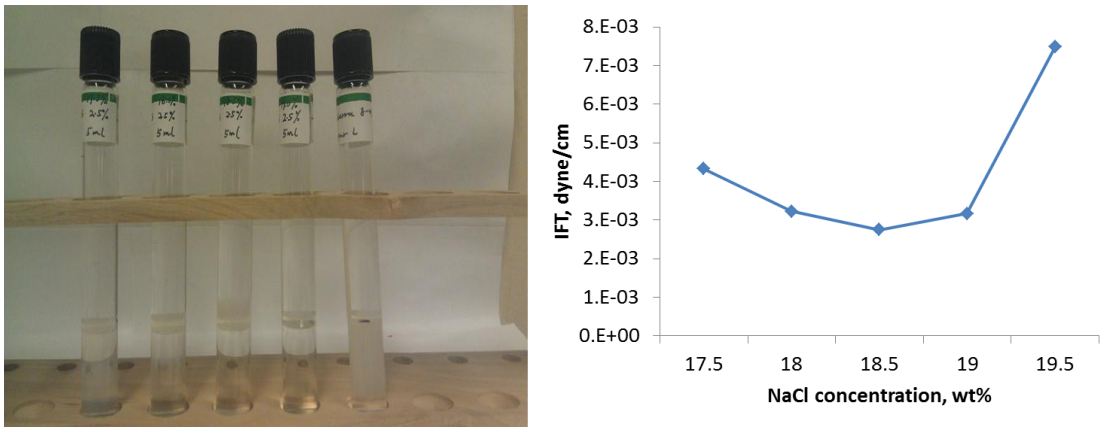

Figure 1- 51: Visual observation of middle phase (left) and their corresponding IFT measurements (right).

The identification of EACN was based on visual observation of middle phase and IFT measurements. Figure 1- 51 shows the vials with salinities between 17.5 and 19.5% and their corresponding IFT measurements. Figure 1- 51 shows that 18.5% salinity corresponds to the lowest IFT. Calibration for AF 8-41S surfactant was done with different oils of known EACN values. The equation governing this surfactant was found to be as shown in Equation 1-7. By back calculation, EACN was found to be 10.7.

$$\ln S = 0.0478(EACN) + 2.4075 \qquad \textbf{Eq. 1- 7}$$

where S is the optimum salinity of aqueous phase. This equation is based on the general equation governing the systems containing hydrocarbon, anionic surfactant, alcohol, and salinity [81]

$$\ln S = K * ACN + f(A) - \sigma \qquad \textbf{Eq. 1- 8}$$

where f(A) is a value specific for alcohol utilized and σ and K are characterisitic surfactant parameters. Based on EACN value, suggested surfactants to be compatible with isopar L were AF-123-8S and Steol CS-460.

1.10.2.2. Middle Phase Investigation for Surfactant Optimum Ratio

Ratio between AF 123-8S and Steol CS-460 can be identified based on phase behavior studies. Using 4000ppm of AF 123-8S and varying Steol concentration from 200 to 1800ppm in API brine and isopar L. The middle phase appeared to be around 1800ppm of Steol after 1 week.

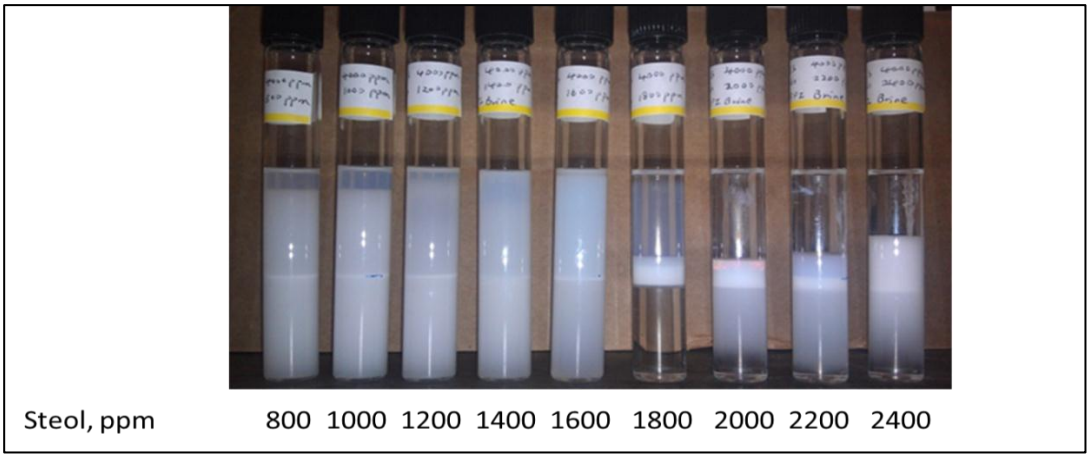

Figure 1- 52: Binary surfactant system scan for middle phase using AF 123-8S and Steol CS-460 in API brine and Isopar L oil.

Using ternary system of 2000ppm of AF and 1600ppm of hexyl glucoside and range of steol concentration, middle phase was found to be around 1200ppm of Steol as shown in figure below.

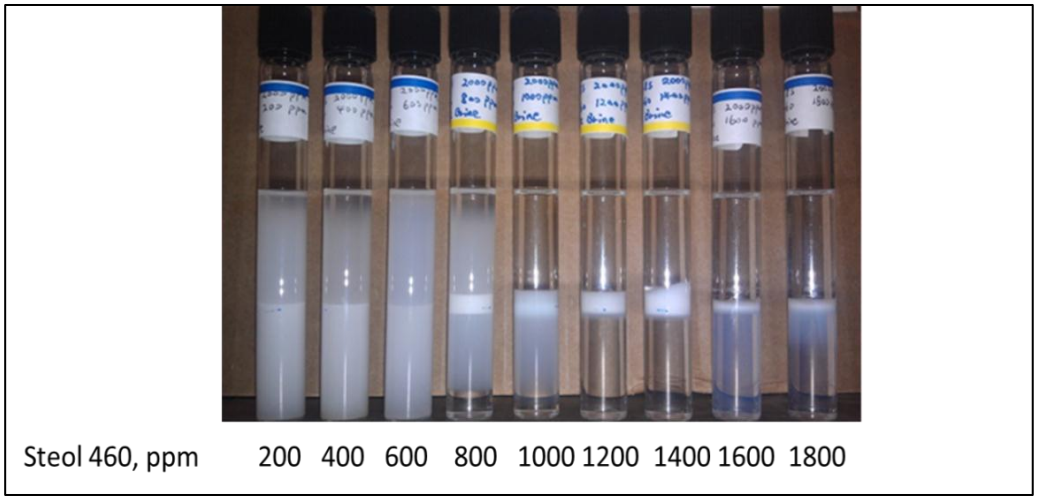

Figure 1- 53: Ternary surfactant system scan for middle phase using AF 123-8S, hexyl glucoside and Steol CS-460 in API brine and Isopar L oil.

1.10.2.3. Dispersion Stability Using AF 123-8S and Steol CS-460

Using 1000ppm of each surfactant and varying amount of salt from 0.1 to 10% and keeping the ratio between sodium chloride and calcium chloride of 4:1. 100ppm of P-MWNT has been sonicated and filtered using 1um filter to check for the possibility of stabilizing dispersion. Table below lists these results.

Table 1- 11: Dispersion concentration using binary surfactant system and varying salt amount.

NaCl concentration	0.1%	1.0%	10.0%
C/C_o after filtration	68%	42%	0

Table 1- 11 shows that we could get stable dispersion at 0.1 and 1% brine. However, there using 10% salt has drastic effect on stability. There is room for enhancement that can be achieved using these surfactants. Further work is needed to investigate dispersion stabilization and adsorption.

1.10.3 Nanohybrids as Surfactant Carrier: General Conclusions

Stronger interactions between nanohybrids and surfactant versus surfactant and reservoir rock wall can allow for using nanohybrids as carriers for surfactants to the oil/water interface. In DI water, adsorption of nanohybrids stabilized by surfactant showed little to no adsorption while the presence of oil inside porous media showed 1PV delay demonstrating the possibility of high interaction between nanohybrids/surfactant and the oil phase. In brine it was necessary to find an optimum system that can both reduce IFT and stabilize nanohybrids dispersion. General grounds for any oil and salinity have been set including: finding EACN, choosing compatible surfactant system (binary or ternary), conducting dispersion stability studies, conducting adsorption isotherms, running column studies in the presence of oil. The preliminary results obtained so far are encouraging and much room for improvement is available.

1.11. Radial Diffusion of Nanohybrids inside a Porous Media

It was expected that dispersion propagation of nanohybrids in sand column does not reflect the anticipated actual retention of particles as particles do not have

enough time to diffuse radially inside the pores. The particle tends to travel in the streamlines because of the small diffusivity anticipated for such particle [82]. This can be understood by inspecting equation 1.4. Reducing the flow velocity or stopping the flow completely will reduce or eliminate convective forces allowing for diffusion to be the dominant. It was suggested to slow down or halt the flow inside the porous media to evaluate the possibility of radial diffusion. Figure 1- 54 shows a snapshot of nanoparticles flow inside porous medium. The particles closer to the center [blue] are traveling faster than the particles closer to the wall (red particles). A series of experiments have been done using sand packed column to demonstrate this phenomenon.

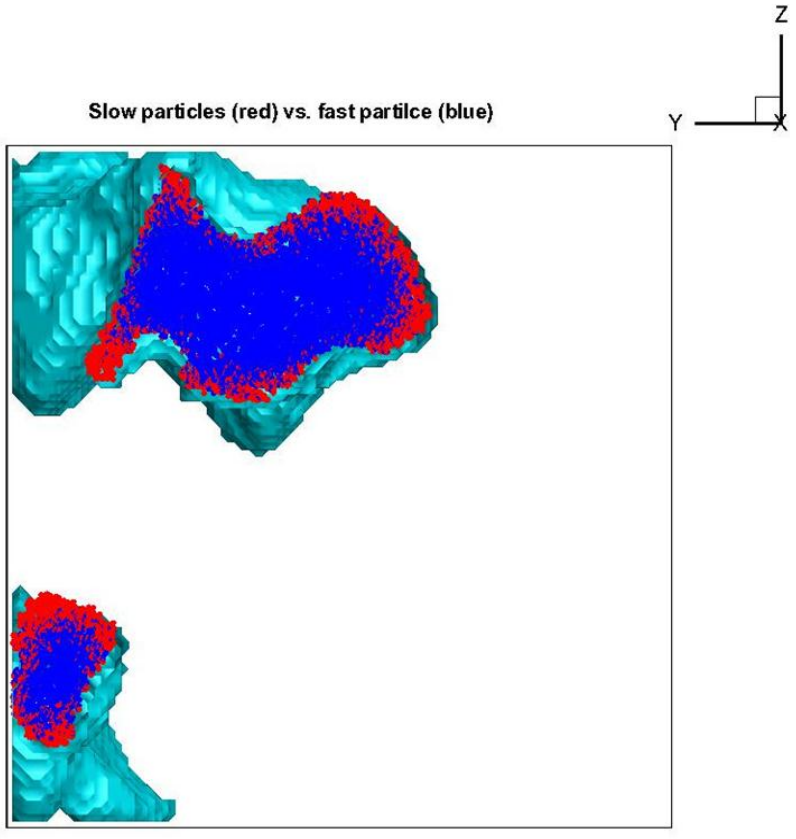

Figure 1- 54: (a) Snapshot of nanoparticles flow simulation[7].

1.11.1 Radial Diffusion of P-MWNT in Ottawa Sand Column

Ottawa sand F-95 of a particle size ranging 53-450 um with approximately 70% of the particles ranging between 100-140um has been used for investigation of radial diffusion possibility in sand packed column [83]. The two experiments were done using 100ppm of P-MWNT, 200ppm of GA and 1600ppm of HEC-10 in 10% API brine. The dispersion was sonicated, centrifuged and filtered the same way mentioned earlier in this chapter. Two columns 3" each packed with Ottawa sand were tested. 5PV of dispersion were injected into the two columns and collected accordingly. The only difference was stopping the flow right after the 5th PV for 24 hrs and then continuing to inject brine. The 24hrs stop was made to allow for radial diffusion if any. Figure 1-55 shows the normalized concentration of P-MWNT and the cumulative recovery.

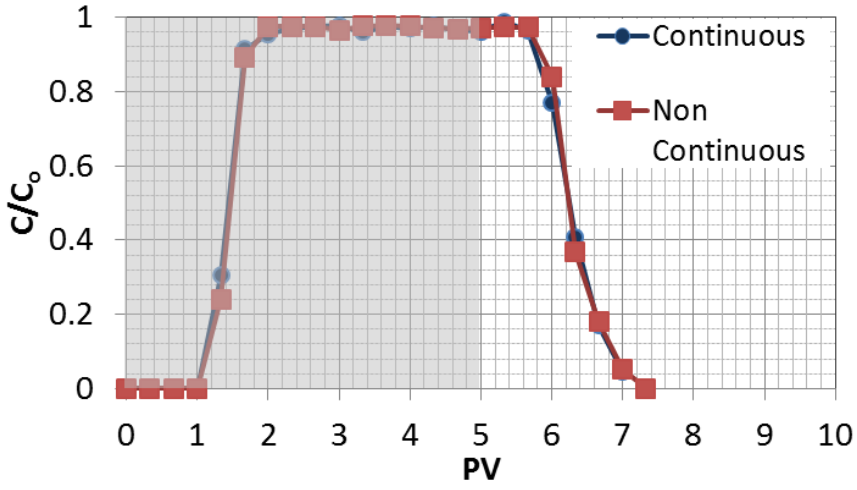

[7] Ongoing simulation effort by the research team (Dimitrios Papavassiliou and others).

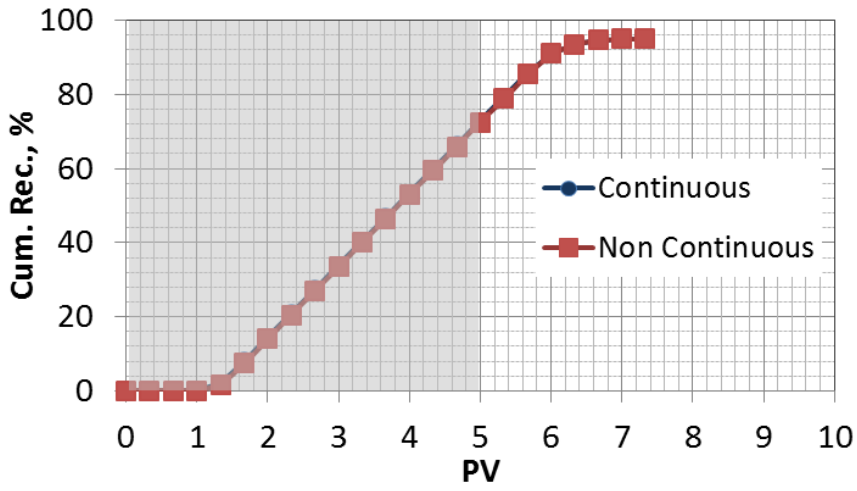

Figure 1- 55: Normalized concentration [top] and cumulative recovery [bottom] corresponding to P-MWNT injection through Ottawa sand.

It was observed that the normalized concentrations and cumulative recoveries for both runs were very similar. The total recovery for both cases was 95.0% which suggests no further interaction between nanohybrids and Ottawa sand particles during the 24 hrs. This can be explained by the lack of clays and dead end pores in Ottawa sand. It suggests also that an excess amount of HEC-10 polymer probably exists which is sterically preventing further nanohybrids adsorption. It is important to highlight the outstanding reproducibility of the results in spite of the 24 hrs stop. Both experiments have same normalized concentration and cumulative recovery indicating the high confidence in our column tests.

1.11.2 Radial Diffusion of P-MWNT in Berea Sand Column

The same previous experiment was repeated in a similar manner using Berea sand packing instead of the Ottawa sand and with one of the experiments the flow being stopped for 24 hrs following the 5th PV. Figure 1- 56 shows the normalized concentration and cumulative recovery for both experiments.

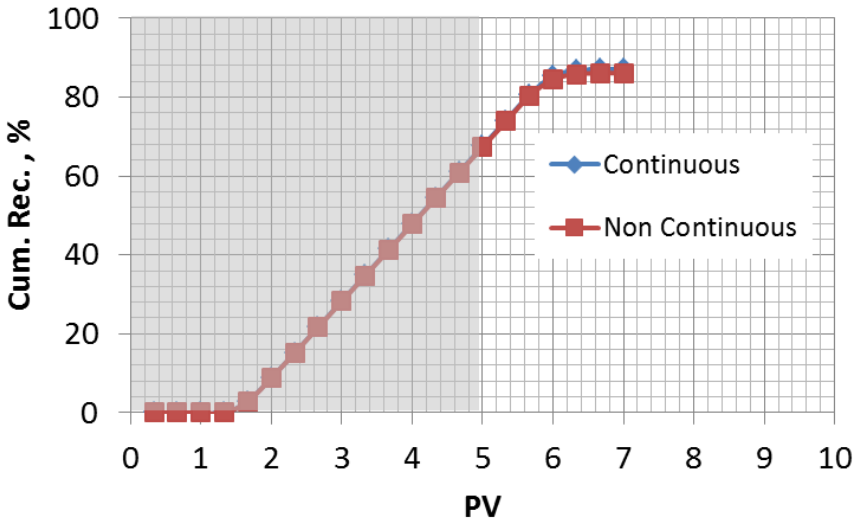

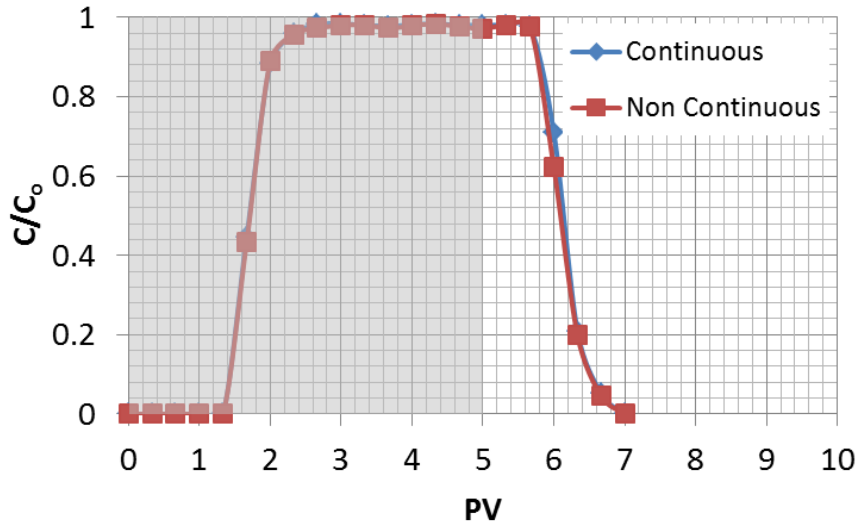

Figure 1- 56: Normalized concentration [top] and cumulative recovery [bottom] corresponding to P-MWNT injection through crushed Berea sand.

By observing Figure 1- 56, no noticeable difference was detected the two experiments particle recoveries and normalized concentration especially during dispersion injection. However, slight change is observed following the 24hrs flow stop. Enlargement of that part of the figure is shown in Figure 1- 57. The main difference in particle recovery or normalized concentration is taking place on the sixth PV due to increased retention of particles.

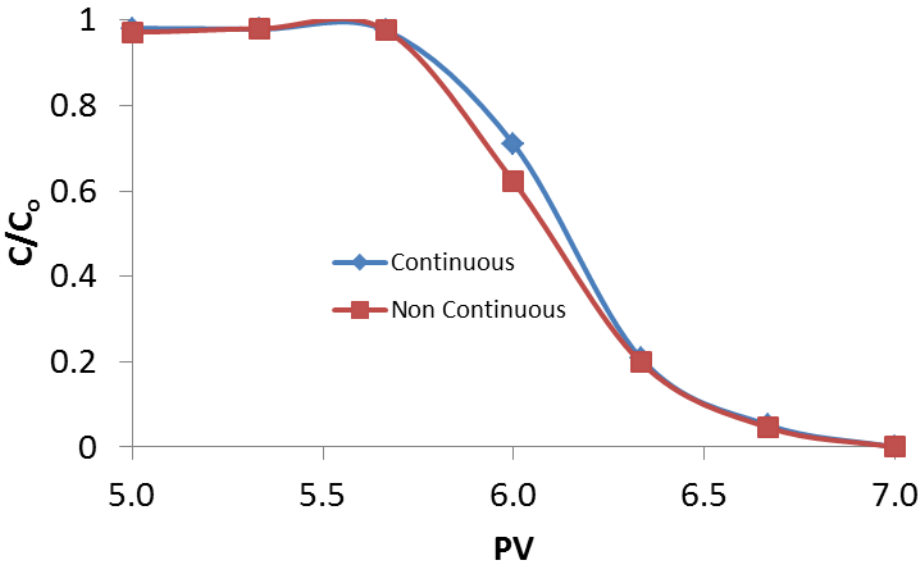

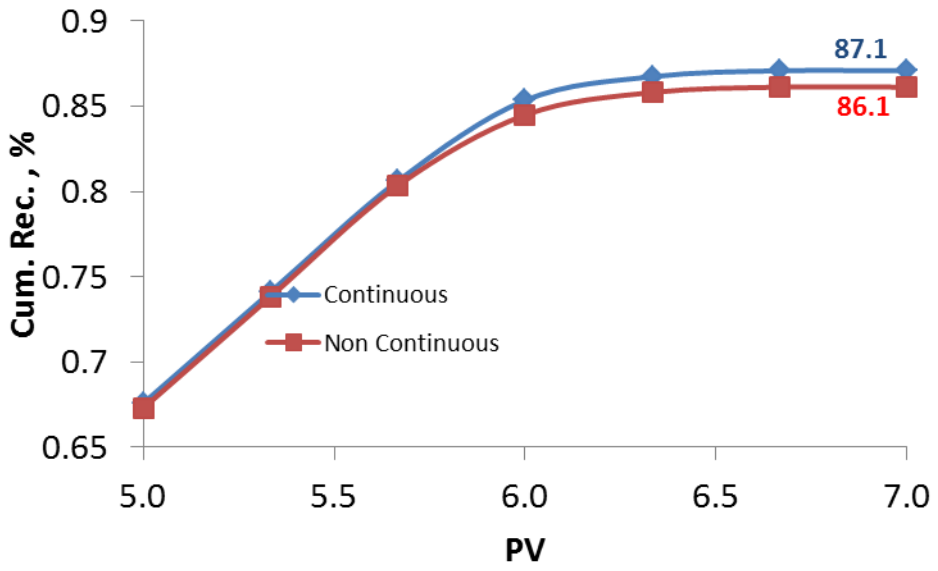

Figure 1- 57: Zoomed in normalized concentration [top] and cumulative recovery [bottom] corresponding to P-MWNT injection through crushed Berea sand.

Two more experiments have been conducted using slightly different injection sequence. The dispersion injection for non-continuous run has been done by injecting 2 PVs of dispersion, stopping the flow for 24hrs and then resuming dispersion injection for the total of 5PVs. The continuous case has also been repeated using same dispersion to avoid the minor changes in concentration that can result from dispersion filtration. Figure 1- 58 shows the normalized concentrations of these experiments. The main change observed in Figure 1- 58 is on the third PV because of the flow stoppage for 24hrs. This difference can be seen more clearly in Figure 1- 59. There are some changes that have been observed in previous figures and that is mainly due to particle adsorption to the small pores. It is suggested to repeat previous experiments in consolidated cores. Consolidated cores will have dead end pores and therefore running in such cores will

presumably reveal this phenomenon more clearly and capture the entrapment of particles inside the dead end pores.

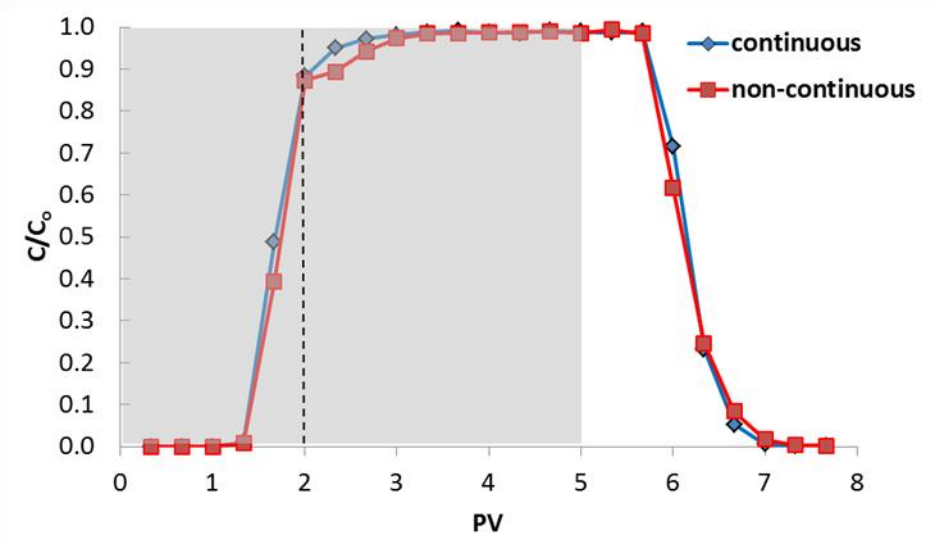

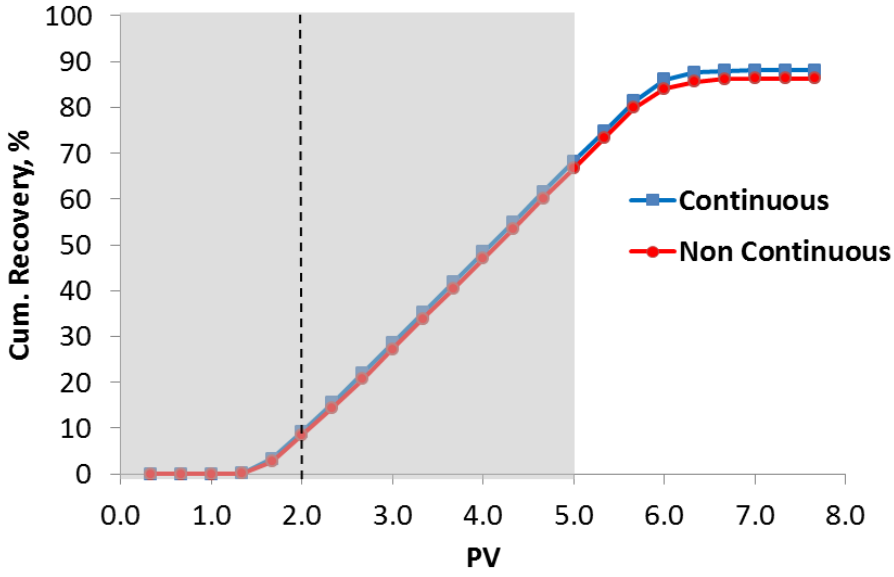

Figure 1- 58: Normalized concentration [top] and cumulative recovery [bottom] corresponding to P-MWNT injection through crushed Berea sand.

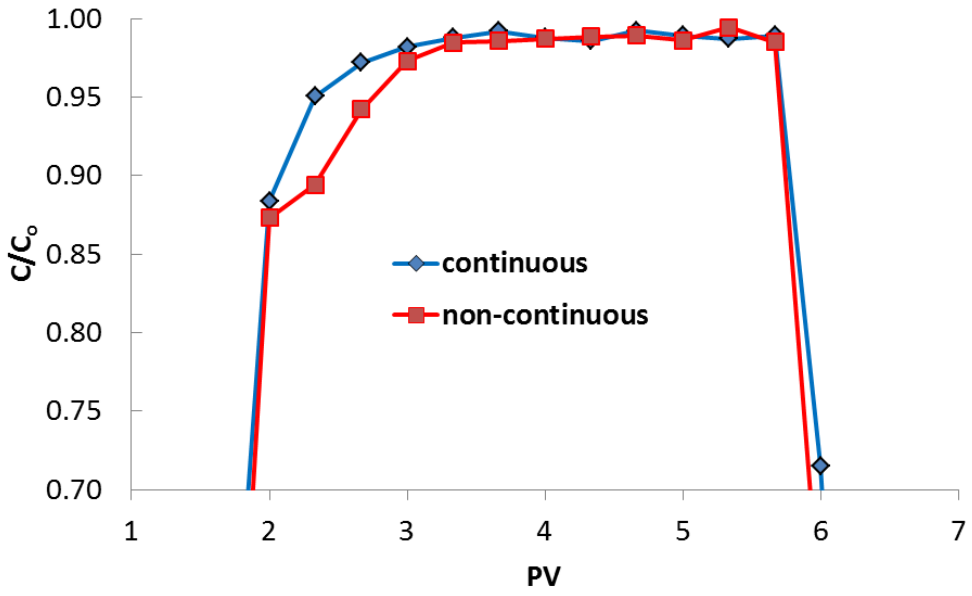

Figure 1- 59: Zoomed in normalized concentration corresponding to P-MWNT injection through crushed Berea sand.

1.12. Nanohybrids as Sensors, Contrast Agents or Tracers

Reservoir characterization is one of the main challenges for effective oil recovery. Reservoir characterization can be defined as the process for quantitatively assigning reservoir properties, recognizing geologic information and uncertainties in spatial variability [84]. One of the main focuses of this research as highlighted in the introduction is the possibility to use nanohybrids as carriers for sensors or contrast agents or to be used as tracer themselves. NMR well logging or Logging While Drilling (LWD-NMR) is one of the currently adopted technology for reservoir characterization [85]. The other technique which was suggested by Schlumberger in a recent publication to be used in similar manner as LWD-NMR is in-situ Electron Spin Resonance (ESR) [86]. Incorporating nanoparticle can revolutionize the technology significantly as will be explained later.

1.12.1. NMR Well-Logging Using NMR Sensitive Elements Loaded to Carbon Nanohybrid

Logging-while-drilling(LWD) NMR tool is being used currently by major oil service companies (e.g. Schlumberger, Halliburton and Baker Hughes) for well fluids characterization, permeability and porosity estimation for a depth of investigation(DOI) up to 16” measured from the borehole [85, 87]. Logging While

Drilling NMR tool has the potential to have the capability to detect element particles not naturally occurring in the formation with high S/N ratio at detectable concentration with real time measurements. It is suggested to attach these formation-alien element particles to nanoparticle carriers that have demonstrated ability to propagate through reservoir rock of a rock permeability of 200mD or less. Detecting changes in elemental/nanohybrids particles presence from LWD-NMR and varying concentration of injected pulses of nanoparticles can be a very useful tool to provide more detailed information through size exclusion of these nanoparticles at small pore throats in the wellbore vicinity or through tracking their movement further inside the reservoir. Figure 1- 60 shows a typical NMR signal of boron, a suggested NMR detectable element, at concentrations of few ppm [88, 89]. Figure 1- 61 shows the design of LWD-NMR.

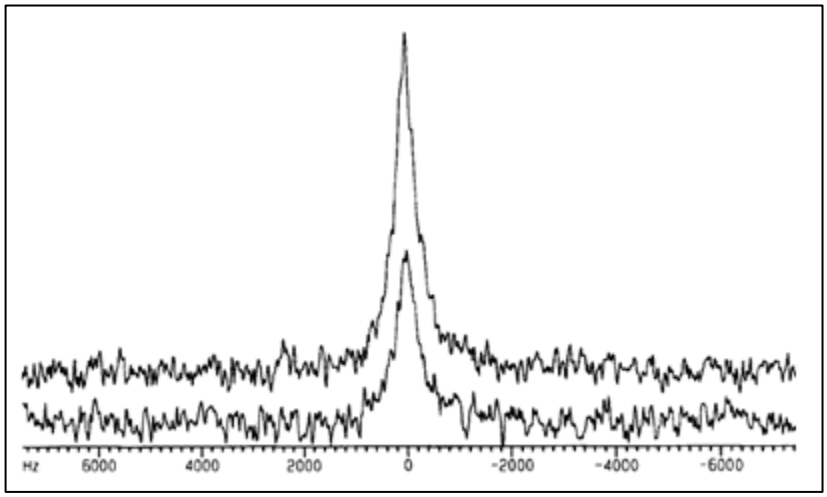

Figure 1- 60: NMR signal of ^{11}B corresponds to few ppm of concentration.

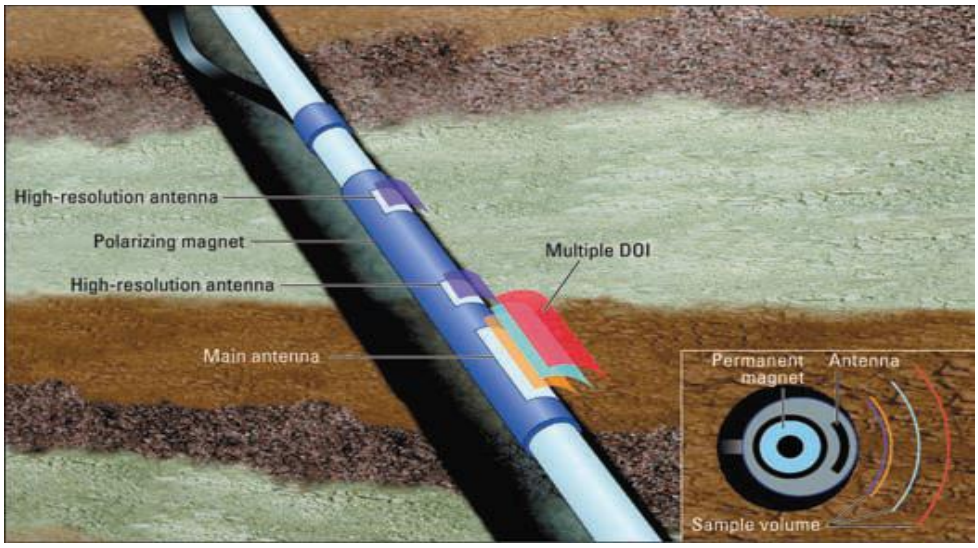

Figure 1- 61: Schlumberger magnetic resonance expert (MRX) wire line tool [85].

It was suggested to use boron as NMR sensitive element. The incorporation of boron was challenging because of the high temperature required to attach boron in contrast to other elements that require relatively mild conditions. Preparation of MWNT/B was done by mixing magnesium boride with P-MWNT at 800^{o}C under continuous flow of nitrogen. It was found that this high temperature is resulting in fusing the tubes together. Figure 1- 62 shows the SEM image where the tubes seemed to be fused together which in turns affect the ability to disperse and propagate the nanohybrids. Further investigation of this technique is necessary to find alternative methods to load boron inside tubes or finding alternative NMR sensitive element. A suggested method that has been employed is loading boron inside carbon nanotubes [90].

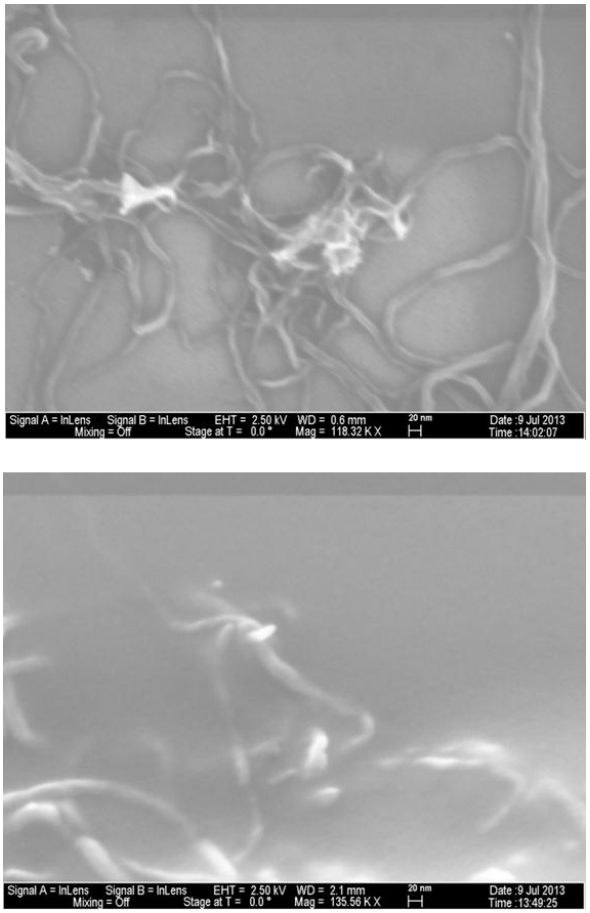

Figure 1- 62: SEM images of boron incorporated nanohybrids.

1.12.2. Electron Paramagnetic Resonance (EPR)

EPR or ESR has the potentials to be used in a similar way as NMR to detect metal species/tracers at dilutions million times lower than standard chemical tracers methods [86, 91]. The detection of free radicals by ESR has been suggested to be viable route for quantification of trace amounts of chemical species. Figure 1- 63 shows an EPR spectra provided by ACTIVE SPECRTUM to detect tempol with a concentration sensitivity as low as 1uM or 0.15ppm [92]. Tempol radical stability is

attributed to the four methyl groups sterically protecting the nitroxyl radical as shown in Figure 1- 64 [93].

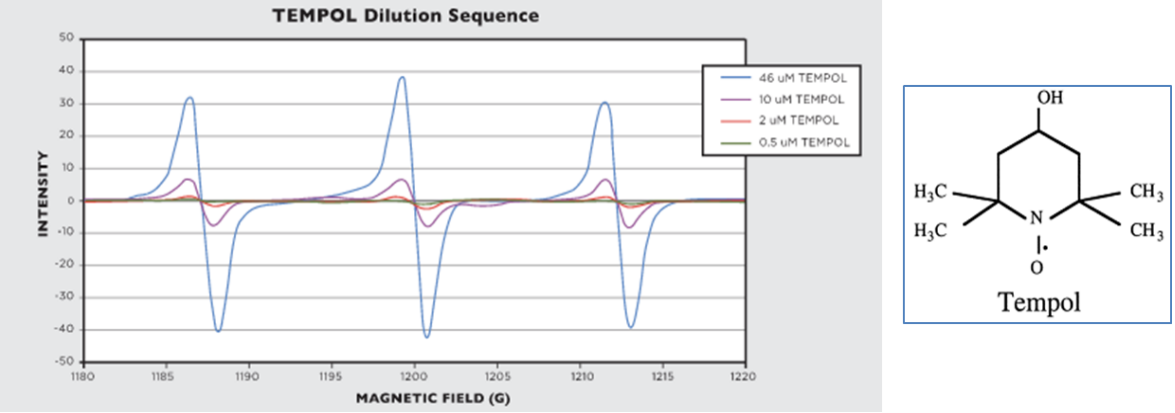

Figure 1- 63: EPR Spectra and chemical formula of Tempol.

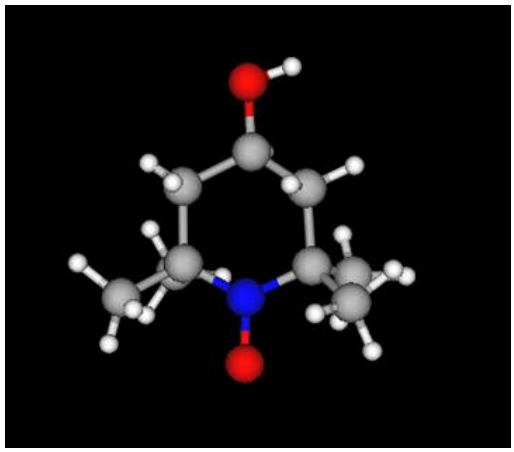

Figure 1- 64: Tempol structure showing the steric methyl group protection for the free radical generated using a ChemAxon free software (Marvin Space) [carbon=gray, oxygen=red,nitrogen=blue].

Schatz et al.(2008) reported grafting Tempo(the ring without alcohol group) into graphene coated cobalt nanoparticles for the selective oxidation of alcohol [94]. Tempol supported into C/Co nanoparticles is shown in Figure 1- 65.

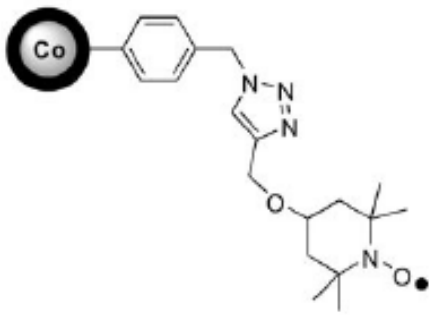

Figure 1- 65: Tempo supported on C/Co nanoparticles [94].

In a similar manner, it is suggested to use similar way to graft Tempo into CNT. Figure 1- 66 shows suggested reaction based on the similar work of Schatz et al.(2008). From left the reactant is azidomethyl benzene functionalized CNT, the product is tempol crafted into nanotube.

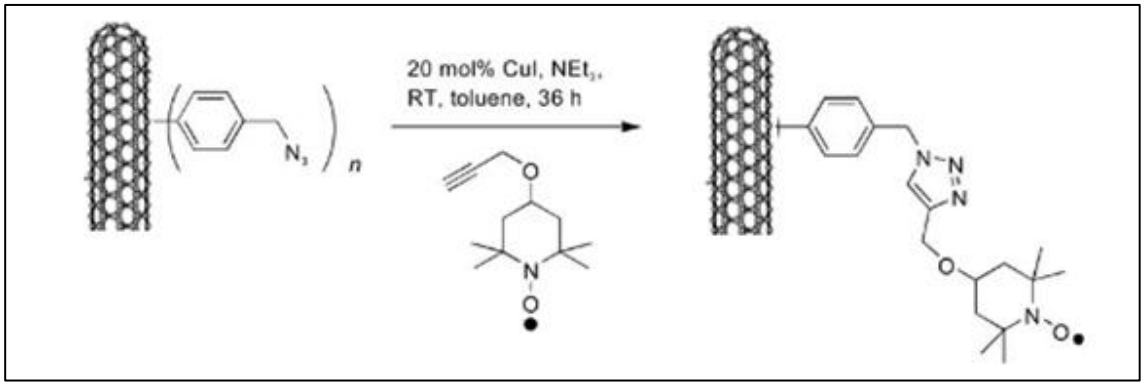

Figure 1- 66: Suggested reaction for crafting tempol into CNT.

Resasco et al. (2005) reported the nanotube functionalization with 4-hydroxymethylaniline[HMA] which can react further with hydrogen azide to produce the azidomethyl functionalized nanoparticles shown on the left side of the reaction [94,95]. Propargyl ether tempo produced by the reaction of propargyl bromide with Tempol was reported elsewhere [96]. Following the reaction scheme in Figure 1- 66 should result in crafting the tempol to the nanohybrids. This reaction was not conducted due to the involvement of hydrogen azide which is an explosive liquid at room temperature and pressure [97].

An alternative route for crafting tempol into MWNT was reported by Wang et al. (2012) as shown in Figure 1- 67. Oxidized-MWNT reacts with thionyl chloride to produce COCl-MWNT. COCl-MWNT reacts with tempol to replace the chlorine and produce Tempo-MWNTs.

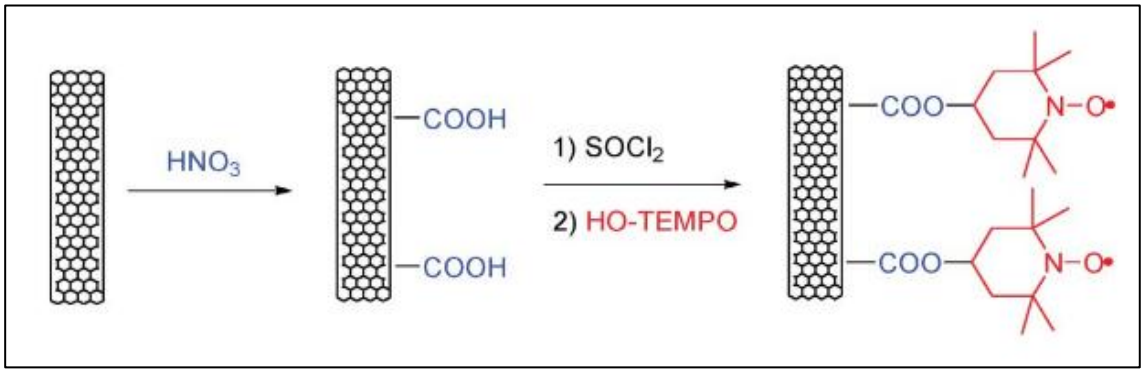

Figure 1- 67: Crafting Tempol onto MWNTs [98].

1.12.2.1 Procedure

1g of P-MWNT was treated with 75mL nitric acid at 80^{o}C under reflux conditions and stirring to generate carboxylic acid groups on the surface. The reaction

mixture was cooled down and filtered using polycarbonate filter and the acid was discarded. The solid material was washed with deionized water multiple times and then suspended in DI water and sonicated for 10 minutes and then filtered again. This procedure was repeated until the pH of the filtrate was close to 7. Oxidized-MWNT was dried overnight in vacuum oven at 80^{o}C. 0.5g of oxidized-MWNT was placed in 100mL flask and with a stirring bar and 1mL of dimethylformamide (DMF) and 50mL of thionyl chloride. The mixture was heated to 65^{o}C under reflux conditions and a gas trap filled with 500mL of 0.01M sodium hydroxide. The mixture was washed with anhydrous tetrahydrofuran (THF) and dried under vacuum at room temperature. Figure 1- 68 shows the reaction setup to produce COCl-MWNT. COCl-MWNT was mixed with Tempol in boiling THF for 48 hrs filtered and washed with THF multiple times and dried under vacuum. Product will be analyzed in Raman to validate the attachment of Tempo onto nanohybrids. Characterization of Tempo-MWNTs will be conducted using Raman spectroscopy with IG/ID increasing by covalently crafting Tempo to the surface of the nanotubes [98].

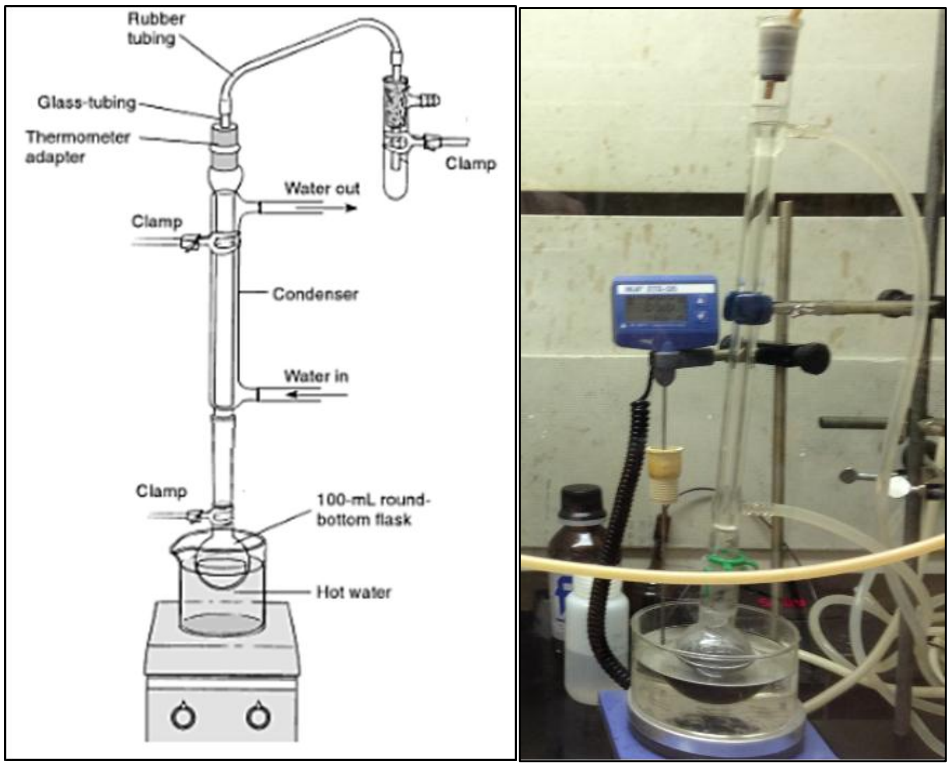

Figure 1- 68: Reaction of oxidized-MWNT with thionyl chloride setup.

1.12.3. Nanoparticles as Oil Tracer

Column studies performed earlier demonstrated an interaction between nanohybrids and oil phase inside porous media. It was found from previous column studies that a typical S_{or} is usually greater than 0.25. An injection scenario where a fraction of oil smaller than S_{or} is to be injected followed by brine flush. The S_{or} inside the column will be controlled by doing so and therefore injection of nanohybrids can have different responses depending on the amount of oil inside the porous media. Three column tests have been done. All three columns were pretreated with brine. The first one was injected with 0.2PV of oil (isopar L), the second one was injected with

0.1 PV of oil and the third one was left with oil injection. All three columns were then injected with 1PV of 100ppm of stable dispersion stabilized by GA and HEC-10. The normalized concentrations and cumulative recoveries are shown in Figure 1- 69

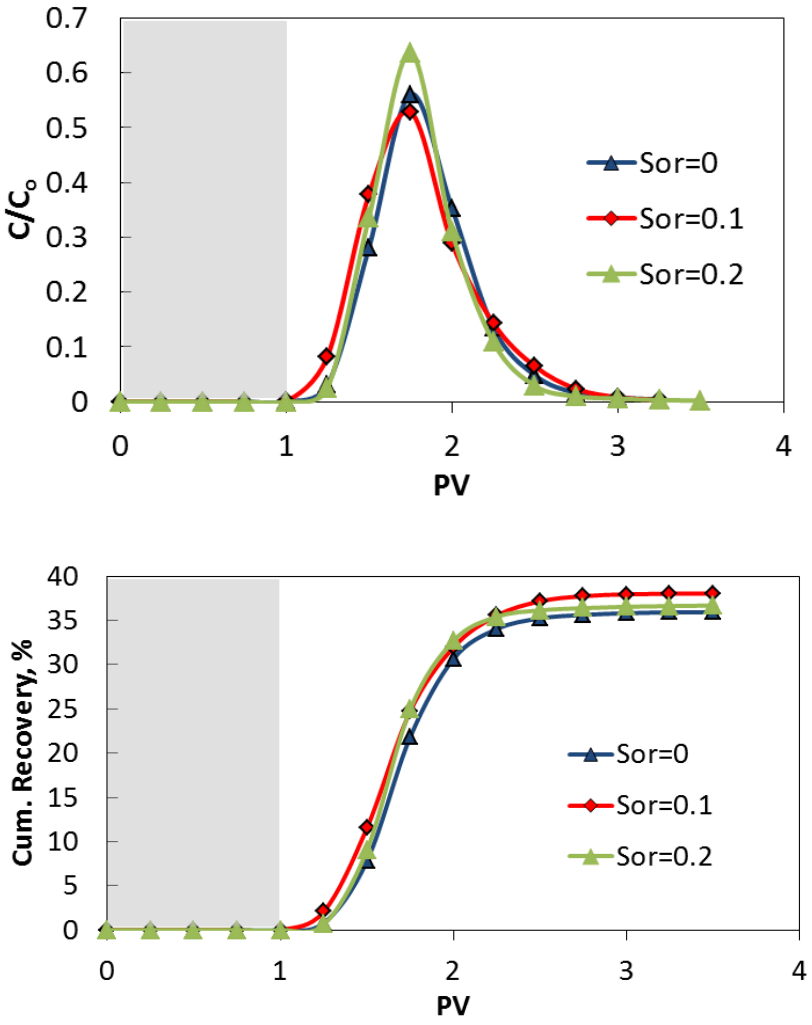

Figure 1- 69: Tracer Test using P-MWNT without flow stoppage. Normalized concentration of P-MWNT[top], cumulative P-MWNT recovery[bottom].

We can observe the highest concentration achieved at highest S_{or} is expected as the nanohybrids tend to bypass the oil and sand without interactions. The faster

breakthrough is not clearly demonstrated and the interaction between nanohybrids and oil is not evident. This is might be due to the lack of enough time for the interactions to take place and the dilution effect by back mixing inside the porous media. Previous experiments were repeated using slightly different technique, following dispersion injection, a ¼ PV of brine was injected and the flow was stopped for 24hrs. The flow of brine was resumed for 2 PVs and the effluent was analyzed. The ¼ PV of brine represent the dead volume from the entrance; that is the volume from the suction line up to the point where the flow would contact the porous media. This was done to make sure that the 1PV of nanohybrids injected is exactly inside the column. Figure 1- 70 and Table 1- 12 show that the normalized concentration and cumulative recoveries for different oil saturations. It is not obvious if the nanohybrids are actually following a specific trend. The maximum normalized concentration achieved is the highest oil saturation but that does not correspond to significant changes in oil recoveries. One of the possible explanations for this behavior is the oil phase blocking the nanohybrids access to the sand by engulfing sand particles. At the same time the oil presence is not reducing adsorption and therefore it is expected there still strong interaction between the oil phase and nanohybrids. In order to understand the extent of such phenomena another 2" sand packed column was tested by dry packing the column and allowing the oil to flow first. 1PV of oil was injected and flushed with 2PVs of brine and then 1PV of dispersion followed by ¼ PV of brine and then the flow was interrupted for 24 hrs. The flow later was resumed and the effluent was analyzed. Figure show a comparison between this test and the oil-free test. The oil

saturation in this test was found to be 0.47 and the total particle recovery was 7%. This result demonstrates the possibility of nanohybrids entrapment by the oil/water interface. Nanohybrids interaction with the oil phase can be studied further by comparing their behavior with oil wet Ottawa sand.

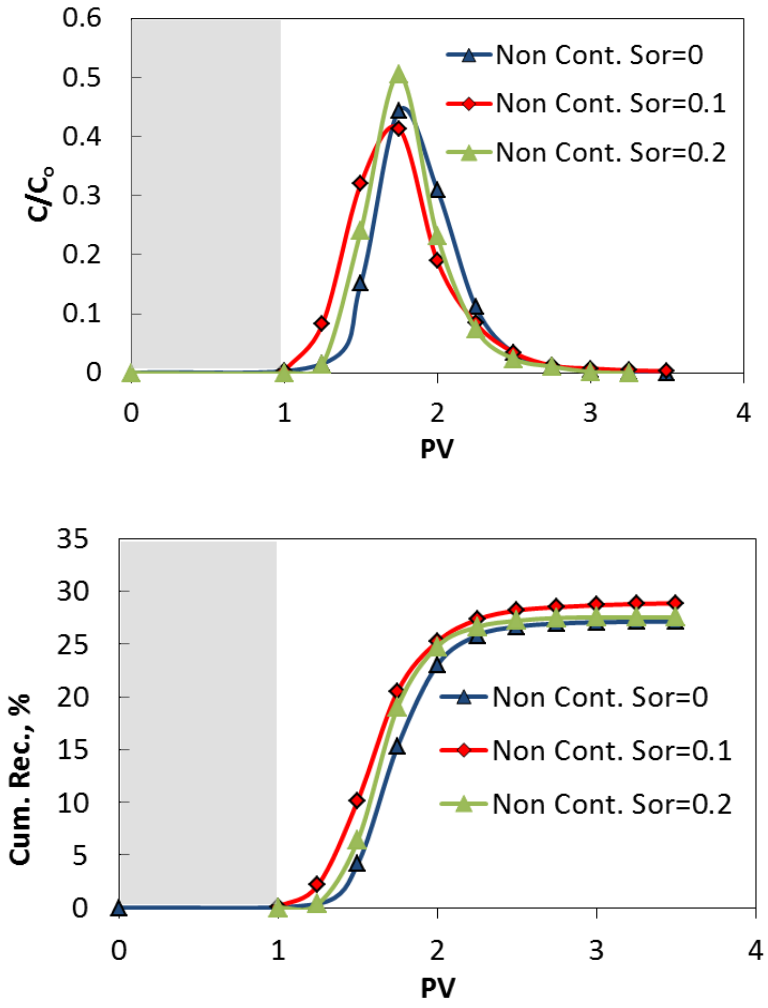

Figure 1- 70: Tracer Test using P-MWNT flow stoppage. Normalized concentration of P-MWNT [top], cumulative P-MWNT recovery [bottom].

Table 1- 12: Tracer test normalized concentration, cumulative recovery and adsorption values.

	Continuous			Non Continuous		
S_{or}	C/C_o max	Cum. Rec., %	Ads. (mg/g)	C/C_o max	Cum. Rec., %	Ads. (mg/g)
0	0.56	36	0.009	0.44	27	0.011
0.1	0.53	38		0.41	29	
0.2	0.63	37		0.50	28	

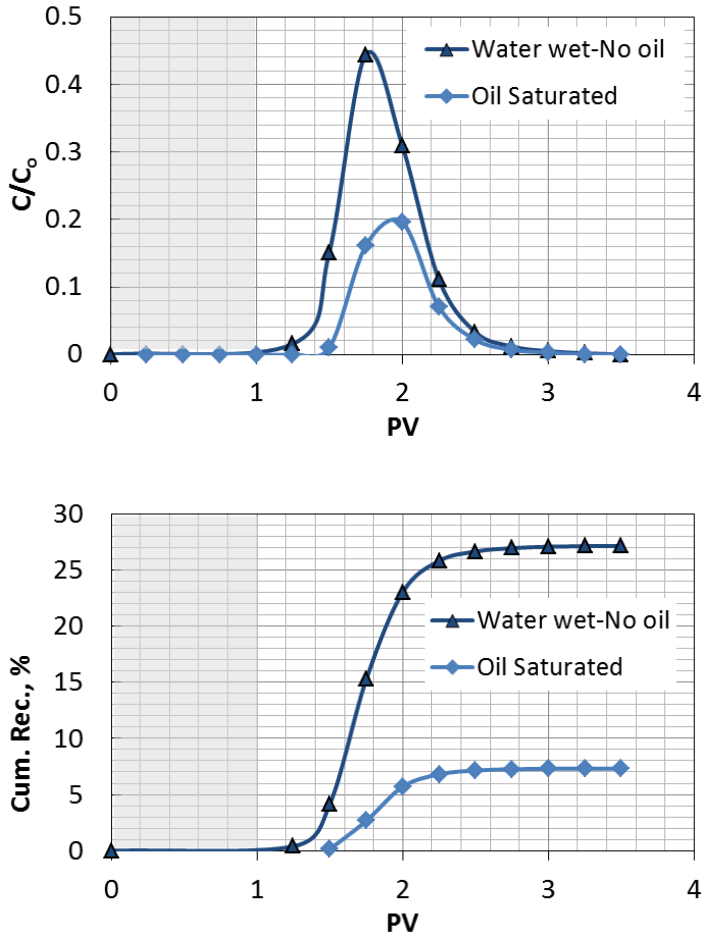

Figure 1- 71: Comparison between oil wet and oil free adsorption of P-MWNT. . Normalized concentration of P-MWNT [top], cumulative P-MWNT recovery [bottom].

1.13. Chapter Conclusions

Carbon nanohybrids have been propagated successfully in consolidated and non-consolidated porous media. Carbon nanohybrids dispersing method were found crucial for successful propagation through porous media. GA or PVP as a primary dispersant in addition to HEC-10 demonstrated outstanding ability to disperse P-MWNT. Using GA or PVP was necessary to de-bundle the tubes into dispersible ones while the HEC-10 is expected to provide steric repulsion to keep the tubes well separated in high salinity brines. GA and HEC-10 system produced better dispersion and less adsorption in comparison to PVP40 and HEC-10. The reason for that is the adsorption due to the charge of the pyrene ring in PVP. The stable dispersion of GA/HEC-10 demonstrated stability at temperatures up to 80^{o}C and 10% brine salinity. At 90^{o}C the dispersion lost it stability due to the GA aerobic degradation and HEC-10 thermal degradation. GPC studies showed that HEC-10 has a molecular weight of 500kD and little degradation corresponding to 10∼20% reduction in molecular weight can take place following two hours of sonication. Successful propagation of nanohybrids through 200mD cores advanced the research significantly towards the application side by incorporating nanohybrids into new novel applications.

The interactions of functionalized nanohybrids dispersion with oil phase inside porous media has been examined and were found that more particle retention take place in the presence of oil. This generated potential towards using nanohybrids as tracers. Using nanohybrids as surfactant carriers were also investigated towards the objective of reducing surfactant adsorption to the reservoir rock and delivering the

surfactant to the oil/water interface for chemical EOR purposes. Preliminary encouraging results were obtained and the research is still under further investigation. Attaching NMR and EPR sensitive functional groups were examined by incorporating them into current reservoir characterization methods such as LWD-NMR or LWD-EPR. As a conclusion, incorporating nanoparticles into reservoir technology is expected to have significant impact on the future of oil production industry.

References

[1] M. Kadhum, D. Swatske, B. Shiau, J. Harwell and D. Resasco, "Propagation of Interfacially Active Carbon Nanohybrids in Porous Media" *Energy and Fuels,* 2013.

[2] L. Villamizar, P. Lohateerparp, J. Harwell, D. Resasco and B. Shiau, "Interfacially Active SWNT/Silica Nanohybrid Used in Enhanced Oil Recovery" *SPE 129901,* 2010.

[3] J. Baez, M. Ruiz, J. Faria, J. Harwell, B. Shiau and D. Resasco, "Stabilization of Interfacially-Active-Nanohybrids/Polymer Suspensions and Transport Through Porous Media" *SPE Paper No. 154052,* 2012.

[4] S. Drexler, J. Faria, M. Ruiz, J. Harwell and D. Resasco, "Amphiphilic Nanohybrid Catalysts for Reactions at the Water/Oil Interface in Subsurface Reservoirs," *Energy and Fuels, 26,4,* vol. 26, no. 4, pp. 2231-2241, 2012.

[5] A. Fletcher and J. Davis, "How EOR Can be Transformed by Nanotechnology" *SPE 129531,* 2010.

[6] J. Faria, M. Ruiz and D. Resasco, "Phase-Selective Catalysis in Emulsions Stabilized by Janus Silica-Nanoparticles" *Adv. Synth. Catal.,* vol. 352, no. 14-15, pp. 2359-2364, 2010.

[7] F. Caldelas, M. Murphy, C. Huh and S. Bryant, "Factors Governing Distance of Nanoparticle Propagation in Porous Media" *SPE 142305,* 2011.

[8] N. Ogolo, O. Olafuyi and M. Onyekonwu, "Enhanced Oil Recovery Using Nanoparticles" *SPE Paper No. 160847,* 2012.

[9] T. Zhang, A. Davidson, S. Bryant and C. Huh, "Nanoparticle-Stabilized Emulsions for Applications in Enhanced Oil Recovery" *SPE 129885-MS,* 2010.

[10] T. Zhang, D. Espinosa and K. Yoon, "Engineered Nanoparticles as Harsh-Conditions Emulsions and Foam Stabilizers and as Novel Sensors" *SPE 21212-MS,* 2011.

[11] E. Rodriguez, M. Roberts, H. Yu, C. Huh and S. Bryant, "Enhanced Migration of Surface-Treated Nanoparticles in Sedimentary Rocks" *SPE 124419-MS,* 2009.

[12] J. Yu, J. Berlin and W. Lu, "Transport Study of Nanoparticles for Oilfield Application" *SPE 131158-MS,* 2010.

[13] B. Aminzadeh, D. DiCarlo, D. Chung, S. Bryant and C. Huh, "Effect of Spontaneous Formation of Nanoparticle Stabilized Emulsion on the Stability of a Displacement" *SPE paper No. 154248-MS,* 2012.

[14] P. McElfresh, M. Wood and D. and Ector, "StabilizingNano Particle Dispersions in High Salinity, High Temperature Downhole Environments" *SPE 154758-MS,* 2012.

[15] M. Onyekonwu and N. Ogolo, "Investigating the Use of Nanoparticles in Enhancing Oil Recovery" *SPE Paper No. 140744,* 2010.

[16] M. Shen and D. Resasco, "Emulsions Stabilized by Carbon Nanotube−Silica Nanohybrids" *Langmuir,* vol. 25, no. 18, pp. 10843-10851, 2009.

[17] M. Ruiz, J. Faria, M. Shen, S. Drexler, T. Prasomsri and D. Resasco,

"Nanostructured Carbon–Metal Oxide Hybrids as Amphiphilic Emulsion Catalysts" *Chem. Sus. Chem.,* vol. 4, no. 7, pp. 964-974, 2011.

[18] S. Crossley, J. Faria, M. Shen and D. Resasco, "Solid Nanoparticles that Catalyze Biofuel Upgrade Reactions at the Water/Oil Interface" *Science,* vol. 327, no. 1, pp. 68-72, 2010.

[19] J. Hwanga, M. Eltohamya, H. Kim and U. Shin, "Self assembly of positively charged carbon nanotubes with oppositely charged metallic surface" *Applied Surface Science,* vol. 258, no. 17, pp. 6455-6459, 2012.

[20] R. Bandyopadhyaya, E. Nativ-Roth, O. Regev and R. Yerushalmi-Rozen, "Stabilization of Individual Carbon Nanotubes in Aqueous Solutions" *Nano Letters,* vol. 2, no. 1, p. 25, 2002.

[21] D. Baskaran, J. Mays and M. and Bratcher, "Noncovalent and Nonspecific Molecular Interactions of Polymers with Multiwalled Carbon Nanotubes" *Chemistry of Materials,* vol. 17, no. 13, pp. 3389-3397, 2005.

[22] V. Moore, M. Strano, E. Haroz, R. Hauge and R. and Smalley, "Individually suspended Single-Walled Carbon Nanotubes in Various Surfactants" *Nano Letters,* vol. 3, no. 10, pp. 1379-7382, 2003.

[23] M.J. O'Connell, P. Boul, R.E. Smalley et al. "Reversible Water Solubilization of Single-Walled Carbon Nanotubes by Polymer Wrapping" *Chemical Physics Letters,* vol. 342, no. 3-4, pp. 265-271, 2002.

[24] P. Hiemenz, Principles of Colloid and Surface Chemistry, 1977.

[25] H.L. Bohn and B.L. McNeal "A qualitative derivation of the diffuse double layer" *Journal of Agronomic Education,* vol. 12, pp. 26-28, 1983.

[26] M. Sharma and T. Yen, "Interfacial Electrochemistry of Oxide Surfaces in Oil-Bearing Sands and Sandstones," *Journal of Colloid and Interface Science, Vol. 98, No. 1, March 1984,* vol. 98, no. 1, pp. 39-54, 1984.

[27] M. Kadhum, D. Swatske, B. Shiau, J. Harwell and D. Resasco, "Propagation of Interfacially Active Carbon Nanohybrids in Harsh Reservoir Conditions," *in press,* 2013.

[28] M.E. Crocker "Wettability and Adsorption Characteristics of Crude-Oil Asphaltene and Polar Fractions" *Journal of Petroleum Technology,* p. 470, 1988.

[29] P. Churcher, P. French, J. Shaw and L. Schramm, "Rock Properties of Berea Sandstone, Baker Dolomite, and Indiana Limestone" *SPE 21044,* 1991.

[30] E. Donaldson, R. Kendall, B. Baker and F. Manning, "Surface-Area Measurement of Geologic Materials" *SPE Journal,* vol. 15, no. 2, pp. 111-116, 1975.

[31] R.F. Scheuerman "Guidelines for Using HEC Polymers for Viscosifying Solids-Free Completion and Workover Brines" *Journal of Petroleum Technology,* vol. 35, no. 2, pp. 306-314, 1983.

[32] S. Attal, R. Thiruvengadathan and O. Regev, "Determination of the Concentration of Single-Walled Carbon Nanotubes in AqueousDispersions Using UV" *Anal. Chem.,* vol. 78, pp. 8098-8104, 2006.

[33] S. Jeong and K. Kim, "Optical absorption spectroscopy for determining carbon

nanotube concentration in solution" *Synthetic Metals,* vol. 157, no. 13-15, pp. 570-574, 2007.

[34] J. Das, N. Das and S. Bandyopadhyay, "Effect of PVP Intermediate Layer on the Properties of SAPO 34 Membrane" *Advances in Materials Science and Engineering,* 2012.

[35] M. Pattanaik, and S.K. Bhaumik "Adsorption behaviour of polyvinyl pyrrolidone on oxide surfaces" *Materials Letters,* vol. 44, pp. 352-360, 2000.

[36] R. Hodge, "HEC Precipitation at Elevated Temperature: An Unexpected Source of Formation Damage" *SPE 38155-PA,* 1998.

[37] H. ShamsiJazeyi, G. Hirasaki and R. Verduzco, "Sacrificial Agent for Reducing Adsorption of Anionic Surfactants," *SPE 164061,* 2013.

[38] E. Mubarekyan and M. and Santore, "Adsorption and Exchange Dynamics in Aging Hydroxyethylcellulose Layers on Silica" *Journal of Colloid and Interface Science,* vol. 227, pp. 334-344, 2000.

[39] Y. Dror, "Structure of Gum Arabic in Aqueous Solution" *Journal of Polymer Science: Part B: Polymer Physics,* pp. 3265-3271, 2006.

[40] M. Sabah El-Kheir, A. Yagoub and A. Abu Baker, "Emulsion-Stabilizing Effect of Gum from Acacia Senegal(L) Willd" *Pakistan Journal of Nutrition,* vol. 7, no. 3, pp. 395-399, 2008.

[41] L. Picton, I. Bataille and G. Muller, "Analysis of a complex polysaccharide (gum arabic) by multi-angle laser light scattering coupled on-line to size exclusion

chromatography and flow field flow fractionation" *Carbohydrate Polymers,* vol. 42, no. 1, pp. 23-31, 2000.

[42] W. Rashmi, A. Ismail, I. Sopyan, A. Jameel, F. Yusof, M. Khalid and N. and Mubarak, "Stability and thermal conductivity enhancement of carbon nanotube nanofluid using gum arabic," *Journal of Experimental Nanoscience,* vol. 6, no. 6, pp. 567-579, 2011.

[43] M. Liu, X. Yan, H. Liu and W. Yu, "An Investigation of the Interaction Between Polyvinylpyrrolidone and Metal Cations" *Reactive & Functional Polymers,* vol. 44, pp. 55-64, 2000.

[44] M. Pattanaik and S. Bhaumik, "Adsorption behaviour of polyvinyl pyrrolidone on oxide surfaces" *Materials Letters,* vol. 44, pp. 352-360, 2000.

[45] C. Metin, L. Lake, C. Miranda and Q. and Nguyen, "Stability of Aqueous Silica Nanoparticles Dispersion" *J. Nanopart. Res.,* vol. 13, pp. 839-850, 2011.

[46] R. Ezell, A. Ezzat, D. Horton and E. Partain, "State of the Art Polymers Fulfill the Need for High Temperature Clay-free Drill-In and Completion Fluids" *American Association of Drilling Engineers,* 2011.

[47] A. Martinez-Richa, "Variation of intrinsic viscosity in the hydrolysis of hydroxyethylcellulose, and its relationship with resistance to enzymatic degradation" *Polymer,* vol. 39, no. 14, pp. 3115-3118, 1998.

[48] C. Wu, Handbook of size exclusion chromatography and related techniques, New York : Marcel Dekker, 2004.

[49] U. Neue, "Waters Columns for SEC" in *Column Handbook for Size Exclusion Chromatography*, Academic Press, 1999, p. 325.

[50] A. Satter, G. Iqbal and J. Buchwalter, Practical Enhanced Reservoir Engineering, 2008.

[51] Z. Li, E. Sahle-Demessie, A.A. Hassan, and G.A. Sorial "Transport and deposition of CeO2 nanoparticles in water-saturated porous media" *Water Research,* vol. 45, pp. 4409-4415, 2011.

[52] A. Sattar, Y. Shum, W. Adams and L. Davis, "Chemical Transport in Porous Media With Dispersion and Rate-Controlled Adsorption" *SPE 6847,* 1979.

[53] Y. Li, Y. Wang, K.D. Pennell and L.M. Abriola "Investigation of the Transport and Deposition of Fullerene (C60)Nanoparticles in Quartz Sands under Varying Flow Conditions" *Environ. Sci. Technol.,* vol. 42, pp. 7174-7180, 2008.

[54] T. Ahmed, Reservoir Engineering Handbook, 2010.

[55] T. Ahmed, Advanced Reservoir Management and Engineering, 2nd ed., Elsevier Publications, 2012.

[56] E. Nikjoo and A. Hashemi, "Effects of non-uniform fluid saturation distribution on pressure transient analysis" *J Petrol Explor Prod Technol,* vol. 2, pp. 141-147, 2012.

[57] "Isoar L Fluid Product Summary" [Online]. Available: http://www.exxonmobilchemical.com/Chem-English/Files/Resources/isopar-summary.pdf.

[58] Z. Sun, X. Zhang, Y. Liang, and H. Li "A facile approach towards sulfonate functionalization of multi-walled carbon" *Journal of Power Sources,* vol. 191, pp. 366-370, 2009.

[59] S. Suganuma, K. Nakajima, M. Kitano et al. "Synthesis and acid catalysis of cellulose-derived carbon-based solid acid" *Solid State Sciences,* vol. 12, pp. 1029-1034, 2010.

[60] B. Srinivas, "Sulfonated carbonaceous materials". Patent US 7241334 B2, 2007.

[61] J. J. Sheng, Modern Chemical Enhanced Oil Recovery, Elsevier Inc., 2011.

[62] S. Thomas, Oil and Gas Science and Technology, vol. 63, 2008, p. 9.

[63] T. Jelmert, N. Chang, L. Hoier "Comparative study of different EOR methods" Report by NTNU 2010.

[64] C. Dang, Z. Chen, N. Nugyen, W. Bae and T. Phung, "Development of Isotherm Polymer/Surfactant Adsorption Models in Chemical Flooding" *SPE 147872,* 2011.

[65] F. Curbelo, A. Garnica, T. Dantas and E. Barros Neto, "Oil Recovery By Ionic Surfactant and Sweep Efficiency Study in Sandstones" *Brazilian Journal of Petroleum and Gas,* vol. 2, no. 1, pp. 9-16, 2008.

[66] T. Goloub, L. Koopal and B. Bijsterbosch, "Adsorption of Cationic Surfactants on Silica. Surface Charge Effect" *Langmuir,* vol. 12, pp. 3188-3194, 1996.

[67] P. Somasundaran and L. Zhang, "Adsorption of Surfactants on Minerals for Wettability Control in Improved Oil Recovery Processes" *Journal of Petroleum Science and Engineering,* vol. 52, pp. 198-212, 2006.

[68] "Upstream Innovation Symposium, 2011," Saudi Aramco, [Online]. Available: http://techquest2011.com/pdf/ReservoirEngTechnology.pdf.

[69] J. Park, G. Kim, D. Yoon, C. Sin, I. Park, T. Bea and M. Lee, "The Effect of Dispersed MWCNTs Using SDBS Surfactant on Bacterial Growth" *Engineering and Technology,* vol. 70, pp. 743-746, 2012.

[70] R. Haggenmueller, S. Rahatekar and J. Fagan et al. "Comparison of the Quality of Aqueous Dispersions of Single Wall Carbon Nanotubes Using Surfactants and Biomolecules," *Langmuir,* vol. 24, pp. 5070-5078, 2008.

[71] M. Strano, V. Moore, M. Miller et al. "The role of surfactant adsorption during ultrasonication in the dispersion of single-walled carbon nanotubes" *Journal of Nanoscience and Nanotechnology,* vol. 3, pp. 81-86, 2003.

[72] H. Zhang and H. Wu., "Role of Surfactant Adsorption in Controlling Morphology of Single-Walled Carbon Nanotubes/Polythiophene Nanohybrid" *Industrial and Engineering Chemistry Research,* 2013.

[73] O. Matarredona, H. Rhoads, Li, Z., H. J.H. and D. Resasco, "Dispersion of Single-Walled Carbon Nanotubes in Aqueous Solutions of the Anionic Surfactant NaDDBS" *J. Phys. Chem.,* vol. B107, pp. 13357-13367, 2003.

[74] Y. Tian, B. Gao and K. Ziegler, "High mobility of SDBS-dispersed single-walled carbon nanotubes in saturated and unsaturated porous media" *Journal of Hazardous Materials,* vol. 186, pp. 1766-1772, 2011.

[75] M. Islam, E. Rojas, D. Bergey, A. Johnson and A. Yodh, "High Weight Fraction

Surfactant High Weight Fraction Surfactant Nanotubes in Water" *Nano Letters,* vol. 3, no. 2, pp. 269-273, 2003.

[76] "Microemulsions & Optimum Salinity Using Novel Ethoxylates and Alfoterra Surfactants," [Online]. Available: http://www.sasoltechdata.com/MarketingBrochures/Microemulsions.pdf.

[77] Y. Wu, S. Iglauer, P. Shuler, Y. Tang and W. Goddard III, "Branched Alkyl Alcohol Propoxylated Sulfate Surfactants for Improved Oil Recovery" *Tenside Surf. Det. 47 (2010) 3,* vol. 47, no. 3, pp. 152-161, 2010.

[78] T. Nguyen, N. Youssef, M. McInerney and D. Sabatini, "Rhamnolipid biosurfactant mixtures for environmental remediation" *Water Research,* vol. 42, pp. 1735-1743, 2008.

[79] A. Witthayapanyanon, E. Acosta, J. Harwell and D. Sabatini, "Formulation of Ultralow Interfacial Tension Systems Using Extended Surfactants" *JOURNAL OF SURFACTANTS AND DETERGENTS,* vol. 9, pp. 331-339, 2006.

[80] E. Donaldson, G. Chillingarian and T. Yen, Enhanced Oil Recovery, II:Processes and Operations, Elsevier, 1989.

[81] B. Wu, B. Shiau, D. Sabatini, J. Harwell and D. Vu, "Formulating Microemulsion Systems for a Weathered Jet Fuel Waste Using Surfactant /Cosurfactant Mixtures" *Separation Science and Technology,* vol. 35, no. 12, pp. 1917-1937, 2000.

[82] P. Lin, D. Wu and Z. Zhu, "Nanoparticle Transportation and Brownian Diffusion in

Planar Jet Flow via Large Eddy Simulation" *Journal of Fluid Dynamics,* vol. 2, pp. 354-358, 2012.

[83] "http://www.sheffield-pottery.com/SILICA-SAND-p/rmsilsanf95.htm" Sheffield Pottery. [Online].

[84] R. Schatzinger and J. Jordan, in *Reservoir Charcterization: Recent Advances Vol. 71*, 1999, p. 4.

[85] F. Robert, "Advances in NMR Logging," *Journal of Petroleum Technology,* pp. 60-66, January 2006.

[86] R. Freedman, G. Krishnamurthy and R. Taherian, "Downhole micro magnetic resonance analyzer". Patent WO 2007130516 A2, 2007.

[87] [Online]. Available: http://www.petrolog.net/webhelp/Logging_Tools/tool_nmr/nmr.html.

[88] C. Vincent, H. Vincent, H. Mourichoux and J. and Bouix, "Characterization by XPS and SEM of reactive chemical vapour deposited boron carbide on carbon fibre" *journal of material science,* vol. 27, no. 7, pp. 1892-1900, 1992.

[89] J. Lao, W. Li, J. Wen and Z. Ren "Boron carbide nanolumps on carbon nanotubes" *Applied phys. Letters,* vol. 80, p. 500, 2002.

[90] R. Nakanishi, R. Kitaura, J. Warner, Y. Yamamoto, S. Arai, Y. Miyata and H. Shinohara, "Thin single-wall BN-nanotubes formed inside carbon nanotubes" *Sci. Rep.,* vol. 3, p. 1385, 2013.

[91] E. Riedel, "Tracing flow of petroleumin underground reservoirs". patent 1976.

[92] [Online]. Available: www.activespectrum.com.

[93] A. Zanocco, A. Canete and M. Melendez, "A Kinetic study of the reaction between 2-p-methoxyphenyl-4-phenyl-2-oxazolin-5-one and 2,2,6,6-tetramethyl-1-piperidinyl-n-oxide" *Bol. Soc. Chil. Quím,* vol. 45, no. 1, 2000.

[94] A. Schatz, R. Grass, W. Stark and O. Reiser, "TEMPO Supported on Magnetic C/Co-Nanoparticles: A Highly Active and Recyclable Organocatalyst" *Chem. Eur. J.,* vol. 14, p. 8262 – 8266, 2008.

[95] F. Buffa, H. Hu and D. Resasco, "Side-Wall Functionalization of Single-Walled Carbon Nanotubes with 4-Hydroxymethylaniline Followed by Polymerization of e-Caprolactone" *Macromolecules,* vol. 38, pp. 8258-8263, 2005.

[96] A. Gheorghe, A. Matsuno and O. Reiser, "Expedient Immobilization of TEMPO by Copper-Catalyzed Azide-Alkyne [3+2]-Cycloaddition onto Polystyrene Resin," *Adv. Synth. Catal.,* vol. 348, p. 1016 – 1020, 2006.

[97] "Hydrazoic Acid: General Description," United States Department of Labor, [Online]. Available: https://www.osha.gov/dts/chemicalsampling/data/CH_245950.html.

[98] Y. Wang, X. Song, S. Shao, H. Zhong and F. Lin, "An efficient, soluble, and recyclable multiwalled carbon nanotubes-supported TEMPO for oxidation of alcohols" *RSC Advances,* vol. 2, pp. 7693-7698, 2012.

[99] in *Technology, Encyclopedia of Physical Science and*, 3rd ed., vol. 18, Academic press, 2001.

[100] P. Somasundaran, Encyclopedia of Surface and Colloid Science, vol. 3, CRC Pr. LLC, p. 1858.

[101] H. Kim and D. and Burgess, "Prediction of Interfacial Tension between Oil Mixtures and Water" *Journal of Colloid and Interface Science,* vol. 241, pp. 509-513, 2001.

[102] M. Azam, I. Tan, L. Ismail, M. Nadeem and M. Sagir, "Static adsorption of anionic surfactant onto crushed Berea" *J Petrol Explor Prod Technol,* vol. 3, pp. 195-201, 2013.

[103] T. Tadros, Emulsion Science and Technology, WILEY-VCH, 2009.

Chapter 2

Enhanced Oil Recovery Using Catalytically Functionalized Carbon Nanohybrids

2.1. Review of Oil Production Phases

Abandonment of oil wells and fields that contains substantial amounts of oil is a growing energy problem. This comprises large amounts of original oil in place (OOIP) that have not been recovered by primary or secondary recovery [1, 2]. While primary recovery is mainly by natural drive energy available in the reservoir, secondary recovery is by injection of external fluids to maintain reservoir pressure, and tertiary recovery or enhanced oil recovery (EOR) is used to recover some additional fraction of the trapped oil. In optimistic production scenarios where rock and fluid properties are optimum, the recovery factor following secondary recovery is ranging from one-third to one-half of the OOIP [3] .To clarify the role of enhanced oil recovery (also called tertiary oil recovery) on oil production, Figure 2- 1 can be inspected. This figure shows a schematic representation of the effect that EOR plays in increasing oil recovery. Primary recovery usually ranges between 5-15% of OOIP. Secondary recovery will bring recovered oil up between 35-45%. Enhanced oil recovery will extract around 10% extra bringing the recovered oil up between 45-55% of OOIP. Enhanced or tertiary oil recovery can be defined as any reservoir process aiming towards changing the existing rock/oil/brine interactions in the reservoir to increase oil production. This includes: thermal recovery, miscible flooding, chemical flooding, and microbial [4]

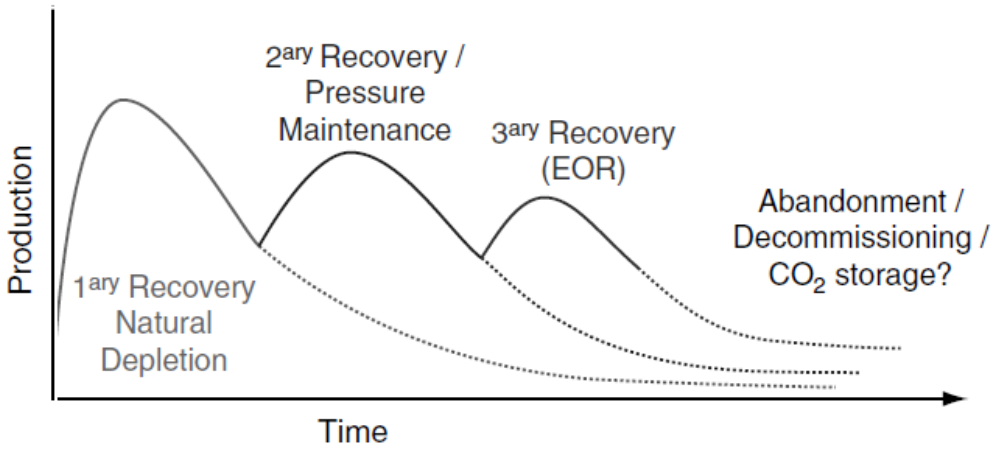

Figure 2- 1: Main phases of field production plan, adapted from Alvarado (2010) [5].

The use of nano-sized particles in enhanced oil recovery has been studied before by focusing on interfering with the nano-scale forces of columbic interaction and disjoining forces. Attempts have been made before to incorporate novel techniques in developing nano-sized materials for optimizing reservoir characterization and current EOR methods [6 - 15]

Due to the unique characteristics of carbon nanoparticles, attention and research efforts have been focused towards utilizing them in a number of fields including EOR and reservoir characterization [7]. This is done by utilizing them to carry catalytic sites to the water oil interface in an oil reservoir and or changing existing interfacial tension [8] or wettability of reservoir rock [16, 17]. The goal behind sending a catalyst to the wellbore is to bring processing to the oil, rather than to bring oil to the processing in refineries [18] in addition to increasing the amount of oil recovered.

In general, using solid nanoparticles has the advantage over surfactants for their ability to stabilize water/oil [19], water/air [20] and oil/air [21] interfaces due to their unique ability to adsorb irreversibly to the interface under inactive conditions [22].

The target of this work is to understand the full potentials of using carbon nanohybrids for oil field applications which require understanding of phenomena involved such as EOR, wettability, adsorption, catalytic conversion.

2.2. Enhanced Oil Recovery Fundamentals

Mobilization of residual oil not produced by primary or secondary recovery is influenced by two main factors: Mobility Ratio (MR) and Capillary Number (N_c). Mobility Ratio can be defined as the ratio between the displacing phase mobility and the displaced phase mobility. Mobility(λ)of a specific phase can be defined as the effective permeability(k) divided by the viscosity(μ) of that phase [23, 24]:

$$\boldsymbol{MR = \frac{\lambda_{displacing\ phase}}{\lambda_{displaced\ phase}}} \qquad \textbf{Eq. 2- 1}$$

$$\boldsymbol{\lambda_i = \frac{k_i}{\mu_i}} \qquad \textbf{Eq. 2- 2}$$

In order to prevent viscous fingering in a reservoir and maintaining good sweep efficiency, Mobility Ratio must be below unity. The other factor that affects EOR

directly is capillary number (N_c) which can be defined as the ratio between viscous forces to interfacial tension forces [25]

$$\boldsymbol{N_c = \frac{v\mu}{\sigma}} \qquad \textbf{Eq. 2- 3}$$

where

v : Darcy velocity

μ : mobilizing fluid's viscosity

σ : oil-water interfacial tension

Capillary Number at the end of a water flood process has a value of $\sim 10^{-7}$. In order to reduce the residual oil saturation to 50% of its original value, Capillary Number must be increased by three orders of magnitude [23].

Oil saturation (S_o) is defined as the fraction of pore volume occupied by the oil phase while the residual oil saturation (S_{or}) is the remaining oil trapped following secondary recovery method [26].

$$\boldsymbol{S_o = \frac{Volume\ of\ oil}{pore\ volume}} \qquad \textbf{Eq. 2- 4}$$

Wettability is another important factor that has major impact on oil recovery. Wettability can be defined as the tendency of a fluid to preferentially adhere or adsorb to a solid surface in a multi-fluid system [27]. This can be demonstrated by measuring contact angle. For instance, a drop of water will assume a position between completely spreading on a surface (infinitely water wet with a contact angle of 0^o) or

round drop resting on a surface (infinitely oil wet with a contact angle of 180^{o}) or anywhere between these extremes. The angle is measured through the dense phase. Figure 2- 2 below shows the configuration of drop for different conditions of wettability [28].

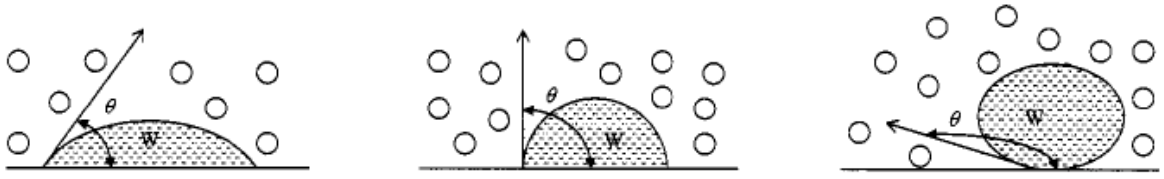

(a) Water wet (b) Neutral (c) Oil Wet

Figure 2- 2: Contact Angle schematic representation [28].

2.3. Summary of Enhanced Oil Recovery Methods

EOR includes thermal and non-thermal methods to recover oil following secondary oil recovery. These are explained briefly in the next few paragraphs. The reason for listing current EOR method is to investigate the possibilities of incorporating any of them with our nanoparticles based method for optimum oil recovery.

2.3.1. Thermal Methods

Thermal methods includes: Steam injection, and in situ combustion. The role of steam injection can be demonstrated from a viscosity stand point. A 13^{o} API oil can have a viscosity of 2,000cp at 110^{o}F and a viscosity of only 60cp at 220^{o}F. This reduction in viscosity by steam injection can increase oil recovery significantly in a typical heavy oil reservoir [29] . Moore et al. (2012) reviewed potentials for in situ

combustion in depleted oil reservoirs by air injection. The authors explained that not all depleted reservoirs are candidates for such techniques. The authors list a number of conditions for successful in situ combustion like: oil must burn at reservoir conditions, successful ignition method, and controlled flow rate of air and monitoring of produced fluids [30]. When all conditions favor combusting the oil, heat will be generated and the injection zone temperature will rise to allow more oil to be displaced from that zone and adjacent zones towards production well. It is also possible to partially oxidize some oils to generate heat without combustion [29].

2.3.2. Chemical Flooding

2.3.2.1. Alkaline Flooding

Alkaline agents aid in displacing the crude oil by raising the pH of the injected flood water. The alkaline reacts with acidic components in crude oil producing in situ surfactants at the interface that will be able to mobilize some oil [31].

2.3.2.2. Carbon Dioxide Flooding

Carbon dioxide can enhance oil recovery by extracting the light to intermediate hydrocarbons. When the pressure is high enough, CO_2 becomes miscible and it can extract wide range of HC ranging from C_2 to C_{30}. Carbon dioxide can swell the net volume of crude oil reducing its viscosity [3]. Nanoparticles can be used to catalyze a reaction that generates CO_2 such as the dissociation of ammonium carbamate or others [32].

2.3.2.3. Nitrogen Flooding

When nitrogen is injected, it can form a miscible front by vaporizing lighter oil components. This front moves away from the injection well and might become miscible. Continuous injection moves the front towards production well [31]**.** Nanoparticles can be used to stabilize foams due to their interfacial activity and therefore there is much potential for enhancing sweep efficiency inside a reservoir [33].

2.3.2.4. Polymer Flooding

In order to achieve aqueous phase mobility closely related to the oil phase one, injection of solutions with higher viscosity is desired as expressed in equations 2-2 and 2-3. This is done by adding polymers to the injected water. The polymers injected could by synthetic such as hydrolyzed polyacrylamide(HPAM) and xanthan gum or naturally occurring polymers such as guar gum, sodium carboxymethyl cellulose, and hydroxyethyl cellulose HEC [4]. Nanohybrids dispersion can increase viscosity of brine due to the presence of HEC-10 which will result in increasing N_c two to three folds and consequently oil recovery.

2.3.2.5. Microbial EOR

Microbial enhanced oil recovery (MEOR) involves the use of reservoir microorganisms or selected bacteria to produce metabolic events that leads to EOR. By

injecting nutrients with added microbes to promote in situ microbial growth and generation of products that mobilize some of the oil phase [31]. Okpokwasili and Ibiene reported 52% recovery factor using biosurfactant in unconsolidated sand column. This result achieved at biosurfactant incubation time (BIT) of 120h] [34]. Carbon nanotubes can provide control over microbial growth as nanotubes have antimicrobial activity [35].

2.4. Catalytic Conversion

Catalytically functionalized carbon nanohybrids used to stabilize water-oil interface were tested to selectively perform reactions in either phases. This was done by attaching catalytic particles to the hydrophobic side, the hydrophilic side or both sides of the nanohybrids and observing the compositional changes of both phases [19, 36]. Similar studies were done on Janus particles to perform such reactions [37].

Selective catalysis of a hydrocarbon that was suggested to be used as a representative of the oil phase is Tetralin. Tetralin (1,2,3,4-Tetrahydronaphthalene), a two ring hydrocarbon with one of the ring saturated, was tested using semi-batch reactor where partial oxidation reaction take place to produce tetralone(3,4-Dihydro-1(2H)-naphthalenone) and tetralol(1,2,3,4-Tetrahydro-1-naphthol) as shown in Figure 2- 3. This was done by creating a Pickering emulsion using sonication which was fed later to a semi-batch Parr reactor. Air was bubbled through the emulsion at 80^{o}C and 200psi. The nanoparticles used in this case to create emulsion was MWNT/alumina with 10% by weight Copper loading. Products showed selectivity towards tetralone

which reduce the interfacial tension of the oil phase making it more mobile in a reservoir-like environment [8].

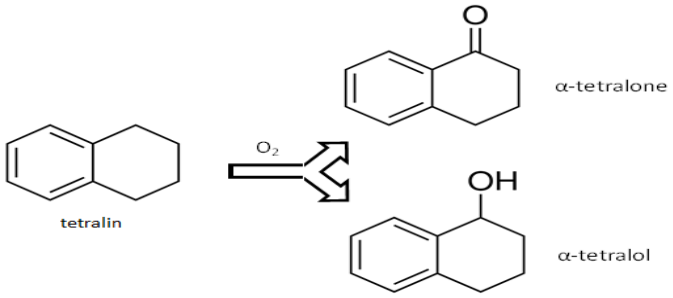

Figure 2- 3: Partial oxidation of tetralin [38].

2.5. Partial Oxidation of Tetralin

Column studies have been performed using the experimental setup designed and constructed by the author of this work. The reaction selection depends on its expected impact on increasing oil recovery. Tetralin as a representative of oil phase has been investigated before using biphasic emulsion reaction. The reaction mechanism and selectivities have been reported elsewhere [8, 38]. Drexler et al.(2012) reported that Tetralin is oxidized into tetralone and tetralol using MWNT/Al_2O_3 with 10% copper loading. The reaction product tetralone has lower interfacial tension with water in comparison to tetralin with water as the generated ketonic oxygen is exposed towards the aqueous phase increasing polarity of oil phase [8]. The reduction in interfacial tension by converting tetralin into tetralone is demonstrated in Figure 2- 4. In this figure, the IFT drops as the mole fraction of tetralone increases in a

tetralin/tetralone mixture. An exponential decay function represents the reduction in interfacial tension as shown in the fit reported by Burgess et al. [39]

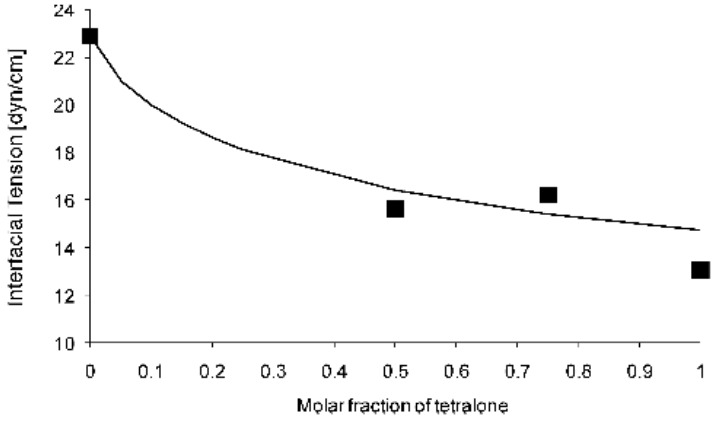

Figure 2- 4: Interfacial tension between mixtures of tetralin/tetralone and water [8].

2.6. Experimental Setup

A packed bed stainless steel flow reactor was designed to conduct partial oxidation reactions. The oil phase (tetralin) is partially oxidized to produce a ketone (tetralone) and alcohol (tetralol) by catalytic conversion as briefly mentioned earlier. Figure 2- 5 shows a schematic representation of the system and the experimental setup. The flow system consists of a syringe pump LC-5000 filled with silicon oil which fills part of pump cylinder and the accumulator. In order to pump dispersions, the pump is set to the reverse cycle and the dispersion is pulled towards the accumulator through a three way valve. After the dispersion is being pulled to the accumulator, the valve is set to the off position and the pump is set to the pumping cycle and the pressure is allowed to increase to the required system pressure. The inert silicone oil is

lighter than the injected aqueous phase and therefore only dispersion is set to continuously flow into the reactor during reaction. The system is connected to a Swagelok back pressure regulator. Once the pressure is the same as the one inside the column, the valve is open and the dispersion is allowed to flow towards the column. The column is a Swagelok stainless steel pipe of 1" OD and variable length depending on the experimental requirement. The column is filled with packing (Hi-Sil silica, glass beads, or crushed Berea sand) and the two ends of the column sealed with 51□m size mesh obtained from Spectrum Laboratories. The column is positioned inside a Thermcraft furnace (XST-3-0-12-V) with a maximum heating temperature of 1100^{o}C. The control unit for the oven is Omega Controller (CN3251-R). Reacting and inert gases are allowed to flow using three mass flow controllers to provide nitrogen or air depending on experiment requirement. The effluent is collected inside a cylinder where liquid is separated from gas. Gas is vented out through a backpressure regulator and the liquid is allowed to flow into another cylinder where it is collected and sampled out frequently. A number of packing have been tested such as glass beads, HiSil200, and crushed Berea sandstone with a number of particle size ranges. The system is pressurized usually using nitrogen. The total pressure was kept at 300psi and the temperature at 90^{o}C. Simultaneous or alternating air and dispersion are set to flow towards the column.

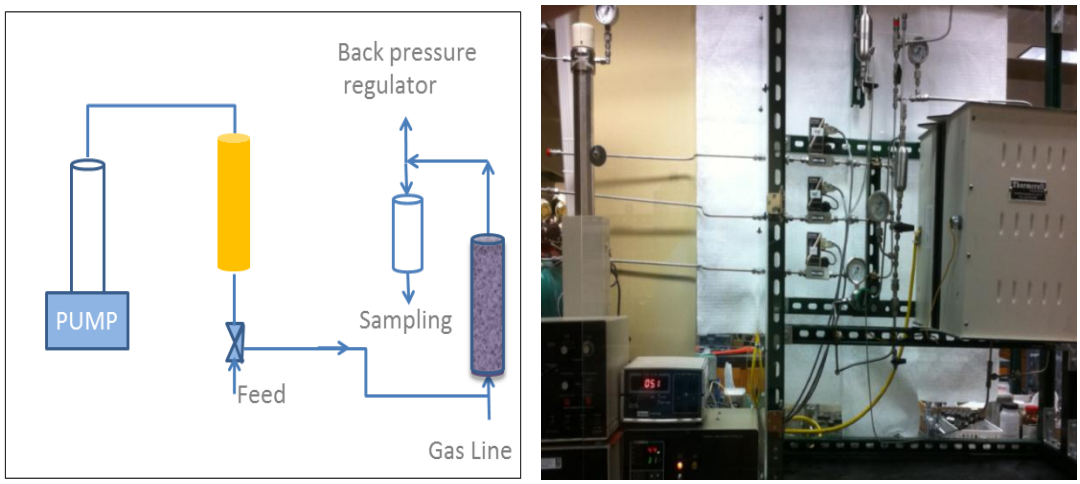

(a) (b)

Figure 2- 5: (a) schematic representation of experimental setup (b) Experimental setup.

2.7. Catalyst Preparation, Characterization, and Dispersion Preparation

MWNT/alumina or purified multi-walled nanotubes (P-MWNT) have been impregnated with catalyst using incipient wetness method in similar way as the one reported by Garcia et al. [40]. The nanohybrids have been obtained from South West Nanotechnology (SWeNT). Copper (II) nitrate was obtained from Sigmaaldrich. Copper nitrate was dissolved in DI water and was added to the nanohybrids drop wise. The addition of copper nitrate solution into the nanohybrids already placed inside the mortar was with continuous pistol mixing with just enough water to avoid extra wetting. The mixture is then dried overnight at 80^{o}C and calcined for 3hrs at 250^{o}C. The metal copper loading was 10% by weight. Figure show schematic representation of impregnation process. In order to characterize the nanohybrids, X-Ray diffraction (XRD) was used. The XRD spectrum showed differences due to the Cu attachment to

nanotubes as reported Xue et al. [41]. The XRD spectrum is shown in Figure 2- 7:a. It has been also shown elsewhere that the two beaks in Figure 2- 7a at $2\theta=36^{o}$ and 39^{o} correspond to copper oxides [42]. SEM images showed bright spots which indicates copper particles attached to the nanotubes as shown in Figure 2- 7b.

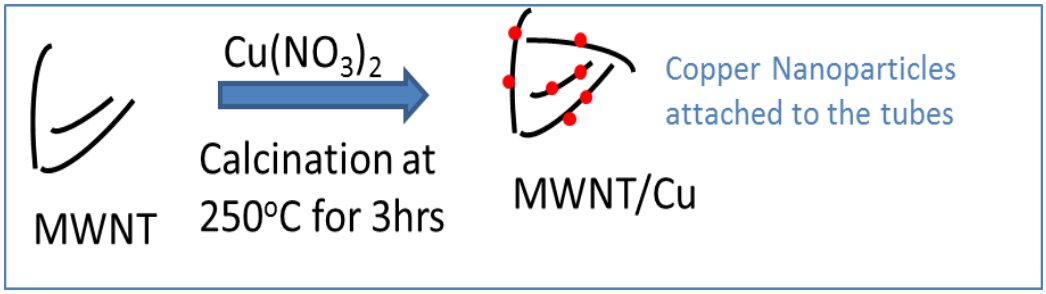

Figure 2- 6: Impregnation of copper onto MWNT.

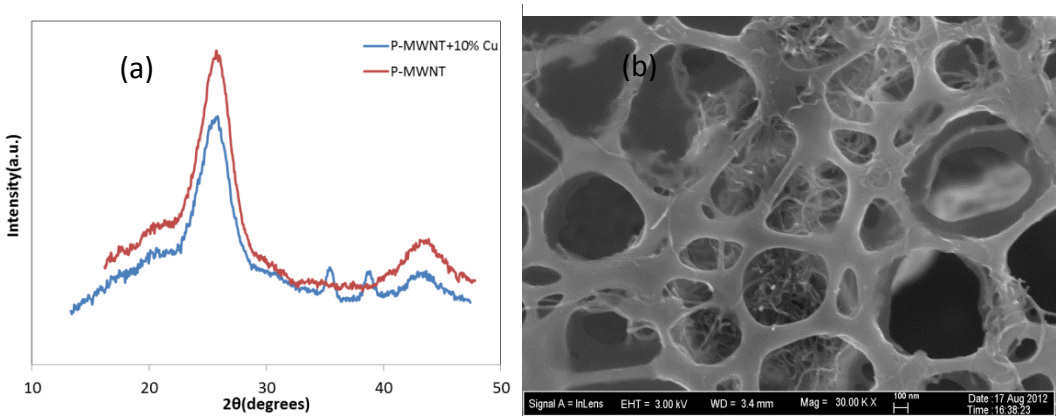

Figure 2- 7: (a) XRD of catalyzed and plain P-MWNT (b) SEM image of functionalized nanohybrids.

The catalytic nanohybrids prepared previously were dispersed in water using sonication. Because of the fast agglomeration encountered in such cases, PVP40 or GA

polymers were used as a dispersant as will be explained earlier. The nanotubes concentration was kept at 100ppm (0.1 mg/ml) and the polymer concentration was kept at 1000ppm. The dispersion was fed directly to the experimental setup. The concentrations of dispersions fed and collected were measured using UV-Vis as explained earlier in Chapter 1.

2.8. Column Flow Studies

Early attempts to partially oxide tetralin in a bed filled with 1000 micron size glass beads were unsuccessful. This is due to the fact that most of retained oil is pushed out of the column by the injected dispersion due to the high porosity or lack of pockets that can retain oil, and high permeability expected in such cases. Therefore different packing was selected to retain oil and be better representative of a reservoir similar environment. HiSil silica and crushed Berea sandstone were selected as candidates for such testing.

2.8.1. HiSil Silica Packing

The subsequent experiments were done using 5" length column packed with HiSil silica packing of a size ranging from 425-850 microns. Dispersion fed at a rate 4mL/hr into the system and the gas stream composing 10% Oxygen and 90% nitrogen with a total flow rate of 20 sccm was simultaneously allowed to flow. The total pressure was 300psi and the temperature was 90^{o}C. The product was identified and analyzed using GC-FID. The product distribution was found to be as shown in Table 2- 1. In this table, overall conversion and yield of products are reported. The

catalyst used in these experiments is MWNT/Alumina with 10% copper loading. Packed column is allowed to be saturated with oil by making the oil climb through the column through upward flow using a large syringe. The column is saturated and rinsed multiple times and the amount trapped in the column is recorded from the weight difference of oil originally used in the syringe. For this experiment, the following table can be constructed.

Table 2- 1:Conversion and yield in HiSil silica column.

RUN	Conversion%	$Y_{tetralone}$	$Y_{tetralol}$	$\frac{Y_{tetralone}}{Y_{tetralol}}$
1	11.7	8.8	4.2	2.1
2	12.4	9.4	4.4	2.1

In the previous table it was shown that the conversion is still low, possibly due to the low residence time since oil phase will float and leave the column as the incoming dispersion replaces it. Following the previous experiments, it was not fully understood if that conversion towards product would directly impact the oil recovered from the column. Therefore, in subsequent experiments, the column was water flooded first to understand the effect of partially modifying the oil phase on recovery. In such experiments, water is first injected to the column at a constant rate and the oil amount leaving the column is collected and analyzed. Once the residual oil is quantified, flow of dispersion and oxidant initiated. In this experiment, the residual oil saturation was reduced by 6% following injection of nanohybrids through the column.

Water flooding and subsequent dispersion injection can be demonstrated in Figure 2-8:. This figure defines a base case scenario for column studies in which an expected impact on oil recovery will be evident from the changes in residual oil saturation.

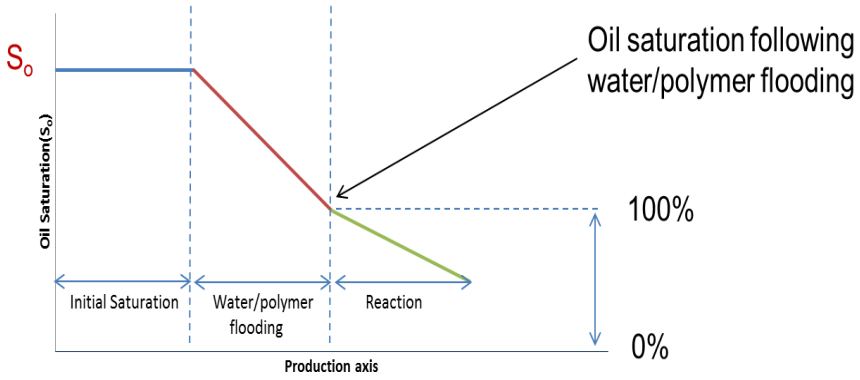

Figure 2- 8: Base case scenario for EOR column experiments.

Inspecting the results from HiSil silica packing did not provide a direct representation of reservoir rock due to the nature of this material of high porosity and affinity to water therefore switching to a different type of packing similar to the reservoir rock was expected to be of great interest.

2.8.2. Crushed Berea Sandstone

Berea sandstone was crushed manually and sieved to the desired size range. The particle size is from 75-25um. The experiment Started by injecting polymer solution of a 1000ppm of PVP40 only and then switching to dispersion at same flow

rate. The oil retained inside the bed after water flooding the bed is estimated. Any more oil leaving the bed is a result of the chemical reaction. The minute amount of oil has been analyzed using GC-FID by dissolving them in a known amount of toluene due to difficulty and uncertainty associated with visual estimation. Quantifying the whole amount of each component in the oil phase can be back calculated from composition. The total residual saturation following the water flooding for the previous setup has been reduced by 6%. Analysis of product gave the following distributions of conversions and ketone to alcohol ratio. From Figure 2- 9 the first 4 vials correspond to water/polymer flooding prior to dispersion injection.

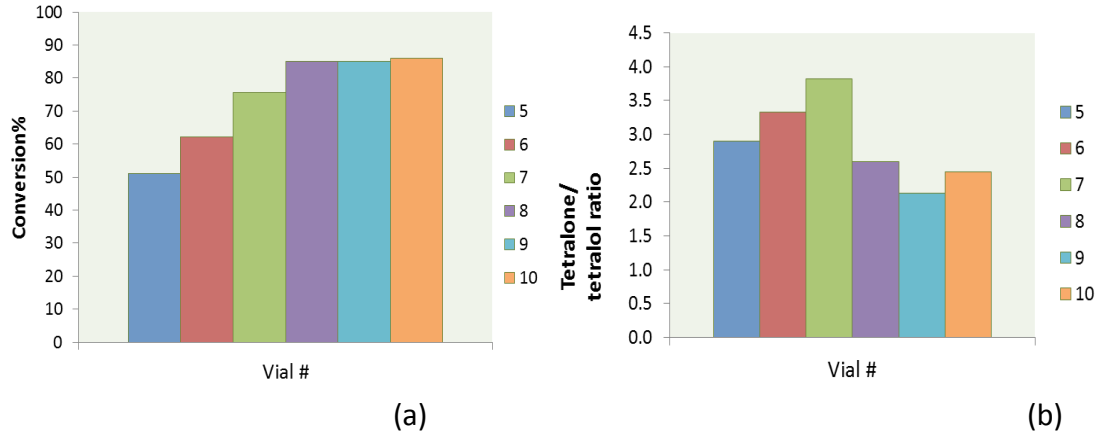

Figure 2- 9: (a) Overall conversion per vial (b) Tetralone to tetralol ratio.

The oil recovered following polymer flooding is due to the reduction anticipated in interfacial tension by the formation of oxygenates from chemical reaction. The anticipated reduction in surface tension has been explained and measured experimentally in previous works [8, 39] and shown in Figure 2- 4:. The drop

in interfacial tension is not significant enough to cause dramatic reduction in residual oil saturation. This will be discussed in further details later.

2.8.3. Anthracene Berea sandstone mixture

In order to increase the entrapment of oil inside the column longer, it is necessary to increase the lipophilicity of sand by mixing it with carbonaceous material. Anthracene which is a three hydrocarbon ring has a melting point of 212^{o}C and a boiling point of 340^{o}C has been used [43, 44]. Mixing sand with a percentage of anthracene was performed to increase entrapment of oil. The anthracene mixed with sand was 5% by weight. Oil collected from water flooding prior to catalyst injection was much less than that for a similar case of tetralin saturated column. After the injection of catalytic dispersion, only traces of oil were collected. This suggests that the reduction in interfacial tension is not significant enough to cause the oil phase detachment from the lipophilic pockets inside the column due to the anthracene presence.

2.8.4. Squalene Mixed with Tetralin

Another experiment where tetralin is mixed with viscous oil (squalene) was conducted. Squalene is 6 times more viscous than tetralin as reported [43]. More oil was trapped inside the column by doing so, however, only traces of oil left the column following reaction.

2.9. Alternating Flow of Gas and Liquid Phase

Earlier work showed in general low retention by co-flowing gas and liquid at the same time. The residual oil saturation in all these experiments was less than 0.25 in all cases. Two phase flow is expected to generate a sweeping effect inside the column and increasing pressure drop [45, 46]. The oil saturation of alternating flow of gas and liquid is around 0.5 at very low flow rate based on experimental measurement as will be explained later.

A 5" column was packed with crushed Berea sand of a size ranging between 75-250um. The column was fully saturated with tetralin (S_o=1) and connected to the column. The flow rate of nitrogen was set to 10sccm and the temperature was set to 90^{o}C. The total pressure was allowed to climb up to 300psi slowly. Once the pressure reached the set point of 300psi, flow of nitrogen stopped and flow of water with 1000ppm of GA was started. The flow was alternated in the manner and the oil leaving the column was collected until no more oil is coming out following few pore volumes of injection. The S_{or} was found to be 0.51. At any time during the experiment only one phase was allowed to flow. Figure 2- 10 shows the flow rates of different phases at any time during experiment. The different colors indicate the four different fluids injected which are (polymer, nitrogen, dispersion, and air). The flow rate of polymer solution or dispersion was 1.5mL/hr while the flow of nitrogen or air was 10sccm.

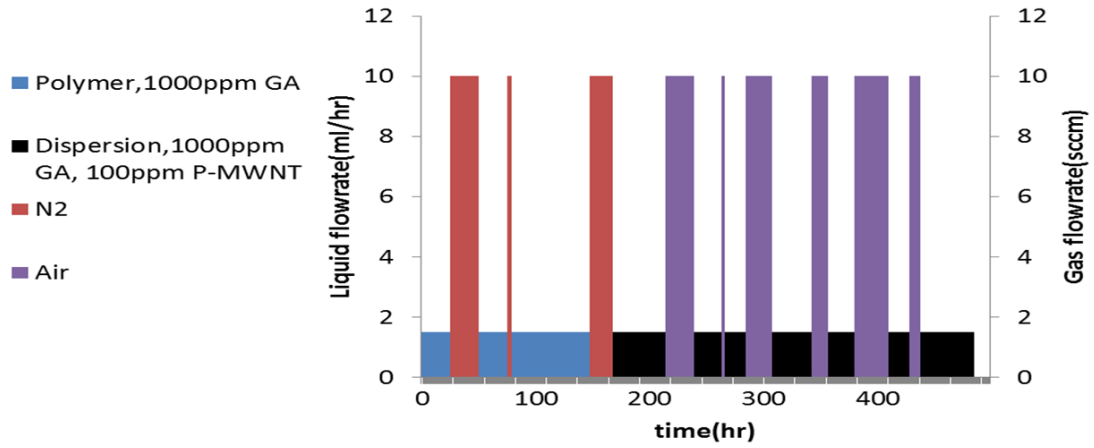

Figure 2- 10: Alternating flow chemical reaction in a Berea sand packed column.

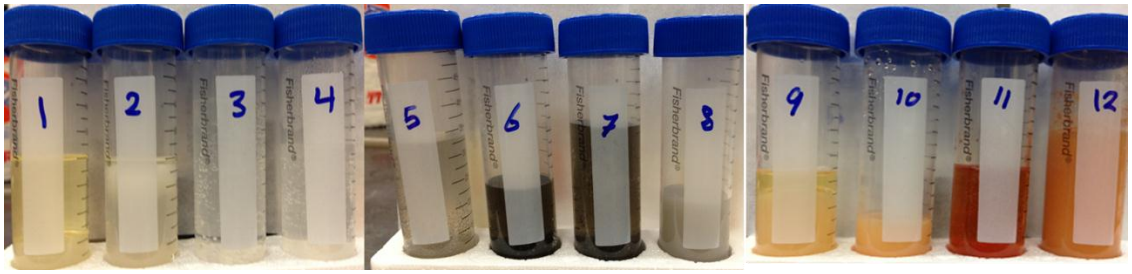

Figure 2- 11: Reaction effluent collected samples.

Figure 2- 11 shows some of the vials collected. One of the important observation from collected samples are color change for vial 6, 7 and 8 which is attributed to the black color of carbon nanotubes dispersion. The vials collected after vial 9 was red colored due to the soluble tetralone in the aqueous phase. The small amounts of oil phase collected were mixed with toluene and analyzed using GC-FID as explained earlier. It is important to mention that the dispersion is being filtered out

following vial 8 and this could be attributed to polymer precipitation or drying due to temperature and air flow inside the column resulting in dispersion filtration.

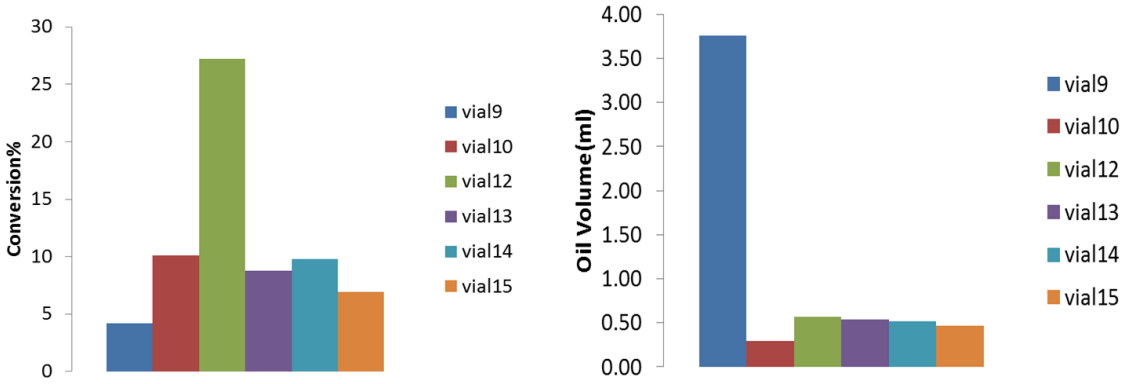

Figure 2- 12: Conversion and amount of oil collected for individual vials.

All vials showed conversion lower than what is reported earlier and some oil despite the fact that more oil was collected. Vial 9 showed around 3.5mL of oil leaving the column which is not substantiated by major oil conversion. The S_{or} by the end of experiment was found to be 0.33. This corresponds to 33% reduction in S_{or}. The amount of oil collected was very high following dispersion injection. Further experiments need to be done to confirm these findings. Although high percentage oil has been recovered in this experiment, there was unexpectedly high pressure drop ranging between 50-120 psi. Yellow residues were observed at the first half inch of the column entrance suggests precipitation of some matter. In accordance with thermal stability studies of GA mentioned in Chapter 1, it is expected that GA are blocking the flow by either degradation at high temperature or drying off by air due to alternating flow cycle.

In general, a reduction in interfacial tension by the reaction is not expected to create significant impact on oil recovery. A 100% conversion of tetralin into tetralone will only result in reducing the interfacial tension from 24 down to 14 dyne/cm (see Figure 2- 4:. This corresponds to 70% increase in N_c assuming that no change in in viscosity or flow rate occurs. This N_c increase is indeed very low to results in significant impact in oil recovery. To demonstrate a comparison between reaction and the usage of surfactant, a 10mM of surfactant can roughly results of up to 3 orders of magnitude reduction in IFT [47]. Therefore, a partial oxidation reaction is not expected to results in a significant oil recovery. However, the effect of producing tetralone might indeed have significant impact on mobility ratio. This effect is believed to be lumped into relative permeability term and could be understood by performing relative permeability experiments to quantify the significance of IFT change.

It is of importance to highlight that converting tetralin into tetralone results in an increase in density from 0.97g/cm^3 to 1.1 g/cm^3 [48]. In terms of upward flow of sweeping phase, this could results in sinking of the oil phase and although switching the flow did not result in significant impact, it is important to highlight this idea. The densities of tetralin and tetralone correspond to specific volumes of 0.136 and 0.133 L/mol respectively which is counted as minor shrinkage in the oil phase following reaction corresponds to 3% only and may have minor adverse effect to the objective of increasing oil recovery since oil will tend to shrink more inside the pores.

2.10 Conclusions and Recommendations

Reducing the interfacial tension of the oil phase by creating polar components at the water-oil interface is not expected to have great impact on oil recovery. The reduction in interfacial tension is not considered a significant contribution towards reducing capillary forces. The maximum reduction in interfacial tension resulted only in a 6% extra recovery for a pure tetralin oil phase feed. When tetralin was mixed with other viscous oils such as squalene, only traces of oil left the column following the injection of reactant gas and catalytic particles. Although oil entrapment following water flooding increased inside the column, no significant amount of oil has been recovered by performing reactions even with overall conversion approaching 80%. It is therefore suggested to modify the wettability of sand as an alternative route rather than just focusing on reducing the IFT. Combined controlled combustion with controlled reaction is also a viable route [49, 50]. A better understanding of relative permeability curve might be helpful in evaluating the possibility of performing in situ reaction.

An alternative route for increasing oil recovery is trying to perform reactions on asphaltenic molecules that are expected to have more significance on oil viscosity and/or rock wettability. Conducting hydrocracking using bi-functionalities (metallic and acidic) of nanotubes could be investigated as well [8, 51, 52].

References

[1] "Maintaining Oil Production from Marginal Fields" Report by Department of

Energy, 1996.

[2] T. Jelmert, N. Chang and L. Hoier, "Comparative study of different EOR methods," Norwegian University of Science & Technology, Trondheim, Norway, 2010.

[3] A. Satter, Practical Enhanced Reservoir Engineering, 2008.

[4] J. J. Sheng, Modern Chemical Enhanced Oil Recovery, Elsevier Inc., 2011.

[5] V. Alvarado, EOR field Planning and Development Strategies, 1st ed., Esevier Inc., 2010.

[6] A. Fletcher and J. Davis, "How EOR Can be Transformed by Nanotechnology," *SPE 129531,* 2010.

[7] M. Kadhum, D. Swatske, B. Shiau, J. Harwell and D. Resasco, "Propagation of Interfacially Active Carbon Nanohybrids in Porous Media" *Energy and Fuels,* 2013.

[8] S. Drexler, J. Faria, M. Ruiz, J. Harwell and D. Resasco, "Amphiphilic Nanohybrid Catalysts for Reactions at the Water/Oil Interface in Subsurface Reservoirs," *Energy and Fuels, 26,4,* vol. 26, no. 4, pp. 2231-2241, 2012.

[9] J. Baez, M. Ruiz, J. Faria, J. Harwell, B. Shiau and D. Resasco, "Stabilization of Interfacially-Active-Nanohybrids/Polymer Suspensions and Transport Through Porous Media," *SPE Paper No. 154052,* 2012.

[10] L. Villamizar, P. Lohateeraparp, J. Harwell, D. Resasco, and B. Shiau "Interfacially Active SWNT/Silica Nanohybrid Used in Enhanced Oil Recovery" *SPE 129901,* 2010.

[11] E. Rodriguez, M. Roberts, H. Yu, C. Huh and S. Bryant, "Enhanced Migration of Surface-Treated Nanoparticles in Sedimentary Rocks" *SPE 124419-MS,* 2009.

[12] M. Kadhum, D. Swatske, J. Harwell, B. Shiau and D. Resasco, "Propagation of Interfacially Active Carbon Nanotube Hybrids in Harsh Reservoir Conditions" *In press,* 2013.

[13] M. Shen and D. Resasco, "Emulsions Stabilized by Carbon Nanotube−Silica Nanohybrids," *Langmuir,* vol. 25, no. 18, pp. 10843-10851, 2009.

[14] C. Hwang, L. Wang, W. Lu, G. Ruan, G. Kini, C. Xiang, E. Samuel, W. Shi, A. Kan, M. Wong, M. Tomson and J. Tour, "Highly Stable Carbon Nanoparticles Designed for Downhole Hydrocarbon Detection" *Energy Environ. Sci.,* vol. 5, pp. 8304-8309, 2012.

[15] J. Berlin, J. Yu, W. Lu, E. Walsh, L. Zhang, P. Zhang, W. Chen, A. Kan, M. Wong, M. Tomson and J. Tour, "Engineered Nanoparticles for Hydrocarbon Detection in Oil-field Rocks" *Energy Environ. Sci.,* vol. 4, pp. 505-509, 2011.

[16] M. Onyekonwu and N. Ogolo, "Investigating the Use of Nanoparticles in Enhancing Oil Recovery" *SPE Paper No. 140744,* 2010.

[17] N. Ogolo, O. Olafuyi and M. Onyekonwu, "Enhanced Oil Recovery Using Nanoparticles" *SPE Paper No. 160847,* 2012.

[18] J. G. Weissman, "Review of processes for downhole catalytic upgrading of heavy crude oil" *Fuel processing technology,* vol. 50, p. 199, 1997.

[19] S. Crossley, J. Faria, M. Shen and D. Resasco," Solid Nanoparticles that Catalyze

Biofuel Upgrade Reactions at the Water/Oil Interface " *Science* vol. 327, no. 1, p. 68, 2010.

[20] B. Binks, "Particles as surfactants—similarities and differences" *Current Opinion in Colloid & Interface Science,* vol. 7, no. 1-2, p. 21, 2002.

[21] B. Binks, A. Rocher, and M. Kirkland "Oil foams stabilised solely by particles," *Soft Matter,* vol. 7, pp. 1800-1808, 2011.

[22] B. Binks, and R. Murakami "Phase inversion of particle-stabilized materials from foams to dry water" *Nature Materials,* vol. 5, pp. 865-869, 2006.

[23] S. Thomas, Oil and Gas Science and Technology, vol. 63, 2008, p. 9.

[24] S. M. Farouq Ali, and S. Thomas "A realistic look at enhanced oil recovery" *Scientia Iranica,* vol. 1, no. 3, pp. 219-230, 1994.

[25] R.A. Meyers, *Encyclopedia of Physical Science and Technology*, 3rd ed., vol. 18, Academic press, 2001.

[26] T. Ahmed, Reservoir Engineering Handbook, 2010.

[27] M.E. Crocker, "Wettability and Adsorption Characteristics of Crude-Oil Asphaltene and Polar Fractions" *Journal of Petroleum Technology,* vol. 40, no. 4, p. 470, 1988.

[28] E. C. Donaldson, Wettability, Gulf Publishing Co., 2008.

[29] T. Ahmed, Advanced Reservoir Management and Engineering, 2nd ed., Elsevier Publications, 2012.

[30] R. Moore, S. Mehta, M. Ursenbach and D. Gutierrez, "Potential for In Situ

Combustion in Depleted Conventional Oil Reservoirs" *SPE Paper No. 154299,* 2012.

[31] J. G. Speight, Enhanced Recovery Methods for Heavy Oil and Tar Sands, Tips Technical Publishing Inc., 2009.

[32] B. Shiau, T. Hsu, B. Roberts and J. Harwell, "Improved Chemical Flood Efficiency by In Situ CO2 Generation" *SPE 129893,* 2010.

[33] D. Resasco, S. Drexler, J. Harwell, B. Shiau, M. Kadhum and J. Faria, "Method and Foam composition for Recovering Hydrocarbons From a Subterranean Reservoir". Patent WO/2013/052359 , 2013.

[34] G. C. Okpokwasili, and A.A. Ibiene, "Enhancement of recovery of residual oil using a biosurfactant slug" *African Journal of Biotechnology,* vol. 5, no. 5, pp. 453-456, 2006.

[35] M. Olivi, E. Zanni, G. De Bellis, C. Talora, M. Sarto, C. Palleschi, E. Flahaut, M. Monthioux, S. Rapino, D. Uccelletti and S. Fiorito, "Inhibition of microbial growth by carbon nanotube networks" *Nanoscale.,* vol. 7, no. 5, p. 19, 2013.

[36] M. Ruiz, J. Faria, M. Shen, S. Drexler, T. Prasomsri and D. and Resasco, "Nanostructured Carbon–Metal Oxide Hybrids as Amphiphilic Emulsion Catalysts" *Chem. Sus. Chem.,* vol. 4, no. 7, pp. 964-974, 2011.

[37] J. Faria, M.P. Ruiz and D.E. Resasco, "Phase-Selective Catalysis in Emulsions Stabilized by Janus Silica-Nanoparticles" *Adv. Synth. Catal.,* vol. 352, no. 14-15, pp. 2359-2364, 2010.

[38] M. Martan, J. Manassen and D. Vofsi, "Oxidation of tetralin, α tetralol and α tetralone : Dependence of alcohol to ketone ratio on conversion" *Tetrahydron,* vol. 26, no. 15, pp. 3815-3827, 1970.

[39] H. Kim and D. Burgess, "Prediction of Interfacial Tension between Oil Mixtures and Water" *Journal of Colloid and Interface Science,* vol. 241, pp. 509-513, 2001.

[40] J. Garcia, H. Gomes, P. Serp, P. Kalck, J. Figueiredo and J. Faria, "Platinum catalysts supported on MWNT for catalytic wet air oxidation of nitrogen containing compounds" *Catalysis Today ,* Vols. 102-103, pp. 101-109, 2005.

[41] B. Xue, R. Liu, Y. Zheng and Z. Xu, "Growth and characterization of bamboo-like multiwalled carbon nanotubes over Cu/Al_2O_3 catalyst" *J. Mater. Sci.,* vol. 44, pp. 4040-4046, 2009.

[42] C.Y. Huang, A. Chatterjee, S. Liu, S. Wu and C. Cheng, "Photoluminescence properties of a single tapered CuO nanowire" *Applied Surface Science,* vol. 256, no. 11, p. 3688–3692, 2010.

[43] N. webbook. [Online].

[44] K. Charleton and E. Prokopchuk, "Coordination Complexes as Catalysts: The Oxidation of Anthracene by Hydrogen Peroxide in the Presence of VO(acac)2" *journal of chemical education,* vol. 88, no. 8, pp. 1155-1157, 2011.

[45] S. Whitaker, "Flow in porous media II: The governing equations for immiscible, two-phase flow" *Transport in Porous Media,* vol. 1, pp. 105-125, 1986.

[46] H. Qingfeng, Z. Youyi, L. Yousong and W. Rui, "Studies on Foam Flooding EOR

Technique for Daqing Reservoirs After Polymer Flooding" *SPE 151955-MS,* 2012.

[47] A. Witthayapanyanon, E. Acosta, J. Harwell and D. Sabatini, "Formulation of Ultralow Interfacial Tension Systems Using Extended Surfactants" *Journal of Surfactants and Detergents,* vol. 9, pp. 331-339, 2006.

[48] "www.sigmaaldrich.com," [Online].

[49] L. Altunina, V. Kuvshinov, S. Ursegov and M. Chertenkov, "Improved Oil Recovery of High-Viscosity Oil Pools" *Oil & Gas Science and Technology,* vol. 63, no. 1, pp. 37-48, 2008.

[50] K. Goodman, "Low temperature oxidation for enhanced oil recovery". Patent US 7,543,638 B2, 2009.

[51] A. Beltramone, D. Resasco, W. Alvarez and T. Choudhary, "Simultaneous Hydrogenation of Multiring Aromatic Compounds over NiMo Catalyst" *Ind. Eng. Chem. Res. 2008, 47, 7161–7166,* vol. 47, pp. 7161-7166, 2008.

[52] Z. Sun, X. Zhang, Y. Liang and H. Li, "A facile approach towards sulfonate functionalization of multi-walled carbon" *Journal of Power Sources,* vol. 191, pp. 366-370, 2009.

Chapter 3

Nanoparticle Stabilized Foams for Oilfield Applications

3.1 Introduction

The use of foams to increase sweep efficiency or drilling fluid control in a typical reservoir have been investigated before [1 - 3]. Surfactants and polymers are often used for stabilizing foams. Nanoparticles foams have been investigated for the possibility of replacing surfactants in that sense by adjusting the particles wettability characteristics [4 - 6]. Hirasaki et al.(2002, 2006, 2010) investigated foam mobilization in porous media using number of surfactants and found that the critical pressure drop for mobilization is inversely proportional to the square root of permeability [1, 7-9].The difference between foams stabilized by solid particles adsorption and the ones stabilized by surfactant adsorption is that surfactant adsorption is reversible while particle adsorption to the interface is irreversible under quiescent conditions when sufficient amount of particles is adsorbed [10]. Additional benefits of using nanoparticles include the less susceptibility to harsh reservoir condition and lower adsorption. Nanoparticles can endure higher reservoir temperature and salinity while many surfactants degrade appreciably at in these harsh reservoir conditions although some alpha olefin sulfonates (AOS) showed less than 10% degradation after treatment for 50 days at a temperature of 200^{o}C [11]. The adsorption of foam generating surfactants is one of the major drawbacks that have been observed in Berea sandstone [12]. The deliverability of nanoparticles through porous media has been thoroughly

discussed through all of Chapter 1. Successful propagation of nanoparticles through cores of 200mD permeability was achieved setting a foundation for developing applications where nanoparticles can play vital rule in oilfield applications. Through this part of work the possibility of generating and stabilizing foams using nanoparticles was examined. The criterion for foam stabilization in a solid-liquid–air systems is that if the sum of solid–air tension (γ_{sa}) and the solid–liquid tension (γ_{sl}) is less than the original liquid–air tension (γ_{la}). This depends on the contact angle of the particle through the liquid phase as given by the Young equation [13]:

$$\cos\theta = \frac{(\gamma_{sa})-(\gamma_{sl})}{(\gamma_{la})} \qquad \textbf{Eq. 3- 1}$$

Foams characterization methods can allow for comparing foam performance. Many techniques in the literature have been identified for foam characterization such as foam quality (Γ) and drainage rate(DR). The quality of foam was defined as [2]:

$$\Gamma = \frac{V_{gas}}{V_{total}} = \frac{V_{total}-V_{liquid}}{V_{total}} \qquad \textbf{Eq. 3- 2}$$

where V_{gas} is the volume of gas, V_{liquid} is the volume of surfactant solution used to generate the foam and V_{total} is the volume of entire foam. Quality of foam (Γ) can provide information about foamability. However, the stability of foam once generated is an important aspect as well. Foam stability can be characterized using a first order kinetic equation as shown in equation below

$$V = V_o(1 - e^{-kt}) \qquad \textbf{Eq. 3- 3}$$

where V_o is initial liquid foaming solution volume and *k* is the time constant. The drainage rate *(DR)* can be defined using the kinetic constant(k)

$$\boldsymbol{DR = \frac{kV_o}{2}} \qquad \textbf{Eq. 3- 4}$$

The half time(t_{half}) which is the time for half of the foam to be drained is also of importance in foam characterization. Although foam quality, half time and drainage rate can provide viable methods to characterize foam stabilized by materials of similar nature; all surfactant or all polymer system, it was found through the scope of this work that it is not wise to use these methods to characterize or differentiate between different kinds of foam stabilization. Therefore, throughout this chapter a simple method comprising the visual observation of normalized foam volume versus time has been used as will be explained later.

Carbon nanotubes stabilized foams can be envisioned to contribute in oil recovery as shown below. In addition to the enhancing mobility control, they can deliver catalytic particle to the oil/air interface facilitating the rate limited partial oxidation reactions by supplying catalytic particles to the already oxidant rich medium in an air enriched medium.

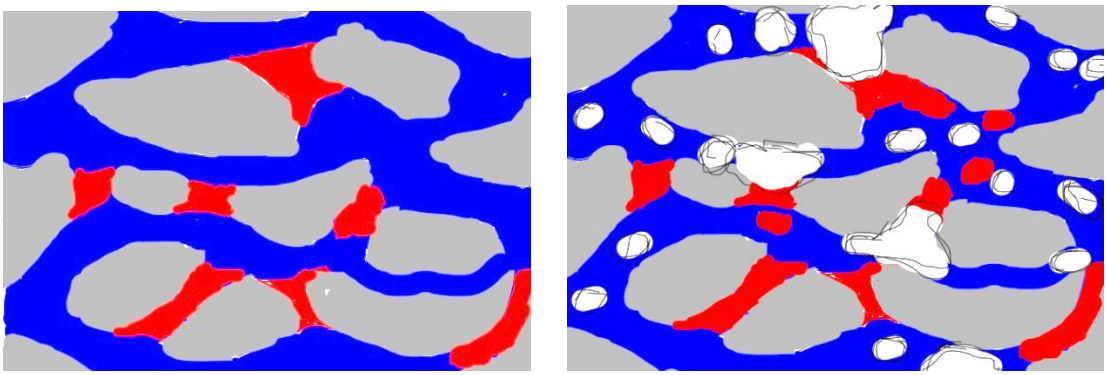

Blue: water, grey: rock, red: oil, white: foams, black: CNT, flow direction from left to right

Figure 3- 1: Envisioned effect of foam stabilization by nanoparticles on displacing oil from reservoir pores.

3.2. Foams Generated in the Lab

3.2.1. Experimental Setup for Foam Generation

Foams prepared in our labs using nanoparticles stabilized dispersion with varying concentration of particles and polymers were compared with known surfactants showed enhanced stability as will demonstrated later. Nanoparticles used in these experiments are purified multi-walled nanotubes (P-MWNT). Polymers used are HEC-10, GA, and PVP40. All experiments were performed in DI water or 10% API brine (8% NaCl and 2% $CaCl_2$). As mentioned earlier, due to the major differences in stabilization methods by using surfactants from that of polymers or nanohybrids, simple visual measurements will only be adopted for different foam comparisons through this work. In this chapter, foam stability and foamability will be compared by measuring the volume of the foam divided by the volume of the liquid that have been

used to generate this foam in RT measurements. Foam prepared using Cole Parmer mixer by mixing the initial liquid at 2000rpm for 5 minutes. Once the foam generated, it is transported to a graduated cylinder for RT visual observation.

3.2.1.1. Foam Generation in DI Water

A number of foams were generated in DI water using a sodium dodecyl benzene sulfonate (SDBS) as a surfactant , HEC-10 as a polymer, and a dispersion of nanohybrids, P-MWNT(CNT), PVP and polymer with the concentration shown in Figure 3- 2 below.

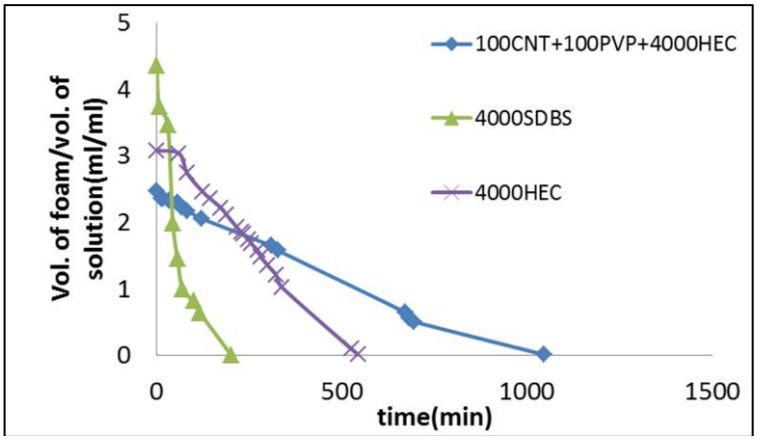

Figure 3- 2: Foams generated in DI water using surfactant, polymer and nanohybrids.

Figure 3- 2 shows the volume generated of the three mixtures used. The foam generated at t=0 reflect the foamability of the mixture while the behavior of the foam over time give indication of which foam is the most stable one. The foamability of SDBS is high initially. However, SDBS foam collapse within relatively short time (t≈3 hrs). HEC-10 foam last longer due to the higher viscosity of this polymer solution which

slows the drainage rate of the foam [14]. The foam lasted for about 9 hours. On other hand, by using carbon nanotubes the stability of the foam was much longer due to the nanotubes interfacial activity. This foam is clearly more stable than other foams since it lasted up to 18 hours. This comparison will be more evident when we discuss foams generated in brine since foams generation will be suppressed by the presence of high ionic strength (high salinity) in solution. It is important to mention that PVP presence in the previous foam has no impact on foam generation. It was used to create stable dispersion of P-MWNT prior to foam generation.

3.2.1.2. Foam Generated in API Brine

Foam stability for surfactant can drop significantly by the presence of salt. Carbon nanotubes stabilized foam showed outstanding performance as will be demonstrated later in terms of their stability in comparison to nanosilica stabilized foams reported elsewhere which can collapse in the presence of high salinity [5]. Dispersions of P-MWNT prepared previously were mixed with different surfactants, polymers to allow for evaluation of foam stability. Figure 3- 3 lists some of the experiments performed in brine. Foam was generated using the mixer according to the procedure mentioned in section 3.2.1. It was not possible to generate appreciable foam using typical surfactant as SDBS as shown in Figure 3- 2. Salt resistant polymer HEC-10 was successful in generating foam. However, the foam collapsed within 10 hours. On the other hand incorporating nanotubes during foam generation showed enhanced stability of the foam. The interfacial activity of nanoparticles can significantly

increase stability. Figure 3- 4 shows two foams one stabilized in the presence of nanohybrids while the other light colored is stabilized by HEC-10 only.

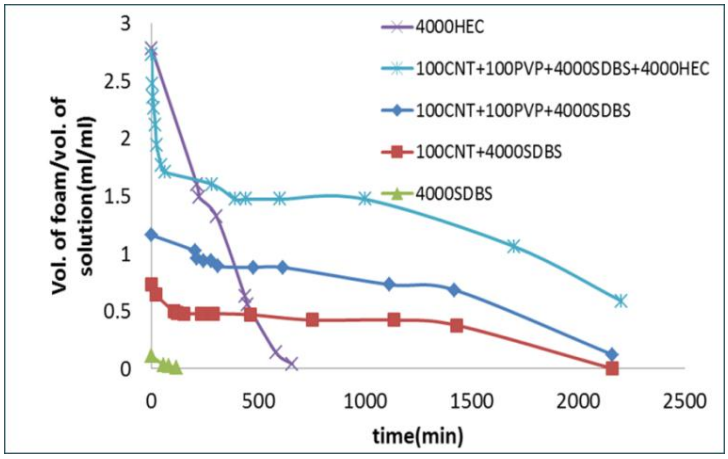

Figure 3- 3: Foams stabilized in API brine [15].

Incorporating nanoparticles in foam generation should significant improvement in foam stability. Nanoparticle size and concentration play important rule in foam stability as particle size decrease or concentration increase, foam stability increases [4]. It is expected that nanoparticles shape can play significant role in stabilizing or destabilizing foam. In this case carbon nanotubes as nano-sized cylinders with questionable definition of using equivalent diameter to model nanoparticle interactions with air/aqueous interface.

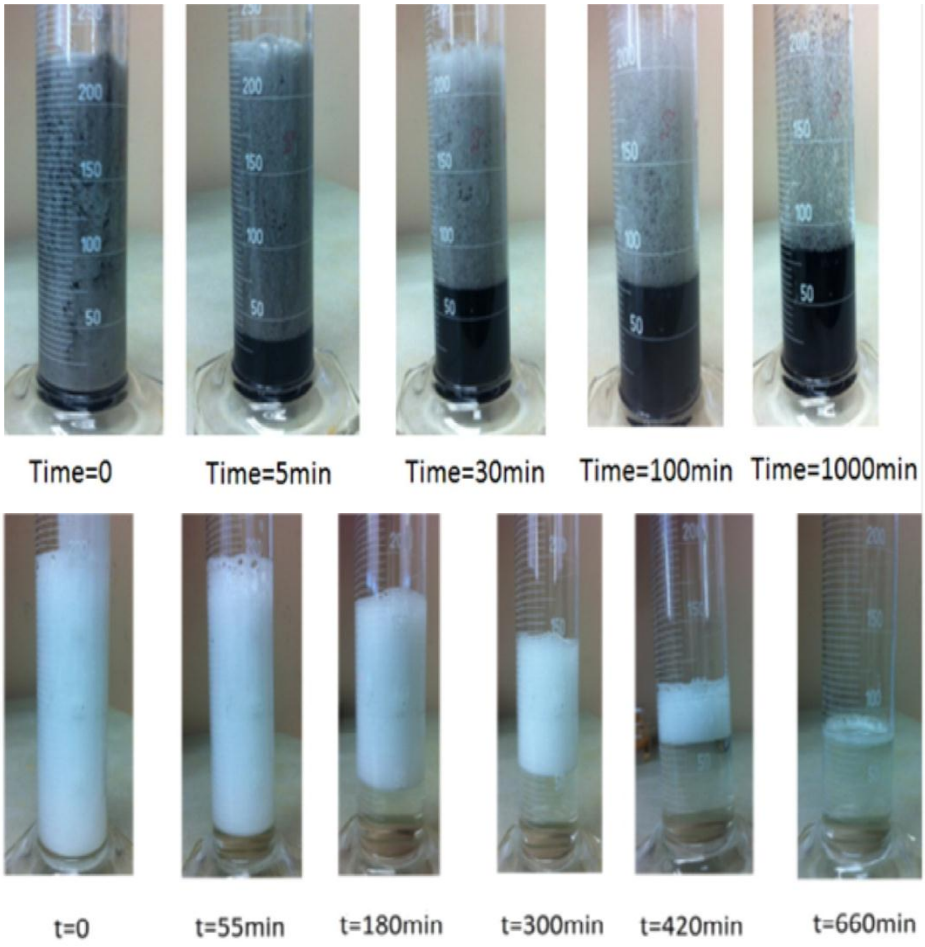

Figure 3- 4: Snapshots of foams in the presence of nanotubes(top) and HEC-10 alone(bottom)

As the length of particle is significantly larger than it is diameter, the alignment of particle with the interface might be playing vital role in increasing or suppressing foam stability. Filtration of large aggregates and polymer concentration might as well play significant role and these could be important aspects to be discussed in future work.

3.2.2. Foam-forming Surfactant and Comparison with Nanohybrids

A number of foam-forming surfactants have been investigated in the literature for the oilfield applications. These include alkyl aryl sulfonates, olefin sulfonates, petroleum sulfonates, and ethoxylated alcohols [1, 12, 16]. Table below lists some of the surfactants that have been selected to be tested for their ability to function in API brine.

Table 3-1 Commercial surfactants test for foamability in API brine.

Surfactant	Actual name, Chemical type	Applicable salinity	Producer	Foamability and foam stability in 10% API brine
POLYSTEP A-18	Sodium(C14-16) olefin sulfonate,Alpha Olefin Sulfonate(AOS)	No info	Stepan	74% quality, stable ✓
STEOL CS-330	Sodium laureth(n≥3) sulfate,alcohol ethoxy sulfate)	No info	Stepan	70% quality, stable ✓
ENORDET O332	Sodium 15-18 internl olefin sulfonate, IOS	high	Shell	50% quality, stable ✓
ENORDET J771	Alcohol alkoxy sulfate, AAS	Low/med	Shell	No foam generated ✗

From previous table, polystep A-18 generated appreciable amount of foam and therefore was adopted to be used for comparison with nanohybrids or for the synergistic possible effect of coupling this surfactant with nanohybrids. Foam stability studies of this surfactant in API brine has been conducted as shown in Figure 3- 5. Polystep A-18 can be used as well to investigate the dispersion stability as well.

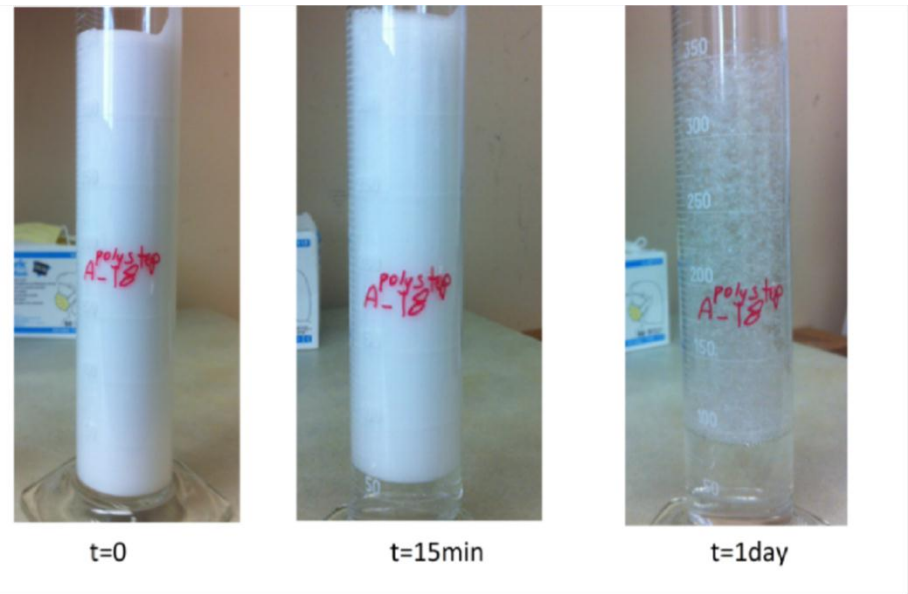

Figure 3- 5: Polystep A-18 foam stability in API brine.

3.2.3. Effect Oil Phase on Foam Stability

Early experiments done on foams stabilized by surfactants or nanoparticles showed that most foam break within two minutes by the addition of bulk oil phase. This can be explained by the effect of an oil droplet in destabilizing a foam lamella by overcoming the electrostatic or steric interaction [1].

Emulsified oil also has an adverse impact on foam stability. Solubilized oil reduces the miceller structuring and accelerate film drainage [14]. Wasan et al.(1994) reported a photo of two dimensional foam using Enordet AE1215-30 and decane where emulsion droplets drained into the plateau borders as shown in Figure 3- 6. Figure 3-6 shows that adding 10mL of emulsion has less severity on foam stability.

The emulsion is made of 1000ppm of P-MWNT and 2mL of decane and 8mL of brine. Foam in this case collapsed completely within 100minutes.

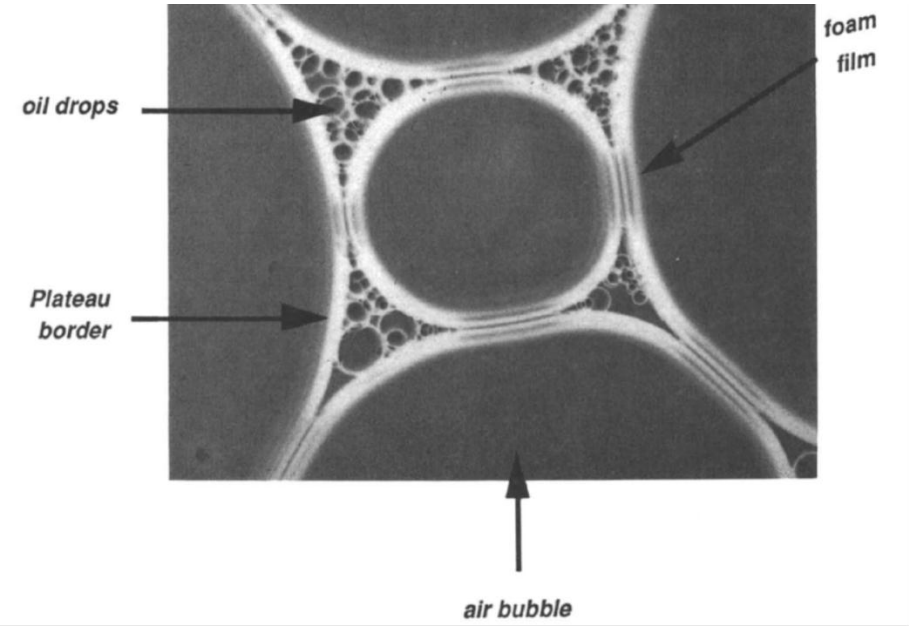

Figure 3- 6: Photomicrograph of a two dimensional foam reported by Wasan et al.(1994).

Incorporating AOS-18 helped foam stability for both foam stabilized by AOS-18 with and without nanoparticles as shown in Figure 3- 8. The red color is due to using the inert Sudan III dye.

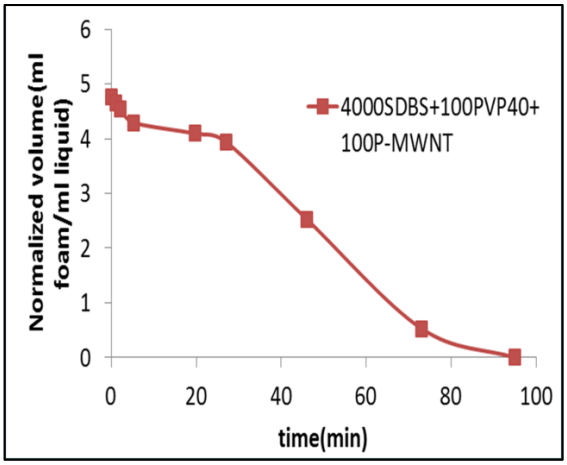

Figure 3- 7: Foam stability in the presence of emulsified decane.

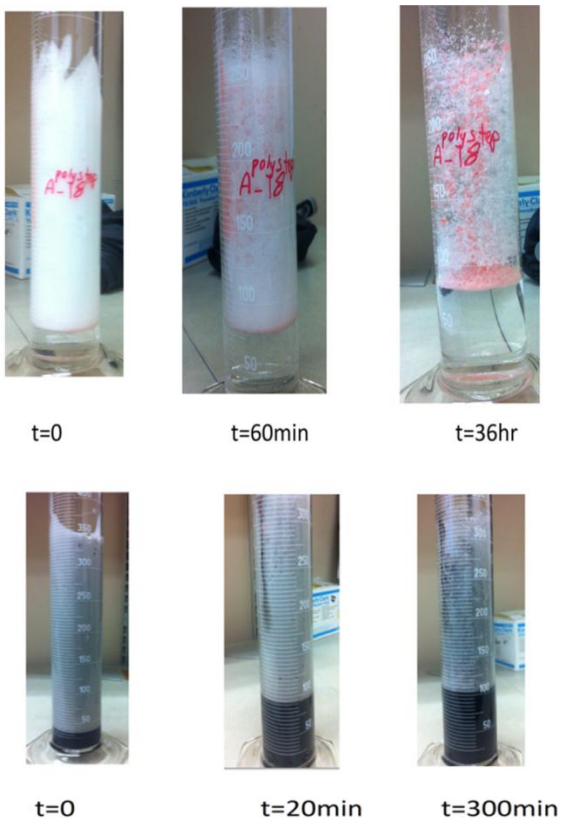

Figure 3- 8: Effect of emulsified oil on foam stabilized(a) by AOS-18(top) and (b) P-MWNT and AOS-18(bottom).

3.3. In Situ Generation of CO_2

Ammonium carbamate has been reported as a source of carbon dioxide for in situ CO2 generation. A molecule can dissociate generating one carbon dioxide molecule and two ammonia molecules as shown below [17, 18, 19]

$$NH_2COONH_4 \leftrightarrow 2NH_3\,(g) + CO_2\,(g) \qquad \text{Eq. 3- 5}$$

Shiau et al. (2010) reported CO_2 generation using ammonium carbamate (AC) titrated with 3M hydrochloric acid or heated at 90°C. These experiments have been repeated and the data has been shown in Figure 3- 9.

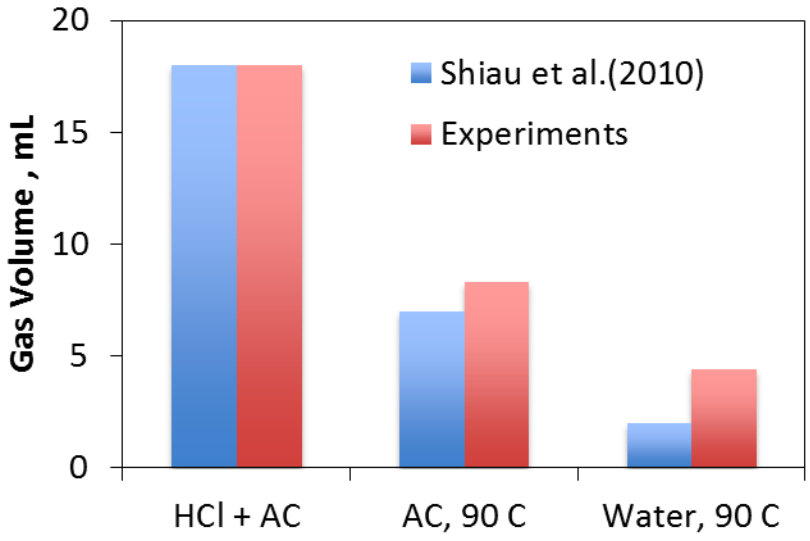

Figure 3- 9: CO_2 generation using ammonium carbamte.

A number of catalysts have been prepared in the lab to investigate the possibility of generating CO_2 controllably. The catalysts tested were P-MWNT with 10% Cu loading, oxidized-MWNT and sulfonated multiwalled nanotube (SO_3-MWNT). The preparation of sulfonated catalyst was according to the method proposed elsewhere

[20] and discussed in Chapter 1. The results shown in Figure 3- 10 indicate no effect of catalytic particles on CO_2 generation. It is therefore thought that CO_2 generation is not acid titration controlled since some experiments performed by slow addition of acid did not result in appreciable gas generation. Only 5 mL of gas was produced following slow addition of HCl which suggests that carbamate dissociation took place due to the heat of dilution resulting from adding acid to the ammonium carbamate solution.

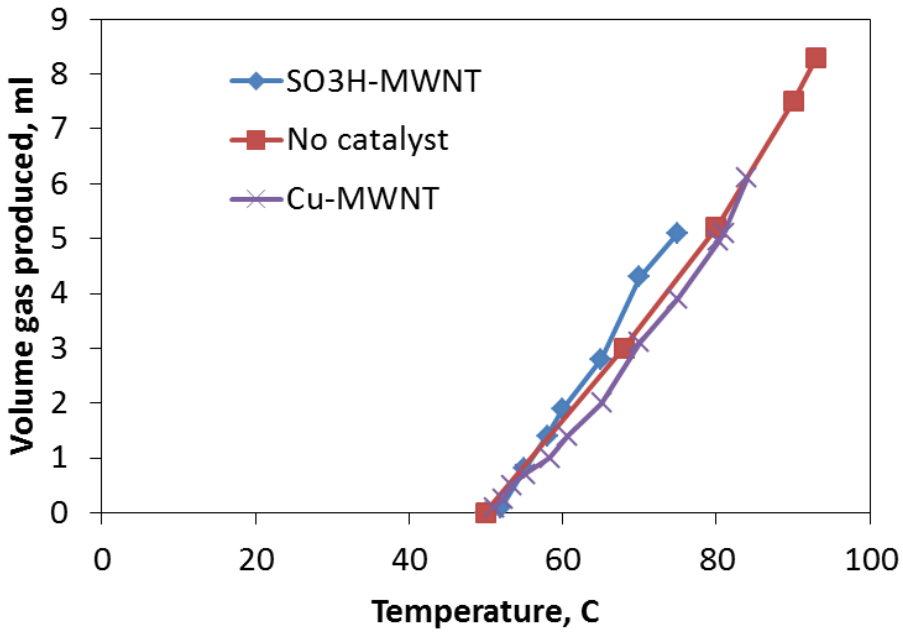

Figure 3- 10: CO_2 generation using a number of catlysts.

3.4. Conclusions

Nanoparticles stabilized foams show significant stability over much longer time. These foams have the possibility to be generated in situ since successful propagation of these nanoparticle has been achieved. The foam stability boost is quite impressive

keeping in mind that very low concentration of these nanohybrids has been used (100ppm). It is possible that carbon nanotubes reduce the drainage rate by extending from the interface to the bulk aqueous phase. It could be that carbon nanoparticle will be covered with adsorbed polymers or surfactants which in turn boost stability by viscosifying the film. Further work including different functionalization of nanohybrids is recommended as a future work.

References

[1] R. Li, W. Yan, S. Liu, G. Hirasaki and C. Miller, "Foam mobility control for surfactant enhanced oil recovery," *SPE 113910,* p. 934, 2010.

[2] B. Herzhaft, A. Toure, F. Bruni and S. Saintpere, "Aqueous Foams for Underbalanced Drilling: The Question of Solids" *SPE 62898 Annual Technical Conference and Exhibition, 1-4 October 2000, Dallas, Texas,* 2000.

[3] Z. Chen, R. Ahmed, S. Miska, N. Takach, M. Yu and M. Pickell, "Rheology and Hydraulics of Polymer (HEC)-Based Drilling Foams at Ambient Temperature Conditions" *SPE-94273-PA,* 2005.

[4] K. Vijayaraghavan, A. Nikolov, D. Wasan and D. Henderson, "Foamability of Liquid Particle Suspensions: A modeling Study" *Ind. Eng. Chem. Res.,* vol. 48, pp. 8180-8185, 2009.

[5] J. Yu, N. Liu, L. Li and R. Lee, "Generation of nanoparticles stabilized supercritical

CO_2 foams" *SPE 150849,* 2012.

[6] T. Zhang, D. Espinosa and K. Yoon, "Engineered Nanoparticles as Harsh-Conditions Emulsions and Foam Stabilizers and as Novel Sensors," *SPE 21212-MS,* 2011.

[7] D. Tanzil, G. Hirasaki and C. Miller, "Conditions for Foam Generation in Homogeneous Porous Media," *SPE 75176,* 2002.

[8] B. Li, G. Hirasaki and C. Miller, "Upscaling of Foam Mobility Control to Three Dimensions" *SPE 99719,* 2006.

[9] D. Tanzil, G. Hirasaki and C. Miller, "Mobility of Foam in Heterogeneous Media: Flow Parallel and Perpendicular to Stratification" *SPE 78601,* 2002.

[10] B. Binks and R. Murakami "Phase inversion of particle-stabilized materials from foams to dry water" *Nature Materials,* vol. 5, pp. 865-869, 2006.

[11] B. Maini and V. Ma, "Thermal Stabiliity of Surfactants for Steamflood Applications," *SPE 13572,* 1985.

[12] K. Mannhardt, J. Novosad and K. and Jha, "Adsorption of Foam-forming Surfactants in Berea Sandstone," *The journal of Canadian petroleum technology,* vol. 33, no. 2, pp. 34-43, 1994.

[13] B. Binks, A. Rocher, and M. Kirkland "Oil foams stabilised solely by particles" *Soft Matter,* vol. 7, pp. 1800-1808, 2011.

[14] D. Wasan, K. Koczo and A. Nikolov, "Mechanisms of Aqueous Foam Stability and Antifoaming Action with and without Oil" in *In Foams: Fundamentals and Applications in the Petroleum Industry*, 1994, pp. 47-56.

[15] D. Resasco, S. Drexler, J. Harwell, B. Shiau, M. Kadhum and J. Faria, "Method and Foam composition for Recovering Hydrocarbons From a Subterranean Reservoir". Patent WO/2013/052359 , 2013.

[16] J. Borchardt, "Foaming Agents for EOR: Correlation of Surfactant Performance and Properties With Chemical Structure" *SPE 16279,* pp. 395-413, 1987.

[17] B. Ramachandran, A. Halpern and E. Glendening, "Kinetics and Mechanism of the Reversible Dissociation of Ammonium Carbamate: Involvement of Carbamic Acid" *J. Phys. Chem.,* vol. 102, no. 22, pp. 3934-3941, 1998.

[18] B. Shiau, T. Hsu, B. Roberts and J. Harwell, "Improved Chemical Flood Efficiency by In Situ CO_2 Generation," *SPE 129893,* 2010.

[19] F. Barzagli, F. Mani and M. Peruzzini, "From greenhouse gas to feedstock: formation of ammonium carbamate from CO2 and NH3 in organic solvents and its catalytic conversion into urea under mild conditions" *Green Chemistry,* vol. 13, pp. 1267-1274, 2011.

[20] Z. Sun, X. Zhang, Y. Liang and H. Li, "A facile approach towards sulfonate functionalization of multi-walled carbon" *Journal of Power Sources,* vol. 191, pp. 366-370, 2009.

Appendix A

A-1 Surface (Interfacial) Tension Derivation

The surface free energy (dG^{σ}) is composed of three terms: an entropy term $S^{\sigma}dT$; an interfacial tension term $Ad\gamma$; and a composition term $\sum n_i d\mu_i$. The Gibbs-Duhem equation at the interface between two bulk phases can be defined as[8]

$$\boldsymbol{dG^{\sigma} = -S^{\sigma}dT + Ad\gamma + \sum n_i d\mu_i} \qquad \text{Eq. A- 1}$$

at constant temperature and composition,

$$\boldsymbol{dG^{\sigma} = Ad\gamma} \qquad \text{Eq. A- 2}$$

$$\boldsymbol{\gamma = \left(\frac{\partial G}{\partial A}\right)_{T,ni}} \qquad \text{Eq. A- 3}$$

[8] Derivation provided by T.F.Tadros. "Emulsion Science and Technology", 1st ed. 2009, Wiley VCH.

Appendix B

B-1 Dispersion loss by filtration and adsorption for HEC-10 and HEC-25

X1, X2 and X3 are concentrations of P-MWNT in ppm.

Table B-1 800ppm of HEC-25

Starting conc. X1	After filtration X2	% loss= $\frac{X1-X2}{X1}100\%$	After adsorption X3	% loss $\frac{X1-X3}{X1}100$
25	9.0	64	7.2	71
50	14.3	71	11.9	76
100	29.5	71	25.7	74
200	49.4	75	42.4	79

Table B-2 1600ppm of HEC-25

Starting conc. X1	After filtration X2	% loss= $\frac{X1-X2}{X1}100\%$	After adsorption X3	% loss $\frac{X1-X3}{X1}100$
25	13.9	44	13.1	48
50	25.4	49	24.6	51
100	49.9	50	48.2	52
200	75.0	62	72.6	64

Table B-3 800ppm of HEC-10

Starting conc. X1	After filtration X2	% loss= $\frac{X1 - X2}{X1} 100\%$	After adsorption X3	% loss $\frac{X1 - X3}{X1} 100$
25	15.1	40	12.2	51
50	27.3	45	19.0	62
100	47.5	53	35.7	64
200	116.3	42	95.1	52

Table B-4 1600ppm of HEC-10

Starting conc. X1	After filtration, adsorption X2,X3	% loss= $\frac{X1 - X2, X3}{X1} 100\%$
25	15.2	35
50	34.2	32
100	66.6	33
200	117.2	41

C-1 Elemental Analysis of HEC-10 and HEC-25

Elemental analysis of the two salinity tolerant polymers has been analyzed for differences in functionalities. Two samples of each polymer have been analyzed for C and H presence. The following table summarizes the results.

Table C-1 Elemental Analysis of HEC-10 and HEC-25

Sample	C%	H%
HEC-10	44.57	5.09
HEC-10	44.65	4.84
HCE-25	44.67	4.89
HEC-25	44.01	4.74